ELECTROCHEMICAL FORMATION OF GERMANENE

by

JIN JUNG

(Under the Direction of John Lewellen Stickney)

ABSTRACT

This dissertation discusses the electrochemical deposition of Ge and germanene on Au. Simply applying an anodic potential on Au electrode in an aqueous Ge solution results in reductive Ge deposition that is limited at a thickness of about 3.5 monolayers (ML), “Bait and Switch” (B&S) method can be used to form a thicker Ge film from aqueous media. Even though Ge film deposited using the B&S method consistently exhibited amorphous Ge Raman signal, electrochemical analysis using cyclic voltammetry (CV) revealed different species of Ge on the Au surface when thin Ge film was deposited on Au surface. One of the species present on the surface is believed to be germanene. Germanene is a crystalline allotrope of Ge and an elemental two-dimensional (2D) material. Similar to graphene, germanene features properties such as ballistic conduction and high optical opacity. Unlike graphene, the energetically favorable structure of germanene has a low-buckling, half of Ge atoms are raised by 0.07 nm.

Electrochemical deposition of Ge and germanene was studied using CV, *in situ* Raman spectroscopy, and electrochemical scanning tunneling microscopy (EC-STM). EC-STM was used to obtain an atomic resolution image of germanene structures on the Au substrate. Atomic resolution images of one ML of Ge film on Au surface

exhibited small domains of germanene surrounded by defective germanene structures, presumably due to nucleation and growth process on polycrystalline Au substrate. The small domains are believed to have limited germanene Raman signal from a Ge deposit.

In situ Raman spectroscopy was used to obtain spectroscopic evidence of electrochemical deposition of germanene. When one ML thick Ge deposit on a SERS active Au substrate was irradiated by 780 nm Raman excitation laser, a sharp germanene Raman peak centered around 296 cm^{-1} was observed. Irradiation using 532 nm Raman excitation laser did not result in the formation of the 296 cm^{-1} peak. Irradiating a SERS active Au substrate with 780 nm laser may have created Au surface plasmon that recrystallized Ge deposit to form larger domains of germanene.

INDEX WORDS: Germanene, Raman spectroscopy, Germanium, SERS, Electrochemistry, Electrodeposition

ELECTROCHEMICAL FORMATION OF GERMANENE

by

JIN JUNG

BS, Mercer University, 2013

A Dissertation Submitted to the Graduate Faculty of The University of Georgia in Partial Fulfillment of the Requirements for the Degree

DOCTOR OF PHILOSOPHY

ATHENS, GEORGIA

2019

ELECTROCHEMICAL FORMATION OF GERMANENE

by

JIN JUNG

Major Professor:	John L. Stickney
Committee:	Tina T. Salguero
	Geoffrey D. Smith

Electronic Version Approved:

Ron Walcott
Interim Dean of the Graduate School
The University of Georgia
December 2019

DEDICATION

For my family.

ACKNOWLEDGEMENTS

I would like to thank Professor John L. Stickney, his guidance was critical for my research projects. I also appreciate former and current members of professor Stickney's group; their passion and expertise were my aspirations. I would like to thank professor Tina T. Salguero and professor Geoffrey D. Smith for spending their valuable time to serve on my committee.

TABLE OF CONTENTS

Page

ACKNOWLEDGEMENTS v

CHAPTER

1 INTRODUCTION AND LITERATURE REVIEW 1

References 12

2 ELECTROCHEMICAL DEPOSITION OF GE 19

Abstract 20

Introduction 20

Experimental 23

Results and discussion 24

Conclusion 47

Acknowledgements 47

References 48

3 *IN SITU* SURFACE ENHANCED RAMAN SPECTROSCOPIC STUDIES OF ELECTROCHEMICALLY FORMED GERMANENE 52

Abstract 53

Introduction 53

Experimental 57

Results and discussion 61

Conclusion 79

Acknowledgements.....80

References.....80

4 PRELIMINARY STUDY OF GERMANENE OXIDATION.....89

Abstract.....90

Introduction.....90

Experimental.....93

Results and discussion.....94

Conclusion.....107

Acknowledgements.....108

References.....108

5 CONCLUSION AND FUTURE STUDIES.....113

References.....116

CHAPTER 1

INTRODUCTION AND LITERATURE REVIEW

Germanene is a 2D material made of germanium.[1] Similar to other group 14 2D materials such as graphene, silicene, and stanene, germanene has a near-planar honeycomb structure.[2,3,4] As illustrated in Figure 1.1, Germanene's structure has low-buckling, meaning that there is 0.07 nm vertical distance between sub-lattices.[5,6] A perfect sheet of free-standing germanene is made of sp^2 hybridized germanium atoms that have interatomic distances of 0.24 nm and germanene ring-to-ring distance of 0.41 nm.[7] Germanene's $2p_z$ orbitals form π orbitals between Ge atoms, forming Dirac points. At Dirac points, valence band and conduction band touch at Fermi level and energy dispersion around the Dirac point is liner. The linear energy dispersion cause electrons to behave like a massless Fermion and travel around 0.3% of the speed of light.[8,9] This is achieved when electrons' mean free path larger than the length of material they are traveling through. In germanene, Ge-Ge π orbitals act as two-dimensional electron gas that provides an environment for electrons to travel without resistivity. The low resistivity is due to negligible internal impurity scattering caused by defects and disorder, also specular scattering at the orbital's edge does not randomize electrons' momentum.[10]

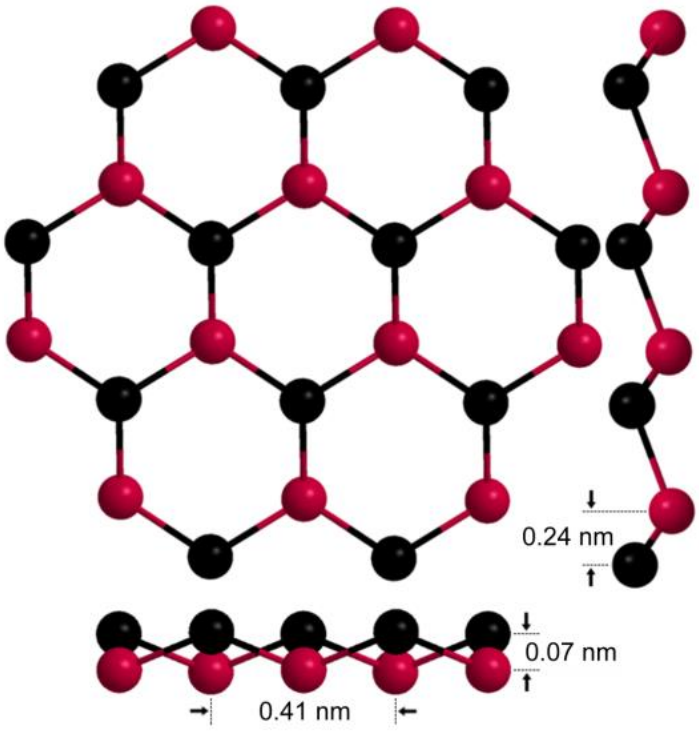

Figure 1.1. Adopted from a publication.[11] The top and side view of the germanene structure has been experimentally measured.[12,13,14] Buckling distance between the top and bottom Ge atoms is 0.07 nm, Ge-Ge bond length is 0.24 nm, and germanene ring to ring distance is 0.41 nm.

The electronic band structure is adjustable via substrate lattice mismatch, external electric filed, functionalization, tensile strain, and low temperature. Germanene's electric band structure is stable when in contact with Au or Ag, albeit with slight band hybridization. The upper half of germanene's Dirac cone is disrupted when germanene is on Cu substrate, and germanene's entire Dirac cone would be disrupted on Al, Pt, and Ir substrates due to band hybridization by covalent bonding between Ge and substrate.[15]

Simply adsorbing molecules such as acetylene, ethanol, methanol, methane, and ammonia increased germanene's bandgap up to 81.0 meV.[16] In addition, applying an external electric field on germanene/adsorbate would open band gap up to 372 meV, and reversing the polarity of the applied electric field closed the band gap.[17] Applying compressive or tensile stress on germanene increased Ge-Ge bond length and decreased buckling. Altered physical dimensions of germanene lead to a reduction in the intrinsic spin-orbit coupling that can change bandgap by 1 meV.[18] Spin-orbit coupling is caused by a magnetic field created by electron's spin interacting with the magnetic field created by relative motion between electron and nucleus, changing the energy of electron's energy level.

Germanene has been studied by other groups previously. The first theoretical study of germanene was reported in 1994, but the first experimental formation of germanene was not reported until 2014.[19,20] Germanene is not a naturally forming structure, and it does not have a graphite equivalent material that is made out of stacked germanene layers.[1,21,22] Thus far, germanene has been mostly formed in an ultra-high vacuum (UHV) environments. The first experimental germanene formation was achieved by evaporating Ge onto Au(111) heated to around 200 ^{o}C in UHV, and the analysis using *in-situ* scanning tunneling microscopy (STM) on the Ge film suggested that $\sqrt{3}$ x $\sqrt{3}$ crystalline germanene was formed.[22] Germanene's 2D structure indicates that when germanene may grow epitaxially if it is formed as deposited, suggesting that substrate lattice constants and germanene lattice constants should match to promote growth. As previously discussed, Ag substrate's lattice constants may not be compatible with germanene, so aluminum nitride layers on Ag(111) was used as the substrate to build

germanene using molecular beam epitaxy (MBE) at a temperature of 450 ^{o}C.[23] Metals were not the only substrates used to form germanene, germanene clusters formed from the edges of highly oriented pyrolytic graphite (HOPG) planes when evaporated Ge was deposited onto HOPG at around 85-120 ^{o}C.[24] Similarly, annealing Pt monolayer on Ge(110) at 826 ^{o}C leads to the formation of the germanene layer covering Ge_2Pt nanocrystal.[25] Epitaxial growth during deposition was not the only way to form germanene, annealing $Si_{0.65}Ge_{0.35}$ layer on Si substrate at 500-800 ^{o}C produced multi-layered germanene.[26] Nonetheless, various techniques have been used to form germanene in a vacuum on a pristine crystalline substrate, but there has been limited research on forming germanene in an aqueous environment.

This group has previously studied the electrochemical formation of Ge from an aqueous media to gorm Ge thin film. Thin film is several angstroms to hundreds of micrometers thick layer, and they are utilized to improve or change a material's surface property. Thin film can be a unique opportunity to use a small amount of materials to obtain the desired property, this is important in applications that do not require a large amount of bulk material such as photovoltaics, sensors, catalysts, and electronics.[27,28] Especially advantageous for nanomaterials that can have a large surface to volume ratio. Thin films referred to in this report will be typically limited to few nanometers thick because electrodeposited Ge in the aqueous phase is limited to 3.5 monolayers (MLs).[29,30] A ML in this dissertation will be defined by the number of the atoms on the Au(111) surface. There are different deposition methods to form such thin films, such as molecular beam epitaxy (MBE), sputtering, chemical vapor deposition (CVD), physical vapor deposition. One of the techniques used to form a thin film is atomic layer

deposition (ALD). ALD forms a thin film of the compound by depositing one layer of an element at a time, taking advantage of surface limited reaction (SLR). A typical ALD refers to deposition from gas to solid in a vacuum, evaporating the source material onto the substrate, but electrochemistry can be used to perform ALD. Electrochemical ALD (E-ALD) is performed in a liquid state to utilize underpotential deposition (UPD) to control SLR, making it easier to handle and scalable. This project's goal was to prove that germanene can be formed using a more energy-efficient and scalable electrochemical method and study the deposition mechanism.

Electrochemical Ge thin film deposition has been studied to develop thin film materials for photovoltaics, semiconductor transistor, and detector.[31,32,33,34] One of the most impactful applications for a thin film is in the semiconductor industry, and germanium could be used as a high-performance semiconductor material due to Ge's oxide thickness and high charge mobility.[35,36] Formation of up to micrometer thick Ge film from various Ge sources such as $GeCl_4$, GeI_4, and $GeBr_4$ in the nonaqueous state have been reported, and suggested that the deposition occurred in two steps: Ge^{+4} to Ge^{+2} and then Ge^{+2} to Ge^0.[37,38,39,40] A typical electrochemical Ge deposition resulted in amorphous Ge film.[41,42] However, crystalline Ge could be formed electrochemically. When Ge^{+4} species was continuously dissolved in the Hg electrode, forming Ge(Hg) alloy and eventually saturating the Hg electrode, and eventually crystalline Ge grew out of the Hg electrode.[43] In another report, indium tin oxide substrate was reduced to form In nanoparticle nucleation sites for crystalline Ge.[44] Suggesting that different Ge structures can be electrochemically formed.

This group already studied electrochemical Ge in an aqueous state before this project started, using Auger electron spectroscopy, cyclic voltammetry, coulometry, electrochemical scanning tunneling microscopy, and Raman spectroscopy.[29,30,45] At the time, the project's focus was to study E-ALD of Ge using electrochemical flow cell shown in Figure 1.2, to develop a method control ML deposition of high-quality Ge. Ge deposition was initially achieved by UPD of Ge on the Au substrate. UPD utilizes SLR where an element deposits on another element, but not onto itself until a larger magnitude of potential is applied, resulting in substrate surface limited deposition of an element. The maximum amount of Ge remained constant around $\frac{4}{9}$ ML when UPD was used to deposit Ge on Au at pH ranging from 1.21 to 9.32. However, pH had a significant influence on the amount of bulk Ge deposition when the more negative potential was applied, and the most amount of Ge was deposited from a basic pH around 9.32. When depositing Ge by simply applying a negative potential, the amount of bulk Ge deposit seemed to plateau at around 3.5 ML after 200 seconds of deposition at all applied potentials, indicating that the Ge deposition process was slow and somehow self-limiting.[29] The limiting amount of bulk Ge deposition was later circumvented by this group by developing a "bait and switch" (B&S) technique.[30] In this technique, the initial maximum amount of bulk Ge was deposited on a substrate, and then bulk Te was deposited on top of the Ge layer. The bulk Te was then reductively stripped down to one ML, leaving the underlying Ge layer intact. Ge was then deposited on top of the remaining Te ML. Finally, remaining Te was reductively removed out from the film, completing a B&S cycle and leaving additional Ge compared to the initial Ge layer. This cycle was then repeated to achieve a desired thickness of Ge film with limited Te contamination. Even though Raman spectra was

used to characterize the bulk Ge film formed using B&S method to be amorphous Ge, nature of the self-limiting Ge deposition was not studied in-depth; leaving the cause of plateud amount of initial layer of Ge on substrate unexplained.

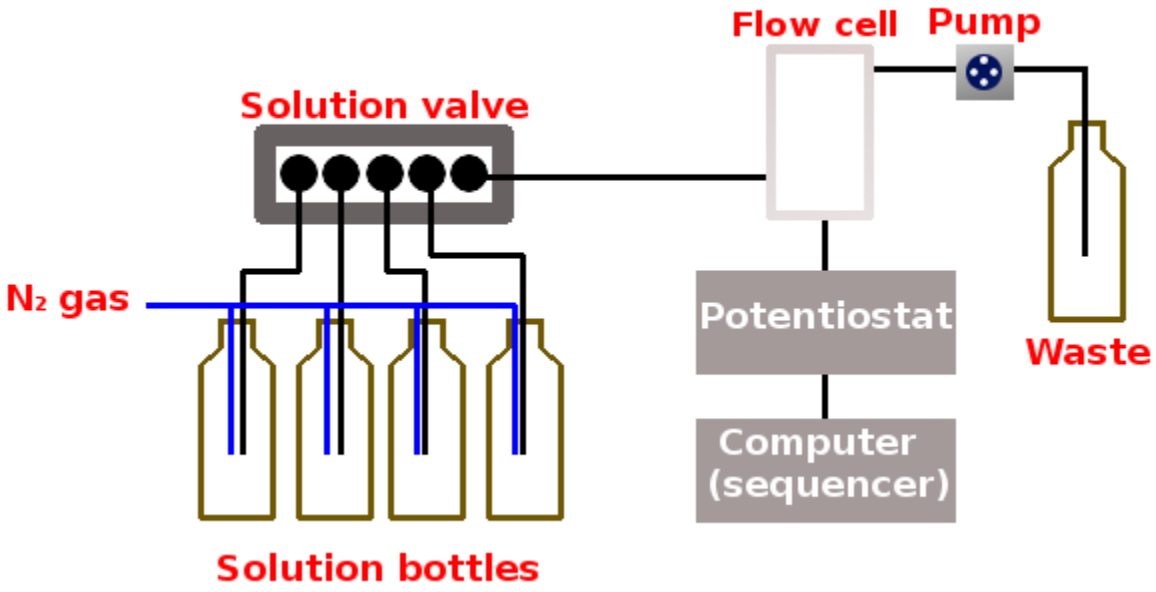

Figure 1.2. Schematics of the EC-ALD flow system. Solutions were degassed by pumping N_2 gas. A pump pulled an individual solution at a time through the flow cell and solution valve block. Flow cell, pump, potentiostat, and solution valve were controlled by the Sequencer program.

Raman spectroscopy provides information about the structure of analyte by measuring the wavelength difference between excitation laser and inelastically scattered Stokes and anti-Stokes Raman scattering of the sample. Rayleigh scattering is the most

common scattering process by far, and the same wavelength as the incoming excitation laser is scattered from the analyte. In Stokes Raman scattering, incoming excitation laser increases electron's energy to a virtual state, and the electron emits a lower wavelength of light than the excitation laser as it relaxes to a higher energy level than the original ground state. In anti-Stokes Raman scattering, incoming excitation laser increases electron's energy level to a virtual state, and the electron emits a higher wavelength of light than the excitation laser as it relaxes to a lower energy level than the original state. The excitation laser causes the molecule to vibrate, but not all bond vibrations lead to Raman emission, because the vibration must polarize the molecule in order to emit Raman emission. The polarizability of an individual vibrational mode can be predicted by studying the molecule's center of inversion. If a vibrational mode stays the same after the pattern is inverted at the center of inversion, it is considered even, but if the inverted pattern changes a vibrational mode, it is considered odd. The even vibrational modes are Raman active, and the odd vibrational modes are IR active.[46]

The Raman spectrometer filters out the excitation laser wavelength and measure the difference between the excitation laser wavelength and the Raman scattering wavelengths.[47] Raman spectrometers typically measure one type of Raman scattering at a time, and all Raman spectroscopy data present in this work will be from Stokes Raman scattering. The Stokes Raman scattering is a rare occurrence that happens once in 10 million scattering incidents, and this leads to poor sensitivity.[48] The intensity of Raman signal is determined by the square of induced Raman dipole that is proportional to Raman polarizability tensor and applied electromagnetic field. In order to improve sensitivity, modern Raman spectrometers adopted high laser density, fast Fourier transform, and

charge-coupled device detector, but they are typically not sensitive enough to measure surface adsorbed analyte by themselves.[49]

Even though conventional Raman spectrometers may not have sufficient sensitivity to measure a thin film on a working electrode, Surface Enhance Raman Spectroscopy (SERS) can achieve necessary sensitivity by amplifying Raman signals by over 10 magnitudes.[50] SERS involves surface plasmon and chemical adsorption on the roughened surface of Au, Ag, or Cu substrate. SERS has been observed in the 1970s and has been since utilized in a wide range of applications including art, archeology, biosciences, solid-state physics, forensics, and nanomaterials.[51,52,53,54,55,56] SERS has been used in this project to study electrochemically formed germanene on the Au substrate. In SERS, electromagnetic enhancement and chemical enhancement mechanisms enable amplification of Raman signals in SERS.

Electromagnetic enhancement in SERS applies to all analytes and is widely considered to be a more impactful enhancement factor. Electromagnetic enhancement in SERS is achieved in two major ways, local field enhancement increasing amplitude of the electromagnetic field applied on the analyte and radiation enhancement increasing Raman dipole. The local field enhancement occurs because the magnitude of the local electromagnetic field at the surface of a metallic surface can be larger than the electromagnetic field from the excitation laser, and the local electromagnetic field induces a Raman dipole just as excitation laser would. The local electromagnetic field enhancement is dependent on the excitation laser wavelength, substrate morphology, and substrate material. Radiation enhancement in SERS occurs because of the analyte's proximity to the metal substrate, radiation pattern modification and an increase in total

power radiated are responsible for the radiation enhancement. Radiation pattern modification is due to Raman emission reflected on the substrate plane, consequentially focusing the Raman emission toward the detector. An increase in total power radiation occurs because the analytes' Raman emission process is altered by the presence of metallic substrate, meaning that the analyte adsorbed on the substrate radiates more Raman signals than analyte in free-space even when the same amplitude of electromagnetic field is applied.[50,57]

Chemical enhancement is considered to have less impact on the overall SERS enhancement. One definition for chemical enhancement is any modification of the Raman polarizability tensor due to adsorption.[58] One mechanism contributing to chemical enhancement is charge transfer. Charge transfer occurs in three different ways. Type 1 leads to a small improvement in Raman signal due to minor change in the adsorbed analyte's electronic structure, altering Raman polarizability tensor to be more favorable but does not require chemical bond between analyte and substrate. Type 2 charge transfer enhances Raman signal when the analyte becomes a surface complex either by covalent binding with the metal or by indirect bonding with another complexing agent. Type 2 mechanism leads to a substantial change in analyte's electronic structure and potentially in Raman polarizability. Type 3 mechanism occurs when the energy difference between the metal substrate's fermi level and analyte's HOMO and LUMO is matched by the excitation laser. Type 3 mechanism leads to a photo-driven charge transfer between analyte and substrate similar to resonance Raman spectroscopy. Just as in resonance Raman spectroscopy, excitation laser's energy matching analyte's electronic transition energy can lead to a change in bond length and polarizability that increases the

probability of Stokes scattering. Another chemical enhancement mechanism is image dipole enhancement. This effect occurs when an laser-induced dipole in the analyte is mirrored by the metal substrate and the mirrored dipole induces a dipole in the analyte, repeating infinitely. However, it has been determined that the image dipole enhancement only has a slight impact.[48,50,57]

One application of Raman spectroscopy is *in situ* Raman spectroelectrochemistry, where Raman spectroscopy is used to measure the analytes on the surface of the working electrode during an electrochemical experiment.[48] Utilizing SERS-active electrode enables quantitative analysis of low concentration species and thin films.[59,60] When performing *in situ* Raman spectroelectrochemistry, water can be mostly ignored because water's broad Raman peak around 3400 cm^{-1} in Raman spectra tend to not overlap with typical analyte's Raman peaks and also water does not absorb analyte's Raman emission.[61] Spectroelectrochemistry is not a simple combination of Raman spectroscopy and electrochemical experiment, and each part of the experiment can affect another. For example, applied potential can change laser absorption and the laser can induce a current or redox reaction at the surface.[48,62] In addition, SERS loses effectiveness when the deposit is too thick, and far away from the SERS-active electrode surface. Even a three-nanometer thick deposit can drastically decrease enhancement effect and make the method ineffective for bulk deposit measurement.[63,64]

REFERENCES

1. Acun, A.; Zhang, L.; Bampoulis, P.; Farmanbar, M.; Houselt, A. v.; Rudenko, A. N.; Lingenfelder, M.; Brocks, G.; Poelsema, B.; Katsnelson, M. I.; Zandvliet, H. J. W., Germanene: the germanium analogue of graphene. *Journal of Physics: Condensed Matter* **2015,** *27* (44), 443002.

2. Kaloni, T. P.; Schreckenbach, G.; Freund, M. S.; Schwingenschlogl, U., Current developments in silicene and germanene. *Physica Status Solidi-Rapid Research Letters* **2016,** *10* (2), 133-142.

3. Geim, A. K.; Novoselov, K. S., The rise of graphene. *Nat Mater* **2007,** *6* (3), 183-191.

4. Zaveh, S. J.; Roknabadi, M. R.; Morshedloo, T.; Modarresi, M., Electronic and thermal properties of germanene and stanene by first-principles calculations. *Superlattices and Microstructures* **2016,** *91*, 383-390.

5. Nijamudheen, A.; Bhattacharjee, R.; Choudhury, S.; Datta, A., Electronic and Chemical Properties of Germanene: The Crucial Role of Buckling. *The Journal of Physical Chemistry C* **2015,** *119* (7), 3802-3809.

6. Ledina, M. A.; Bui, N.; Liang, X.; Kim, Y. G.; Jung, J.; Perdue, B.; Tsang, C.; Drnec, J.; Carlà, F.; Soriaga, M. P.; Reber, T. J.; Stickney, J. L., Electrochemical Formation of Germanene: pH 4.5. *Journal of The Electrochemical Society* **2017,** *164* (7), D469-D477.

7. Derivaz, M.; Dentel, D.; Stephan, R.; Hanf, M.-C.; Mehdaoui, A.; Sonnet, P.; Pirri, C., Continuous Germanene Layer on Al(111). *Nano Letters* **2015,** *15* (4), 2510-2516.

8. Castro Neto, A. H.; Guinea, F.; Peres, N. M. R.; Novoselov, K. S.; Geim, A. K., The electronic properties of graphene. *Reviews of Modern Physics* **2009,** *81* (1), 109-162.

9. Novoselov, K. S.; Geim, A. K.; Morozov, S. V.; Jiang, D.; Katsnelson, M. I.; Grigorieva, I. V.; Dubonos, S. V.; Firsov, A. A., Two-dimensional gas of massless Dirac fermions in graphene. *Nature* **2005,** *438* (7065), 197-200.

10. Beenakker, C. W. J.; van Houten, H., *Quantum Transport in Semiconductor Nanostructures*. 2004; Vol. 44.

11. Jung, J.; Bui, N. N.; Shen, S.; Reber, T. J.; Brezner, J. M.; Mubeen, S.; Stickney, J. L., In Situ Surface-Enhanced Raman Spectroscopic Studies of Electrochemically Formed Germanene. *The Journal of Physical Chemistry C* **2018,** *122* (27), 15696-15705.

12. Bechstedt, F.; Matthes, L.; Gori, P.; Pulci, O., Infrared absorbance of silicene and germanene. *Applied Physics Letters* **2012,** *100* (26), 261906.

13. Ledina, M. A.; Bui, N.; Liang, X.; Kim, Y.-G.; Jung, J.; Perdue, B.; Tsang, C.; Drnec, J.; Carlà, F.; Soriaga, M. P.; Reber, T. J.; Stickney, J. L., Electrochemical Formation of Germanene: pH 4.5. *Journal of The Electrochemical Society* **2017,** *164* (7), D469-D477.

14. Bui, N. N.; Ledina, M.; Reber, T. J.; Jung, J.; Stickney, J. L., An Electrochemical Scanning Tunneling Microscopic Study of the Potential Dependence of Germanene Growth on Au(111) at pH 9.0. *ACS Nano* **2017**.

15. Wang, Y.; Li, J.; Xiong, J.; Pan, Y.; Ye, M.; Guo, Y.; Zhang, H.; Quhe, R.; Lu, J., Does the Dirac cone of germanene exist on metal substrates? *Physical Chemistry Chemical Physics* **2016,** *18* (28), 19451-19456.

16. Wang, Y. P.; Ji, W. X.; Zhang, C. W.; Li, S. S.; Li, F.; Li, P.; Ren, M. J.; Chen, X. L.; Yuan, M.; Wang, P. J., Enhanced band gap opening in germanene by organic molecule adsorption. *Materials Chemistry and Physics* **2016,** *173*, 379-384.

17. Liu, G.; Luo, W. W.; Wang, X.; Lei, X. L.; Xu, B.; Ouyang, C. Y.; Liu, S. B., Tuning the electronic properties of germanene by molecular adsorption and under an external electric field. *Journal of Materials Chemistry C* **2018,** *6* (22), 5937-5948.

18. Kaloni, T. P.; Schwingenschlögl, U., Stability of germanene under tensile strain. *Chemical Physics Letters* **2013,** *583*, 137-140.

19. Takeda, K.; Shiraishi, K., Theoretical possibility of stage corrugation in Si and Ge analogs of graphite. *Physical Review B* **1994,** *50* (20), 14916-14922.

20. Dávila, M. E.; Xian, L.; Cahangirov, S.; Rubio, A.; Le Lay, G., Germanene: a novel two-dimensional germanium allotrope akin to graphene and silicene. *New Journal of Physics* **2014,** *16* (9), 095002.

21. Bundy, F. P., Phase Diagrams of Silicon and Germanium to 200 kbar, 1000°C. *The Journal of Chemical Physics* **1964,** *41* (12), 3809-3814.

22. Davila, M. E.; Le Lay, G., Few layer epitaxial germanene: a novel two-dimensional Dirac material. *Scientific Reports* **2016,** *6*.

23. d'Acapito, F.; Torrengo, S.; Xenogiannopoulou, E.; Tsipas, P.; Velasco, J. M.; Tsoutsou, D.; Dimoulas, A., Evidence for Germanene growth on epitaxial hexagonal (h)-AlN on Ag(111). *Journal of Physics-Condensed Matter* **2016,** *28* (4).

24. Peng, W.; Xu, T.; Diener, P.; Biadala, L.; Berthe, M.; Pi, X.; Borensztein, Y.; Curcella, A.; Bernard, R.; Prévot, G.; Grandidier, B., Resolving the Controversial Existence of Silicene and Germanene Nanosheets Grown on Graphite. *ACS Nano* **2018,** *12* (5), 4754-4760.

25. Bampoulis, P.; Zhang, L.; Safaei, A.; Gastel, R. v.; Poelsema, B.; Zandvliet, H J W., Germanene termination of Ge 2 Pt crystals on Ge(110). *Journal of Physics: Condensed Matter* **2014,** *26* (44), 442001.

26. Tsai, H.-S.; Chen, Y.-Z.; Medina, H.; Su, T.-Y.; Chou, T.-S.; Chen, Y.-H.; Chueh, Y.-L.; Liang, J.-H., Direct formation of large-scale multi-layered germanene on Si substrate. *Physical Chemistry Chemical Physics* **2015,** *17* (33), 21389-21393.

27. Vaidyanathan, R.; Stickney, J. L.; Cox, S. M.; Compton, S. P.; Happek, U., Formation of In2Se3 thin films and nanostructures using electrochemical atomic layer epitaxy. *Journal of Electroanalytical Chemistry* **2003,** *559*, 55-61.

28. Ulman, A., Formation and Structure of Self-Assembled Monolayers. *Chemical Reviews* **1996,** *96* (4), 1533-1554.

29. Liang, X.; Kim, Y.-G.; Gebergziabiher, D. K.; Stickney, J. L., Aqueous Electrodeposition of Ge Monolayers. *Langmuir* **2010,** *26* (4), 2877-2884.

30. Liang, X.; Zhang, Q.; Lay, M. D.; Stickney, J. L., Growth of Ge Nanofilms Using Electrochemical Atomic Layer Deposition, with a "Bait and Switch" Surface-Limited Reaction. *Journal of the American Chemical Society* **2011,** *133* (21), 8199-8204.

31. Szekely, G., Electrodeposition of Germanium. *Journal of The Electrochemical Society* **1951,** *98* (8), 318-324.

32. Malaquias, J. C.; Wu, M.; Lin, J.; Robert, E. V. C.; Sniekers, J.; Binnemans, K.; Dale, P. J.; Fransaer, J., Electrodeposition of germanium-containing precursors for Cu2(Sn,Ge)S3 thin film solar cells. *Electrochimica Acta* **2017,** *251*, 651-659.

33. Claeys, C.; Simoen, E., *Germanium-based technologies: from materials to devices*. elsevier: 2011.

34. Buca, D.; Winnerl, S.; Lenk, S.; Mantl, S.; Buchal, C., Metal–germanium–metal ultrafast infrared detectors. *Journal of Applied Physics* **2002,** *92* (12), 7599-7605.

35. Kamata, Y., High-k/Ge MOSFETs for future nanoelectronics. *Materials Today* **2008,** *11* (1), 30-38.

36. Chui, C.; Kim, H.; Chi, D.; Triplett, B. B.; McIntyre, P. C.; Saraswat, K. C., *A sub-400°C germanium MOSFET technology with high-κ dielectric and metal gate*. 2002; p 437-440.

37. Endres, F.; El Abedin, S. Z., Electrodeposition of stable and narrowly dispersed germanium nanoclusters from an ionic liquid. *Chemical Communications* **2002,** (8), 892-893.

38. Endres, F.; Zein El Abedin, S., Nanoscale electrodeposition of germanium on Au(111) from an ionic liquid: an in situ STM study of phase formation Part II. Ge from GeCl4. *Physical Chemistry Chemical Physics* **2002,** *4* (9), 1649-1657.

39. Endres, F.; Schrodt, C., In situ STM studies on germanium tetraiodide electroreduction on Au(111) in the room temperature molten salt 1-butyl-3-methylimidazolium hexafluorophosphate. *Physical Chemistry Chemical Physics* **2000,** *2* (24), 5517-5520.

40. Endres, F., Electrodeposition of a thin germanium film on gold from a room temperature ionic liquid. *Physical Chemistry Chemical Physics* **2001,** *3* (15), 3165-3174.

41. Jawad, M. J.; Hashim, M. R.; Ali, N. K.; Córcoles, E. P.; Sharifabad, M. E., An Alternative Method to Grow Ge Thin Films on Si by Electrochemical Deposition for Photonic Applications. *Journal of The Electrochemical Society* **2011,** *159* (2), D124-D128.

42. Huang, Q.; Bedell, S. W.; Saenger, K. L.; Copel, M.; Deligianni, H.; Romankiw, L. T., Single-Crystalline Germanium Thin Films by Electrodeposition and Solid-Phase Epitaxy. *Electrochemical and Solid-State Letters* **2007,** *10* (11), D124-D126.

43. Carim, A. I.; Collins, S. M.; Foley, J. M.; Maldonado, S., Benchtop Electrochemical Liquid–Liquid–Solid Growth of Nanostructured Crystalline Germanium. *Journal of the American Chemical Society* **2011,** *133* (34), 13292-13295.

44. Mahenderkar, N. K.; Liu, Y.-C.; Koza, J. A.; Switzer, J. A., Electrodeposited Germanium Nanowires. *ACS Nano* **2014,** *8* (9), 9524-9530.

45. Liang, X.; Jayaraju, N.; Thambidurai, C.; Zhang, Q.; Stickney, J. L., Controlled Electrochemical Formation of GexSbyTez using Atomic Layer Deposition (ALD). *Chemistry of Materials* **2011,** *23* (7), 1742-1752.

46. Appendix B - The bond-polarizability model. In *Principles of Surface-Enhanced Raman Spectroscopy*, Le Ru, E. C.; Etchegoin, P. G., Eds. Elsevier: Amsterdam, 2009; pp 491-498.

47. Le Ru, E. C.; Etchegoin, P. G., Chapter 1 - A quick overview of surface-enhanced Raman spectroscopy. In *Principles of Surface-Enhanced Raman Spectroscopy*, Elsevier: Amsterdam, 2009; pp 1-27.

48. Allen J. Bard, L. R. F., *Electrochemical Methods: Fundamentals and Applications, 2nd Edition*. John Wiley & Sons, Inc: New York, 2001.

49. Le Ru, E. C.; Etchegoin, P. G., Single-Molecule Surface-Enhanced Raman Spectroscopy. *Annual Review of Physical Chemistry* **2012,** *63* (1), 65-87.

50. Le Ru, E. C.; Etchegoin, P. G., Chapter 4 - SERS enhancement factors and related topics. In *Principles of Surface-Enhanced Raman Spectroscopy*, Le Ru, E. C.; Etchegoin, P. G., Eds. Elsevier: Amsterdam, 2009; pp 185-264.

51. Fleischmann, M.; Hendra, P. J.; McQuillan, A. J., Raman spectra of pyridine adsorbed at a silver electrode. *Chemical Physics Letters* **1974,** *26* (2), 163-166.

52. Jeanmaire, D. L.; Van Duyne, R. P., Surface raman spectroelectrochemistry: Part I. Heterocyclic, aromatic, and aliphatic amines adsorbed on the anodized silver electrode. *Journal of Electroanalytical Chemistry and Interfacial Electrochemistry* **1977,** *84* (1), 1-20.

53. Albrecht, M. G.; Creighton, J. A., Anomalously intense Raman spectra of pyridine at a silver electrode. *Journal of the American Chemical Society* **1977,** *99* (15), 5215-5217.

54. Banaei, N.; Foley, A.; Houghton, J. M.; Sun, Y.; Kim, B., Multiplex detection of pancreatic cancer biomarkers using a SAB - Early diagnosis of pancreatic cancer (PC) is critical to reduce the mortality rate of this disease. Current biological analysis approaches cannot robustly detect several low abundance PC biomarkers in sera, limiting the clinical application of these biomarkers. Enzyme linked immunosorbent assay and radioimmunoassay are two common platforms for detection of biomarkers; however, they suffer from some limitation. This study demonstrates a novel system for multiplex detection of pancreatic biomarkers CA19-9, MMP7 and MUC4 in sera samples with high sensitivity using surface enhanced Raman spectroscopy. Measuring the levels of these biomarkers in PC patients, pancreatitis patients, and healthy individuals reveals the unique expression pattern of these markers in PC patients, suggesting the great potential of using this approach for early diagnostics of PCs. ERS-based immunoassay. *Nanotechnology* **2017,** *28* (45), 455101.

55. Cortés, E.; Etchegoin, P. G.; Le Ru, E. C.; Fainstein, A.; Vela, M. E.; Salvarezza, R. C., Monitoring the Electrochemistry of Single Molecules by Surface-Enhanced Raman Spectroscopy. *Journal of the American Chemical Society* **2010,** *132* (51), 18034-18037.

56. linear, W. K. T.-R. a. i.; nonlinear Raman, s., II.

57. Le Ru, E. C.; Blackie, E.; Meyer, M.; Etchegoin, P. G., Surface Enhanced Raman Scattering Enhancement Factors: A Comprehensive Study. *The Journal of Physical Chemistry C* **2007,** *111* (37), 13794-13803.

58. Moskovits, M., Surface-enhanced spectroscopy. *Reviews of Modern Physics* **1985,** *57* (3), 783-826.

59. Fanjul Bolado, P.; Martín Yerga, D.; Junquera Pérez, A.; González García, M. B.; Hernández Santos, D., Surface-Enhanced Raman Spectroelectrochemistry with Screen-Printed Electrodes for Quantitative Analysis. *Meeting Abstracts* **2018,** *MA2018-01* (36), 2119.

60. Munce, C. G.; Parker, G. K.; Holt, S. A.; Hope, G. A., A Raman spectroelectrochemical investigation of chemical bath deposited CuxS thin films and their modification. *Colloids and Surfaces A: Physicochemical and Engineering Aspects* **2007,** *295* (1), 152-158.

61. Auer, B. M.; Skinner, J. L., IR and Raman spectra of liquid water: Theory and interpretation. *The Journal of Chemical Physics* **2008,** *128* (22), 224511.

62. Liu, C. Y.; Bard, A. J., Effect of excess charge on band energetics (optical absorption edge and carrier redox potentials) in small semiconductor particles. *The Journal of Physical Chemistry* **1989,** *93* (8), 3232-3237.

63. Stiles, P. L.; Dieringer, J. A.; Shah, N. C.; Van Duyne, R. P., Surface-Enhanced Raman Spectroscopy. *Annual Review of Analytical Chemistry* **2008,** *1* (1), 601-626.

64. Mosier-Boss, P. A., Review of SERS Substrates for Chemical Sensing. *Nanomaterials (Basel)* **2017,** *7* (6), 142.

CHAPTER 2

ELECTROCHEMICAL DEPOSITION OF GE[1]

[1]Jung, J.; Ledina M.A.; Bui, N.; Stickney J.L. To be submitted to Journal of the Electrochemical Society

2.1 ABSTRACT

Sub-monolayer electrodeposition of Ge and the "Bait and Switch" method to form thicker Ge film was studied to optimize Ge film formation and investigate germanene growth. Using cyclic voltammetry (CV), coulometry, electrochemical scanning tunneling microscopy (EC-STM), and Raman spectroscopy, the Ge film formation method was improved and encouraging signs of germanene formation were observed. Sub-ML Ge film on Au deposited at potentials positive of -0.9 V suggested the existence of multiple species of Ge. When Ge was deposited at around pH 9, the reductive deposition from Ge^{+4} to Ge^{0} started to occur around -0.3 V vs. Ag/AgCl and about one ML formed around -0.9 V vs. Ag/AgCl. A complete germanene structure was not observed when the Ge coverage was low, but germanene structures were observed using EC-STM when at least one ML of Ge was deposited. In addition, B&S deposition conditions were studied to develop a deposition process more supportive for germanene formation, but Raman spectroscopy determined that all Ge films newly formed from the B&S method resulted in amorphous Ge film with no sign of germanene.

2.2 INTRODUCTION

Ge is one of the prominent semiconductor material, even though it has been overshadowed by Si due to stability, abundancy, and price.[1] However, Ge's unique bandgap, electron mobility, dielectric constant, and other material characteristics can be utilized to make a high-performance materials for electronics beyond natural limitations of Si [2] Si may not be entirely replaced by Ge in near future, but the potential of Ge integration in semiconductor circuit is being explored.[2] Common deposition techniques to

form a Ge film are atomic layer deposition (ALD), chemical vapor deposition (CVD), pulsed laser deposition, and sputter deposition.[3,4,5] Those methods are well understood and widely adopted but require a vacuum and high temperature that is energy inefficient and costly. Alternatively, electrochemical methods to deposit Ge could lead to a cheaper and versatile deposition method in ambient temperature and pressure.

Electrochemical deposition of Ge has been studied for decades, mostly in nonaqueous media to avoid hydrogen evolution, because the anodic potential needed to reduce Ge cations dissolved in water to Ge atom on the working electrode is high enough to induce hydrogen evolution reaction (HER) of water. Nonaqueous solvents tend to require much higher overpotential to break down compared to water, and the stability and limited HER in the nonaquous media is an advantage over aqueous methods.[6,7,8,9,10] The mechanisms of electrochemical deposition of Ge in ionic liquid has been studied by Endres, et al., and reported that electrochemical deposition of Ge^{+4} first start with reduction of Ge^{+4} to Ge^{+2} and then Ge^{+2} to Ge^{0}, the Ge deposition in the nonaqueous media results in a bulk deposition, where Ge deposits on top of other Ge atoms, and form few nm think Ge deposits.[11,12] Ge deposition in aqueous media is limited to approximately 3.5 monolayers (MLs), one ML is defined by the number of the atoms on the Au(111) surface, as discussed in this group's previous works.[13,14]

Multiple Ge structures can be formed via electrochemical deposition. Reports suggested that Ge nanowires as small as approximately 50 nm diameter could be formed, but those Ge deposits' structures were amorphous.[15,16] However, other reports suggested that crystalline Ge could be formed. One example was using the Hg working electrode, by forming Hg-Ge alloy in the electrode before expelling crystalline Ge out of the Hg

electrode.[17] Another method to obtain crystalline Ge formation was made possible by electrodepositing Ge on In nanoparticles.[18]

This group has been studying the electrochemical deposition of Ge in aqueous media and has developed the B&S method to overcome the previously mentioned 3.5 ML limitation of direct electrochemical deposition.[13] This method is initiated by depositing 3.5 ML thick Ge deposit on a working electrode, then bulk deposit Te on top of the Ge, then strip Te to one ML, then deposit Ge on the Te ML, and strip away the Te. The second layer of Ge remained on the surface after these steps were followed, and this step could have been repeated multiple times to develop thicker Ge deposits. Further efforts to study and optimize the B&S method are discussed in this chapter. Few variables investigated to optimize the method included substrates, pH, cycle time, applied potential, and ion concentrations.

One of the Ge deposited samples on a Cu substrate using the method mentioned above exhibited a Raman peak attributed to germanene on few spots.[19,20] The observed peak centered around 296 cm^{-1} was distinguishable compared to amorphous Ge peak centered around 270 cm^{-1}.[21] The same peak was also observed in germanene deposits on Au and Si formed in UHV. [22,23] The electrochemical deposition process of Ge and germanene on Au and Cu in various pH was studied as a continuation of reports from Liang and Ledina.[13,19]

2.3 EXPERIMENTAL

Electrochemical experiments were performed using an automated electrochemical flow cell system (Electrochemical ALD L.C., Athens, GA).[24] The working electrode

(substrate) was a 100 nm thick polycrystalline Au film vapor deposited on a 5 nm thick Ti film on the glass. The reference electrode was Ag/AgCl (3 M NaCl, BASI, West Lafayette, IN), and all potentials were reported with respect to it. The substrate was cycled in 0.1 M H_2SO_4 from -0.2 V to 1.45 V before each experiment.

In situ STM studies were performed by Maria Ledina using Nanoscope III (Digital Instruments, Veeco) in an in-house built STM cell.[19] The substrate was Au bead annealed in hydrogen flame, cooled in a hydrogen atmosphere, and then quenched in hydrogen saturated water, producing large Au(111) crystalline terraces. The tips were made by etching 0.25 mm W wire in 1M KOH using 15 V AC. The reported STM studies were performed in constant current mode (height mode) and calibrated using HOPG. A further detailed description of the cell is described in a report.

All solutions were prepared using 18 MΩ ultrapure water from a Millipore-Q system (Barnstead, Dubuque, IA). GeO_2 and blank solutions were either adjusted to around pH 4.7 using perchlorate or buffered to pH 9.0 using 50 mM $Na_2B_2O_4$ (Baker analyzed, 99.5%) and contained 0.1M perchlorate as a supporting electrolyte. The solutions were degassed for at least 2 hours by flushing with nitrogen gas before experiments.

2.4 RESULTS AND DISCUSSION

Figure 2.1, illustrates a series of CVs of polycrystalline Au in pH 4.5 Ge solution with an anodic potential limit of 0.5 V and a cathodic potential limit of -0.5 V with varying time where the potential was held constant at the cathodic potential. The open circuit potential (OCP) was around 0.1 V, and the initial reductive deposition of Ge^{+4} into

Ge^0 in pH 4.5 started when -0.5 V was applied on the working electrode as shown in Figure 2.1. This Ge deposit was reversible, suggested by the small potential difference between the reduction potential and oxidation potential, -0.5 V and -0.25 V respectively. The reductive Ge deposition seems to have slow kinetics when comparing the red and green CVs in Figure 2.1. The cathodic limit potential had to be applied for a few minutes instead of returning to anodic potential immediately to deposit a measurable amount of Ge. Also, the amount of Ge deposition seemed to be limited at the applied potential. As shown in the black and green CV in Figure 2.1, the deposited amount plateaued to around 0.09 ML after applying cathodic potential for 500 s and holding the potential for a longer time did not result in additional Ge deposition. The slow deposition kinetics and plateaued deposition quantity may suggest surface alloy formation.[25] The Ge solution was flowing the entire time during the experiment and the quantity of deposited Ge was magnitudes lower than the quantity of Ge ions in the bulk solution, suggesting that Ge ion quantities should not have been a limiting factor.

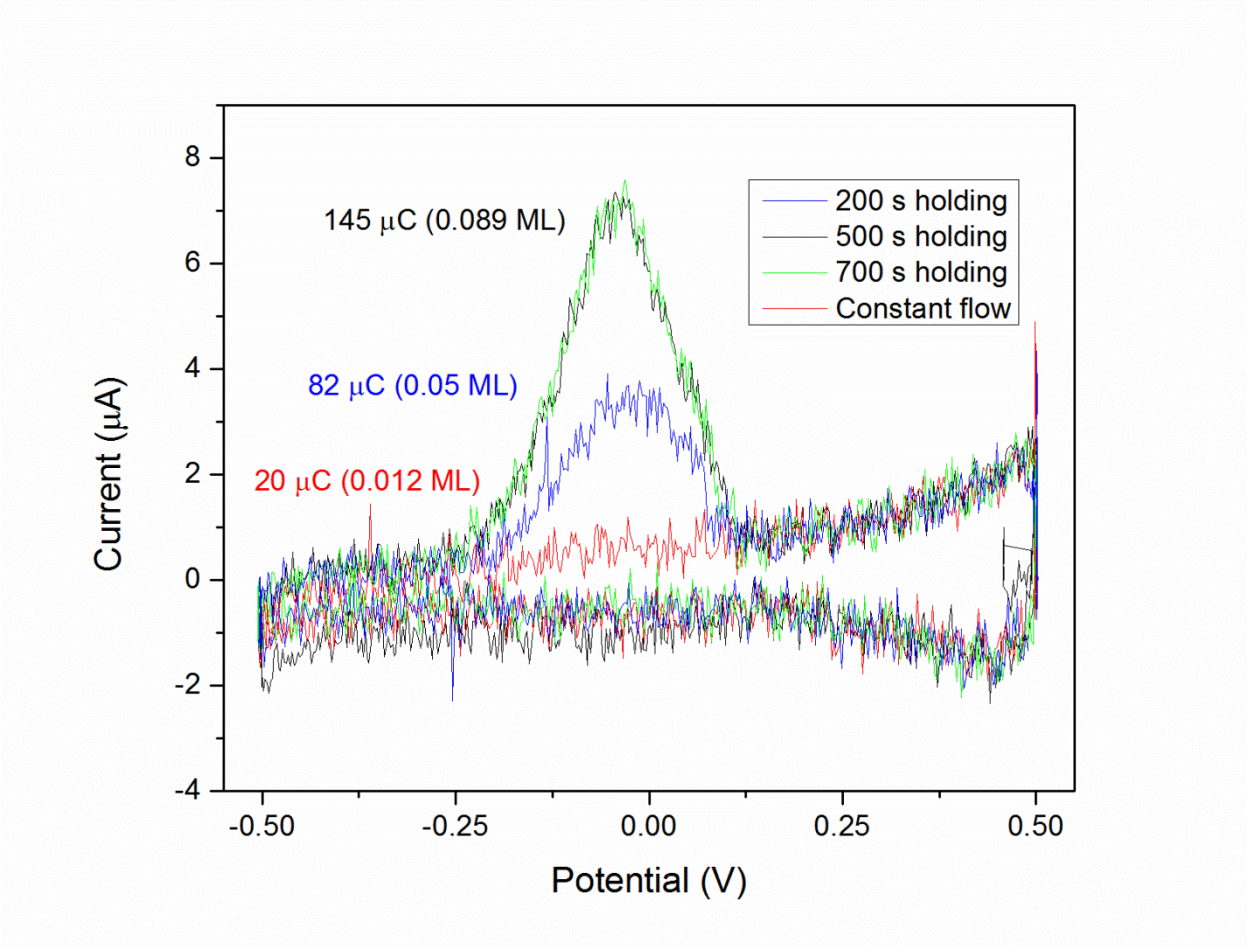

Figure 2.1. CVs of polycrystalline Au in 1 mM GeO_2 in pH 4.5, the cathodic limit potential was applied for varying amounts of time. The cathodic limit potential in red CV was applied for 0 s, blue CV for 200 s, black CV for 500 s, and green CV for 700 s. The amount of deposited Ge quantified by the integrated value of the oxidative peak centered on around 0 V that the deposition plateaus to 0.089 ML around 500 s.

The structure of Ge deposited in Figure 2.1 can't be determined with a CV, but EC-STM suggested that germanene is not formed until more negative potential was applied, around -0.9 V or lower. Deposited Ge atoms until around -0.9 V was applied

were mostly forming a surface alloy with Au. The EC-STM studies that suggested the surface alloy formation were performed by Ledina and shown in Figure 2.2. First Ge atoms seem to deposit and alloy with Au at or below the Au surface, resulting in raised islands across the surface. The height of such islands was reported to be around 0.1 nm, indicating that they simply Ge atoms adsorbed on top of the surface, since the height is smaller than the radius of a Ge atom, suggesting that the reduced Ge atoms are being buried underneath the surface and as forming an alloy with Au substrate. The alloy formation and Au surface disruption were further corroborated from surface X-ray diffraction (SXRD) studies performed by Drnec.[20] In the SXRD studies, reciprocal space map showed Au reconstruction rods disappeared when Ge was deposited at -0.5 V. Suggesting that the Au (111) surface is disrupted by the alloyed Ge atoms.

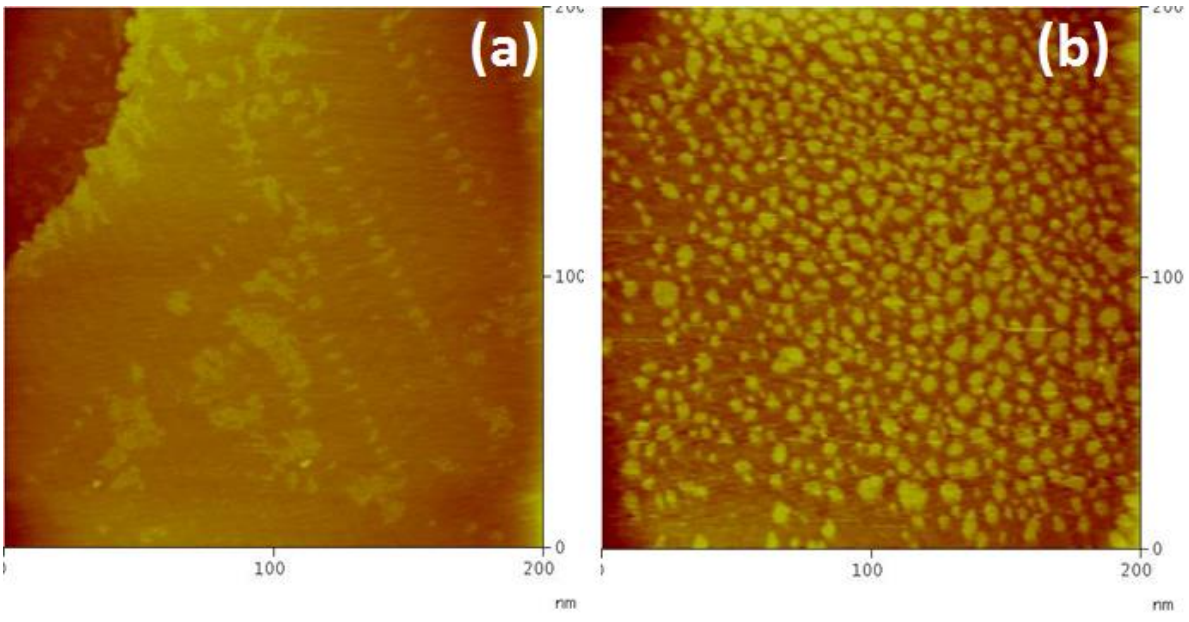

Figure 2.2. Adopted from Ledina's work, STM images of Au(111) surface in 1 mM GeO_2 in pH 4.5. -0.9 V was applied for 0 s in (a) and 480 s in (b).[20] The brightness of the

images indicates height, and the yellow spots on (b) are believed to be due to deposited Ge atoms forming Ge-Au alloy and raising the Au surface.

The Ge deposition's potential and kinetics dependence were further studied by applying a cathodic potential at -0.6 V. As shown in Figure 2.3, holding potential at the cathodic potential limit resulted in a higher oxidation charge, further corroborating slow kinetics of reductive Ge deposition. The amount of Ge deposition was plateaued when the cathodic potential was applied for 700 s (blue), and it had significantly increased overall Ge deposition compared to the shorter deposition time. A new oxidation peaks emerged when more negative cathodic potential was applied, when the Ge deposition was accomplished by applying -0.5 V, the only oxidation peak was around 0 V, but a new oxidation peak centered around -0.5 V appeared when applying -0.6 V. It is believed that the new oxidation peak centered around -0.5 V is from the first ML of Ge on the substrate surface forming Ge-Ge bond. The time-dependent deposition process and resulting Ge structure were further studied in Figure 2.4 by first reducing Ge by applying -0.5 V, rinsing in blank solution, and reducing further in a more negative cathodic potential. The resulting CVs indicated an increased oxidation charge from reduced Ge on the surface. The increased Ge deposit did not support the partial oxidation process, considering that the integrated area of the peaks centered around -0.6 V and 0 V are different. Meaning that if the process was indicative of partial oxidation, where Ge^0 is oxidized to Ge^2 around -0.6 V and Ge^2 is oxidized to Ge^4, the two oxidation peaks should have the same area. It should be noted that Ge ions should not be present in the solution after the

solution was exchanged with the blank solution. The overall increased oxidation may be due to adsorbed Ge ion on the surface that was not previously reduced after -0.5 V was applied but remained on the surface even after rinsing with the blank solution.

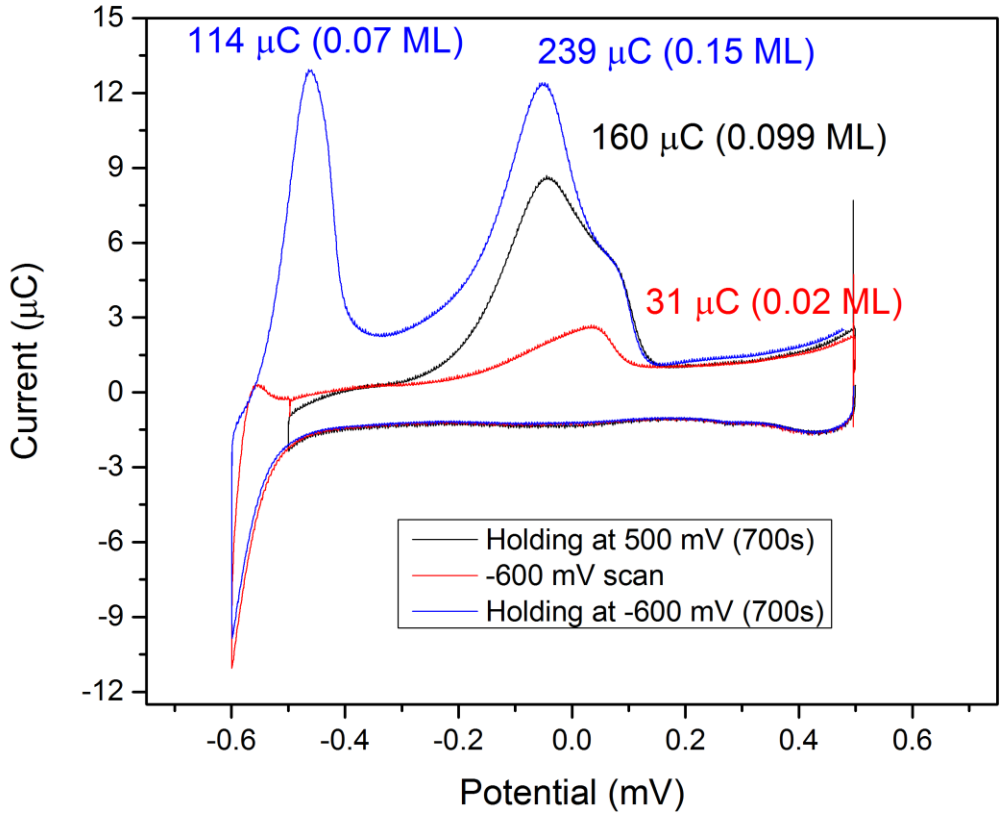

Figure 2.3. CVs of polycrystalline Au in 1 mM GeO_2 in pH 4.5, the cathodic potential limit at -600 mV was applied for varying amounts of time, 0 s for red CV and 700 s for blue CV. Black CV was from a similar experiment to the black CV for 500 s. The amount of deposited Ge quantified by the integrated value of the oxidative peak centered on around 0 V that the deposition plateaus to 0.089 ML around 500 s.

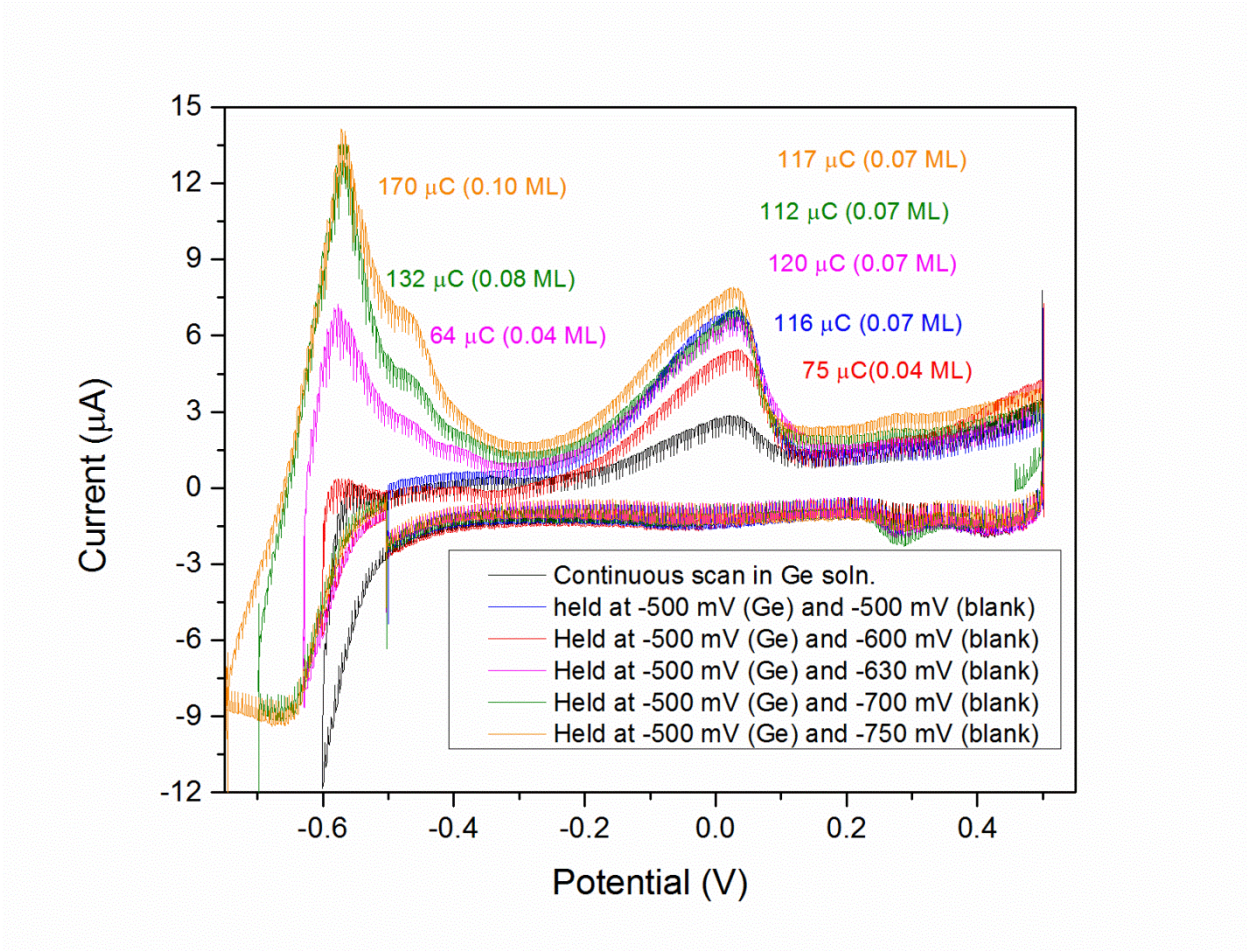

Figure 2.4. CVs of polycrystalline Au in 1 mM GeO_2 in pH 4.5, cathodic potential at -0.5 V was applied for 500 s in Ge solution and at a more negative cathodic potential for 500 s at a blank solution: -0.5 V (blue), -0.6 V (red), -0.63 V (pink), -0.7 V (green), -0.75 V (orange). The solution was rinsed for at least 3 minutes with the blank solution before scanning to a more negative potential. One CV was performed as a standard by continuously scanning in Ge solution from 0.5 V to -0.6 V (black). The oxidation peaks centered around 0 V and -0.6 V increased in their sizes as more negative potential was applied, indicating an increased amount of reduced Ge on the surface.

As shown in Figure 2.5 below, the kinetics of bulk Ge deposition in a plateaued Ge deposit amount was studied by applying -1.4 V on polycrystalline Au in pH 4.5 Ge solution and then holding potential at -0.9 V for various amounts of time. It was hypothesized that holding a negative potential at -0.9 V for a longer time would lead to an increase in Ge coverage that can be observed by the increase in the oxidation peak's area, just as the deposition time was crucial in Figure 2.3 and 2.4 when less cathodic potential was applied. However, the result shown in Figure 2.5 suggested that holding potential at -0.9 V did not change the amount of Ge deposition, oxidation peaks showed that about 3.5 ML thick Ge deposits were formed every time, just like depositing Ge simply by applying -1.4 V. This suggested that when forming multiple MLs of Ge, performing bulk deposition, the deposition process was fast enough that deposition time did not have a noticeable impact. Another possibility is that sub-ML deposition is highly dependent on substrate crystallinity, and bulk Ge deposition is not dependent on the substrate surface. According to reports from Ledina, the lack of further Ge reduction and hydrogen evolution at -0.9 V was critically advantageous when studying the surface using STM using *in situ* STM because it allowed observation of a consistent germanene surface.[20]

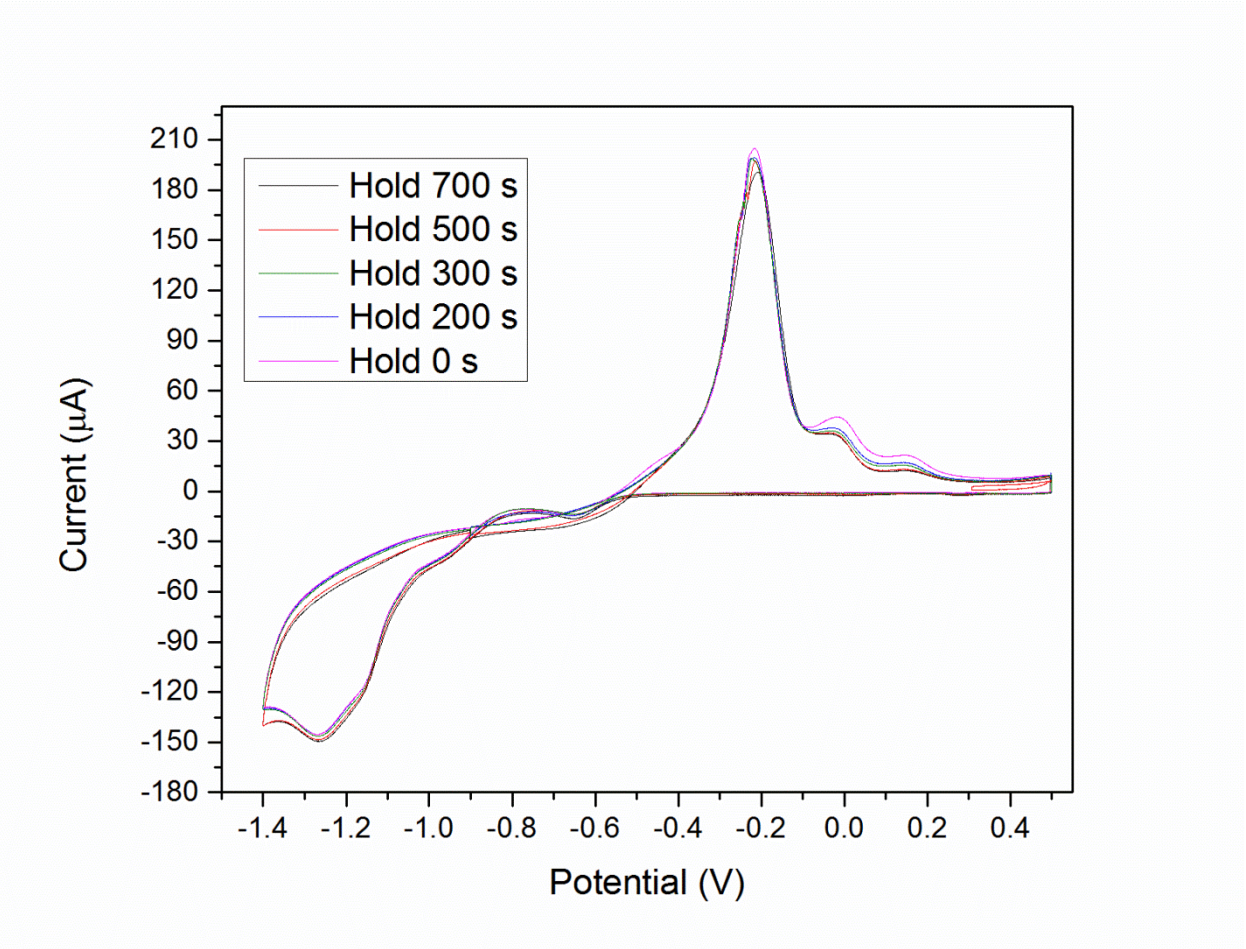

Figure 2.5. CVs of polycrystalline Au in 1 mM GeO_2 in pH 4.5, after reaching cathodic potential limit at -1.4 V, the potential was scanned toward -0.9 V and stopped scanning at -0.9 V for various amounts of time before resuming scan to anodic potential limit at 0.5 V. The entire CV was performed in Ge solution, and in each CV potential was held at -0.9 V for 0 s (pink), 200 s (blue), 300 s (green), 500 s (red), and 700 s (purple). -0.9 V was chosen to avoid excessive hydrogen evolution and stop further Ge reduction or oxidation.

Electrochemical Ge deposition on Cu substrate was studied to examine differences between using Cu and Au, in addition to identifying favorable bulk Ge deposition conditions, evidence of germanene formation was further investigated. The surface of Cu substrates get oxidized when they are exposed to the air, so when the Cu substrate was assembled into the flow cell sulfuric solution was always flown in first under cathodic potential control, typically around -0.1 V, to reduce any existing copper oxide at the surface and protect the Cu surface from oxidation. Cu substrate was never exposed to potentials that may cause oxidation in all experiments unless expressly noted. As seen in Figure 2.6, Ge deposition on a Cu surface behaved similarly to Ge deposition on an Au surface. The 3.5 ML deposition limit was still present and applying more cathodic potential or applying the cathodic potential for a longer time did not increase the amount of Ge deposit. It was noted that when multilayered Ge reduction started around -0.9 V, a little earlier than on Au. The bulk Ge reduction peak also had a shoulder before a sharp diffusion-limited peak. The identity of the shoulder peak was not extensively studied, but it was noted that the shoulder was not present or was difficult to distinguish when the substrate was not cleaned thoroughly. Moreover, applying the B&S method on top of a Ge deposit formed without the shoulder peak seemed to result in a less uniform and thinner deposit. Considering that the sharp change in current is an indication of substrate crystallinity, a sharp current peak indicates that a large amount of reduced species is forming at one type of crystalline surface simultaneously, and cleaning the Cu surface prior to deposition seemed to sharpen the shoulder peak. The shoulder may be the first coherent ML of Ge forming on the Cu surface.

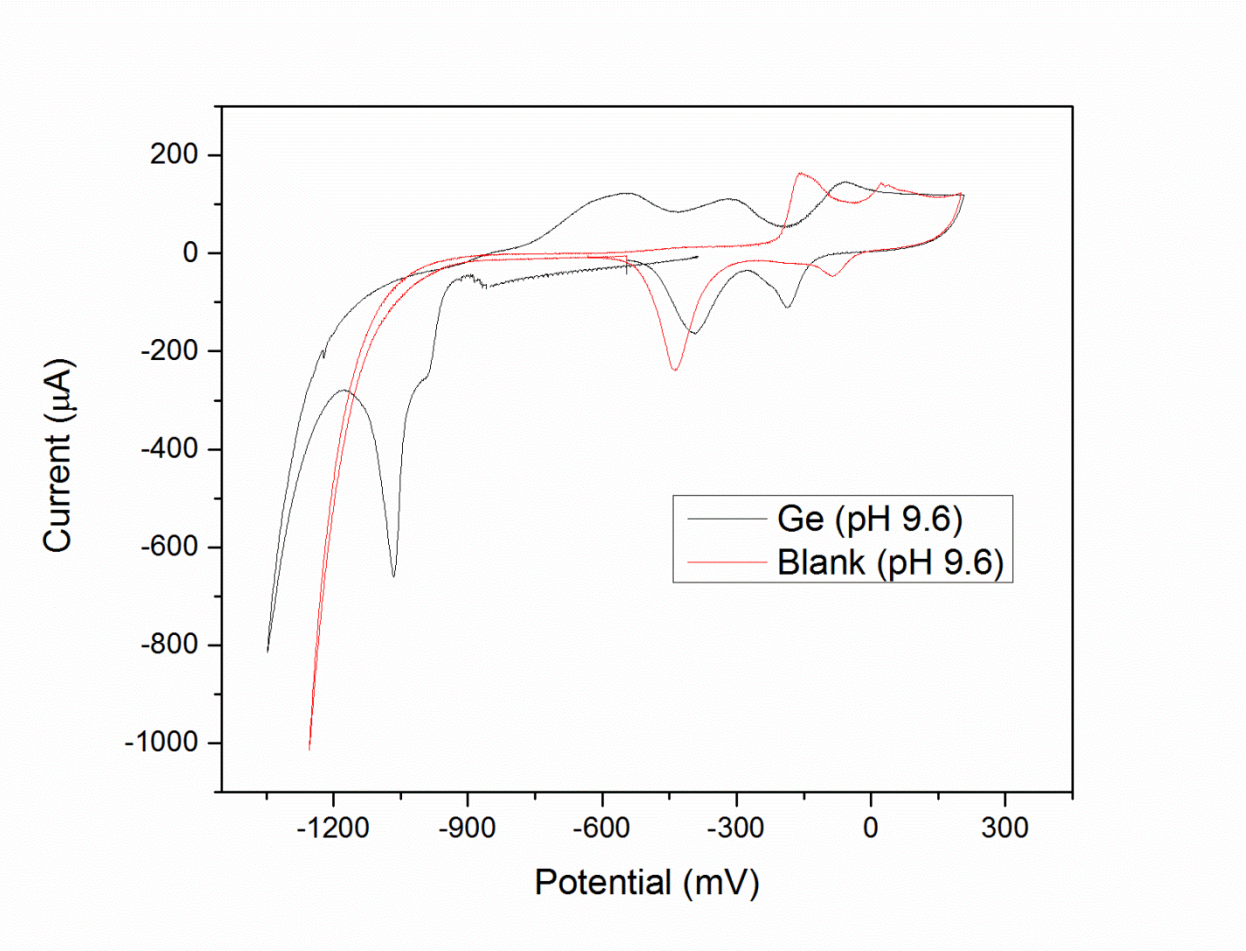

Figure 2.6. CVs of reductive Ge deposition and oxidative stripping on polycrystalline Cu in pH 9.6 1 mM GeO_2 (black) and pH 9.6 blank solution (red). Significant hydrogen evolution occurs around -1 V in the blank solution, and around -1.25 V in the Ge solution. HER seemed to be less favorable to occur in Ge solution since Ge deposited surface required larger overpotential to evolve hydrogen. Also, Cu oxidation is observed around -0.15 V, and the oxidized Cu was reduced around -0.35 V. Ge reduction in Ge solution start to occur around -0.6 V, but the only sub-ML amount of Ge is deposited around that potential. Ge deposition over 1 ML occurs at or more negative than -0.9 V.

Depositing Ge on Cu required additional steps and considerations to protect against oxidation, compared to when depositing on Au, but Cu's higher hydrogen evolution reaction (HER) overpotential was useful when using the B&S method to form thicker Ge deposits. The Ge deposits from B&S method on Cu seemed to be more uniformly and reliably plated compated to on Au. The larger HER overpotential allowed more cathodic potential to deposit Ge and reductively strip Te to one ML. Ge deposition and Te stripping are critical steps in B&S a Ge deposit, and reductive Te stripping is directely benefited by application of more cathodic potential. Therefore, most of the efforts toward studying and optimizing the B&S method involved Cu substrates.

An example of the B&S method is shown in Figure 2.7. The particular program seemed to produce a uniform Ge deposit consistently. Variables to optimize and improve Ge deposition process included, but not limited to, temperature, Ge deposition potential, solution flow speed, blank solution flow time, Te UPD stripping potential, Te UPD stripping time, potential change method (ramp or step), initial Ge deposit, solution pH, and buffer presence. A few important variables that seemed to have improved Ge deposits were increasing volume of blank solution flown in after Te strip to ML to rinse away leftover Te ions and spending a longer time around -1.4 V in Ge solution. It is presumed that residue ions present on the surface may be affecting the quality of deposits every cycle and rinsing away residue by flowing blank and Ge solutions and giving Ge sufficient time to depsoit on a rinsed surface may be improving the quality. The improved B&S cycle showed a linear increase in the amount of deposited Ge and a small presence of Te as shown in Figure 2.8, indicating a successful development of a B&S program and a room for further optimize removal of Te. Minimizing Te presence was one of the key

objectives because it was believed that Te in the Ge deposit could have been disrupting the surface crystalline structure or potentially forbid germanene formation via poor lattice matching. Unfortunately, complete elimination of Te was never achieved. It has been suspected that Te may be alloying or strongly interacting with the Au substrate.

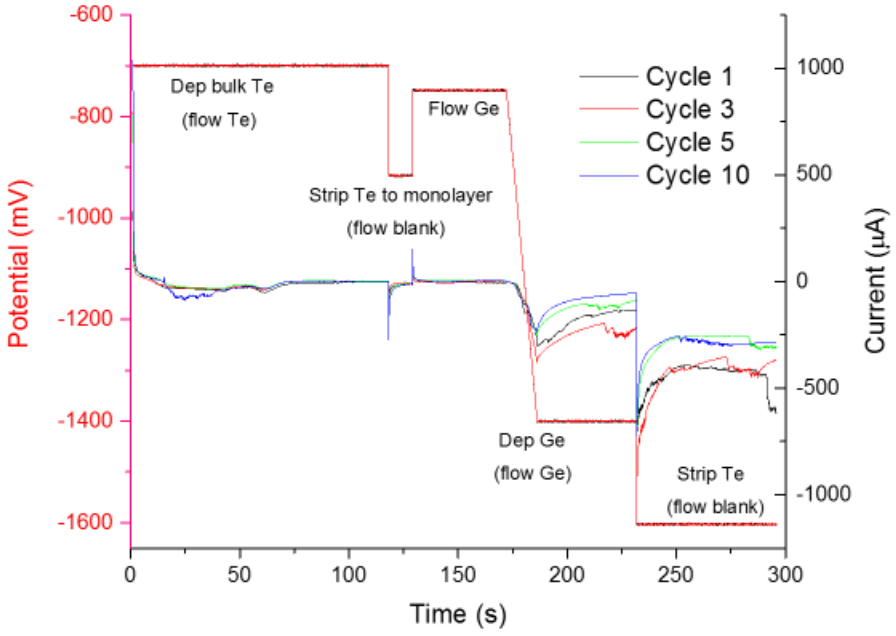

Figure 2.7. An example of a current time trace plot diagram of the Ge B&S deposition process. Red line indicates the applied potential during the program, and the black, red, green, and blue lines are the currents from cycles 1, 3, 5, and 10 respectively. After the initial 3.5 ML Ge was deposited on Au by applying -1.35 V, Te solution was rinsed in at -0.7 V to deposit bulk Te. The Te deposit was then reductively stripped to monolayers by applying -0.9 V while flowing blank solution. Afterward, Ge solution was rinsed in at -0.7 V to avoid any further Te deposition from leftover Te ions. A negative potential

around -1.45 V was then applied to deposit as much Ge as possible. Afterward, in a blank solution, leftover ML Te was reductively stripped off by applying -1.6 V. Hydrogen bubble formation was prominent, and consistent attention to remove hydrogen bubble on the working electrode was necessary.

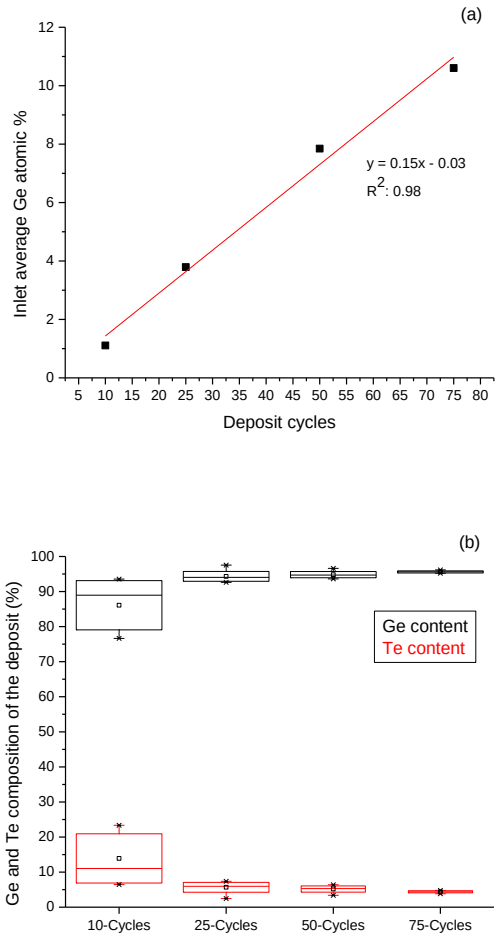

Figure 2.8. A series of EPMA measurements of Ge deposits on Cu from a program described in Figure 2.7 (Figure 2.8a) using 10, 25, 50, and 75 cycles. The amounts of Ge deposition increased linearly from the number of deposit cycles, indicating that the

number of cycles is directly responsible for a thicker Ge deposit. Meanwhile, as Ge deposition was from increased cycles was linearly increasing, Te contents in the deposits were plateaued despite the cycles used to form the deposit (Figure 2.8b). The consistent amount of Te may be due to surface-limited deposition of Te on Au and the leftover Te from last few deposit cycles remained on the surface.

One avenue explored to study and optimize Ge deposition on Cu was to take advantage of Cu's larger HER overpotential and use more acidic solution. Acidic solutions evolve hydrogen at lower overpotential due to increased presence of hydrogen ions in the solution, but it was hoped that Cu's larger HER overpotential could offset the effect. The pH dependence in electrochemical Ge deposition was reported in a previous study from this group.[8] However, as shown in Figure 2.9, the lower overpotential needed for HER from a solution with lower pH was much greater compared to the Cu substrate's larger overpotential for HER. This was further examined in Figure 2.10, but the excessive hydrogen evolution made a close examination of deposition difficult and the lack of Ge oxidation from the CVs indicated that significant Ge deposition did not occur. Perhaps this could have been optimized by adjusting the sulfuric acid and buffer concentration, but the HER-prone conditions and less crystalline surface of Cu made STM studies using the same conditions difficult, and further investigation of Ge deposition on Cu in acidic condition was considered an unfruitful topic for research.

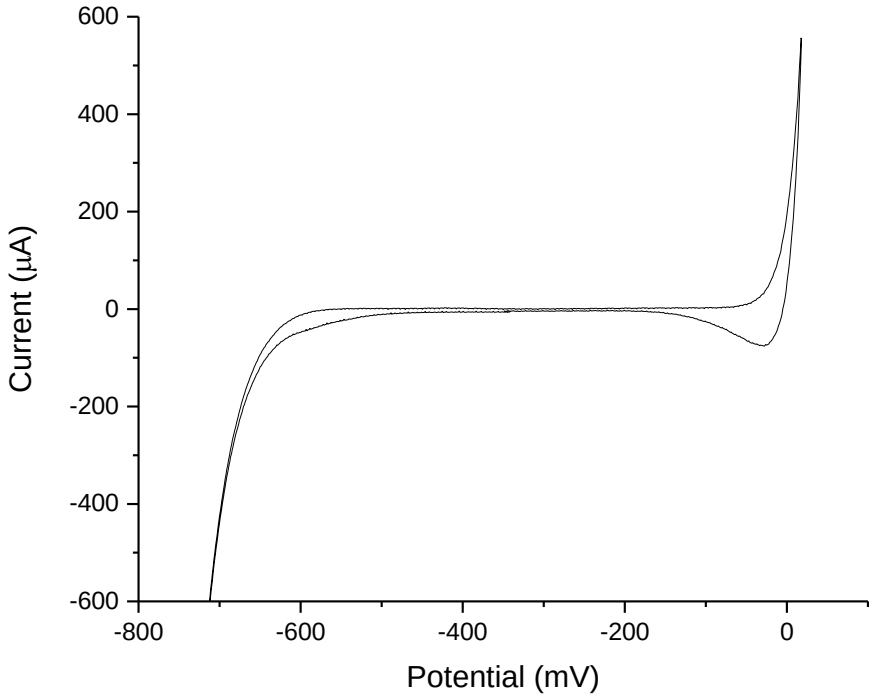

Figure 2.9. A CV of polycrystalline Cu in 0.5 M sulfuric acid. Cu reduction can be seen around -0.05 V. The abrupt increase in oxidation current over 0 V is oxidation of Cu. Unlike Au oxidaiton, oxidized Cu in acid dissolves in the solution, removing the Cu layer to reveal Ti adhesive layer underneath.

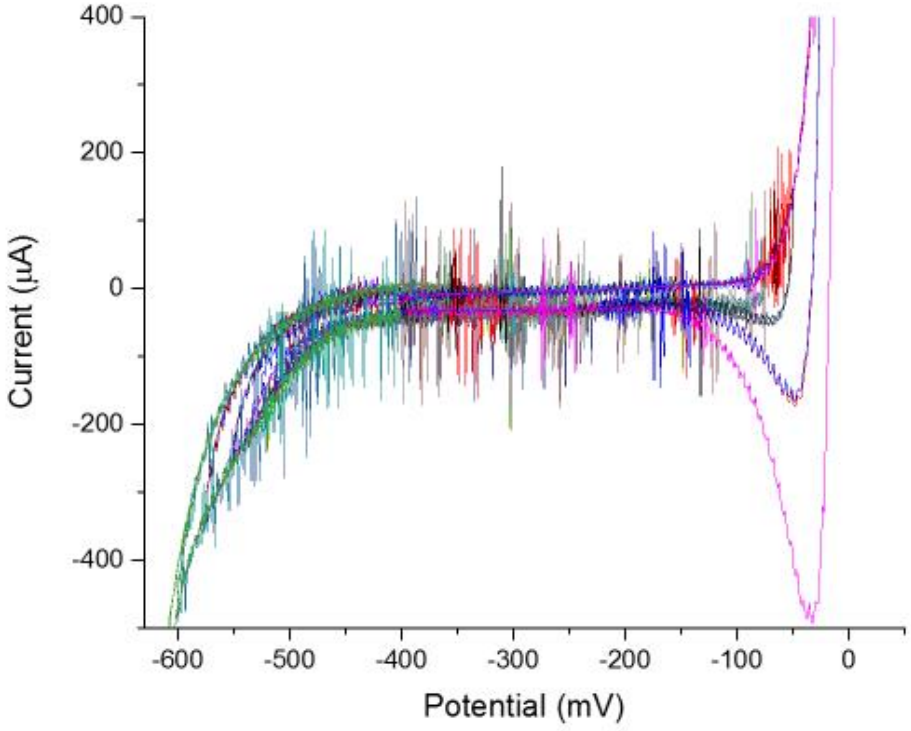

Figure 2.10. A series of CVs of polycrystalline Cu in 0.5 mM GeO_2 dissolved in 0.5 M sulfuric acid. The vertical lines were unwanted noises that originated from excessive hydrogen or oxygen bubble formation. Apart from the artifacts, the CVs show almost no difference from Figure 2.6, indicating little to no Ge deposition on the surface. It is believed that the Ge deposition did not occur because the applied potential before the hydrogen evolution became the dominant reaction was not enough to start the significant Ge reduction.

Another approach to optimize the B&S method was to decrease the number of solutions used from three (blank, Ge, and Te) to one solution containing both Ge and Te. As previously discussed, one of the challenges with the B&S method was that one cycle

could take approximately 5 minutes, and constant supervision was necessary to limit hydrogen bubbles affecting deposition. Bubbles present on the surface of working electrode effectively disconnects the area from the rest of the cell and stop reaction at the spot. Such limitations made it difficult to increase the thickness that a person can deposit in a day. Running the automated deposition program continue overnight without oversight was attempted, but the forementioned hydrogen bubbles formation proved to be problematic and potential control was lost within an hour. It was theorized that using only one solution to deposit both Ge and Te would eliminate the need for solution exchange and reduce necessary steps per cycle, resulting in a shorter time per cycle and enable much thicker deposition. A CV of polycrystalline Au in the Ge and Te solution in Figure 2.11 indicated that the attempt at one solution deposition method may have been ineffective. In this experiment, the initial 3.5 ML worth of Ge was deposited and two potentials, -0.9 V to deposit Te and -1.35 V to deposit Ge and strip Te, were cycled. However, the resulting amount of Ge deposit measured from oxidizing the film did not show any change. It should be noted that the anodic scan does not show any Te peaks, so the applied cathodic potential was sufficient enough to reductively strip Te. The root cause of the ineffective cycle was not clear, but it has been speculated that Ge may not have been sufficiently deposited on Te because the Te was stripped off too early before Ge deposition. This method may not have shown a promising result yet, but this avenue is still believed to be potentiaully effective and further optimization may allow one solution deposition of thick Ge film in an aqueous state in future.

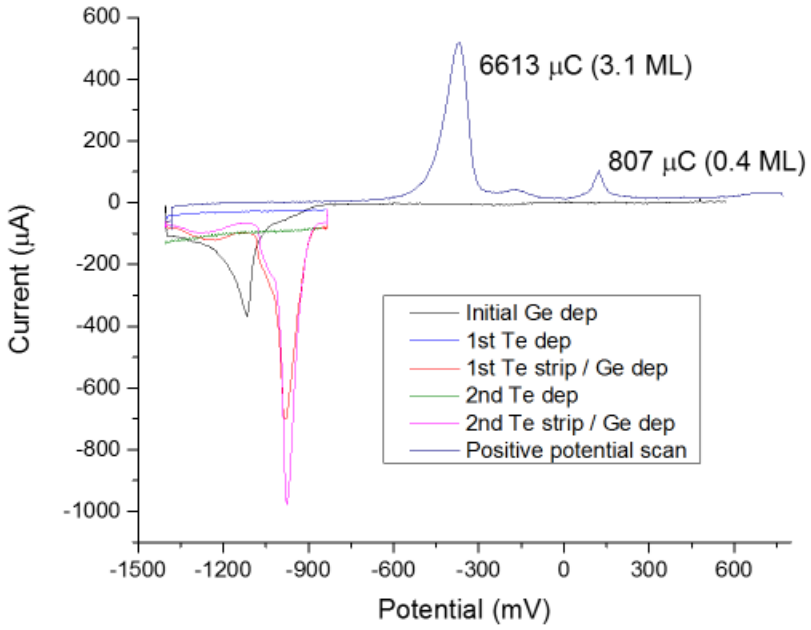

Figure 2.11. CVs of a series of potential sweeps of polycrystalline Au in 0.5 mM Ge, 0.2 mM Te in pH 9 solution. The legend is chronologically ordered. Starting at 0.6 V, the potential was scanned to -1.35 V and held constant at the cathodic limit for 5 mins while the solution was flowing (black). Afterward, it was scanned to -0.9 V (blue) and scanned back to -1.35 V to reductively strip Te while depositing Ge for 5 mins (red). It was then scanned to -0.9 V (green) and back to -1.35 V (pink) again. Lastly, the potential was scanned to 0.6 V in a blank solution to oxidize all deposited films and measure its quantity. The charge from integrating the oxidation peak centered around -0.4 V and 0.15 V, listed next to their respective peaks, suggested little to no additional Ge deposit.

Au substrate was most frequently used to study germanene formation in this report because Au's EC-STM compatibility enabled side-by-side studies with EC-STM

and CV. In addition, Au substrate is compatible with germanene.[26] EC-STM studies of germanene on Au formation in pH 4 has been studied mostly by Ledina,[20] and similar studies in pH 9 has been performed by Bui.[27] The result of the studies are only briefly summarized in this report, detailed descriptions of the EC-STM studies can be found in the cited articles. In pH 4, the first sign of germanene structure was observed when Ge was deposited at -0.4 V, but only in nanoribbon structures. This step is analogous to Figure 2.1, where sub-ML of Ge was deposited for over 700 s. These structures seemed to have been partially imbedded into the Au substrate, but the Au reconstruction was still visible, indicating that the surface crystallinity was not entirely disturbed. The STM images and representation of nanoribbon structures are shown in Figure 2.12, adopted from a previously published report.[20] The small coverage of the surface is in accordance with the CV studies discussed in Figure 2.1.

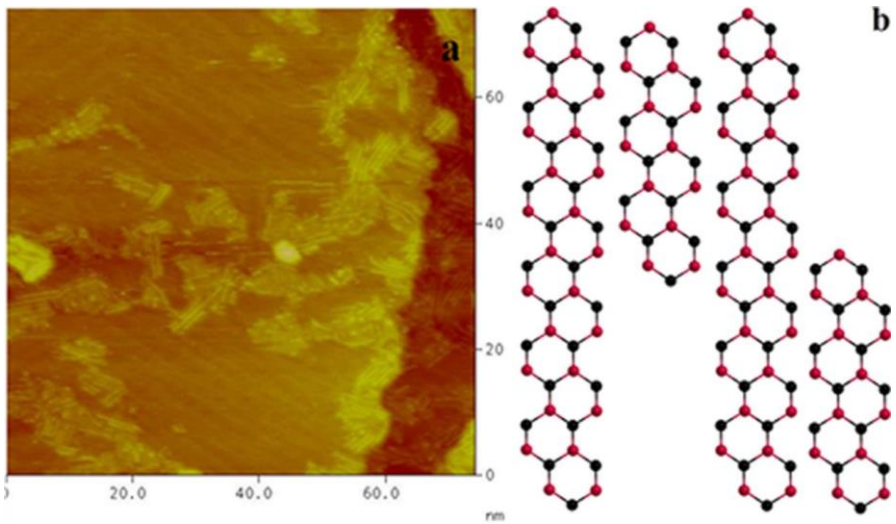

Figure 2.12. This figure was adopted from a previously published report by Ledina *et al.*[20] STM image of Au(111) in a pH 9 Ge solution at -0.4 V (a). The Au herringbone

reconstruction is still visible, but germanene nanoribbon structures are present, suggesting that the amount of Ge deposit may not be high enough to disrupt the surface crystallinity. A drawing of a proposed nanoribbon structure is presented in (b).

When more negative potential around -1.4 V was applied, the bulk Ge film covered the entire surface, as shown in Figure 2.13. Moreover, the atomic resolution images of the surface revealed that the deposit exhibited hexagonal structures with the same physical dimensions as germanene.[20] The image of the germanene structure was obtained from the top layer of the 3.5 ML of Ge deposit, suggesting that the structure is not due to Ge-Au alloy. Close examination of the STM images in Figure 2.13 e and f showed that pristine germanene structures were only apparent in small domains. The crystalline germanene domains were surrounded by defective germanene structures, typically 5 or 7 membered rings. The defective germanene formation surrounding small domains was a persistent observation in all electrochemically deposition of germanene. As shown in Figure 2.14, the defective rings and small domain sizes were also found in germanene formed in pH 9. Unlike the STM experiments performed in pH 4, the experiments in pH 9 focused on obtaining images from the first ML germanene. Nonetheless, small domains of germanene structures on the surface of Au(111) surrounded by defecting germanene structures surrounding them were reproducibly observed in pH 9. The defective structures are presumably due to the nature of nucleation and growth in an electrochemical deposition.[28] It is believed that domains of germanene

form simultaneously and grow laterally, and defective germanene structures form when adjacent domains with different lattice direction meet.

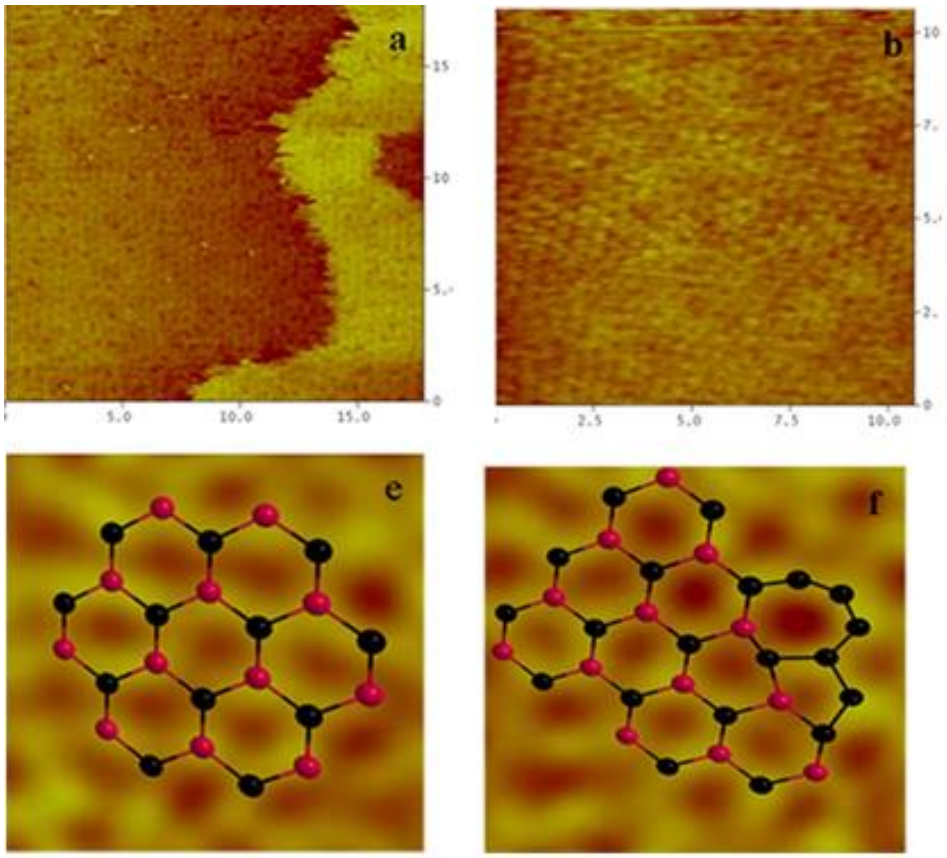

Figure 2.13. This figure was adopted from a previously published report by Ledina *et al.*[20] STM images of Au(111) in a pH 4 Ge solution. -1.4 V was applied to deposit Ge before scanning back to -0.9 V to observe the deposit without any further reaction (a, b). Superimposed image of germanene drawing, including 5 and 7 membered ring structures are present on a STM image after FFT filter was applied (e,f).

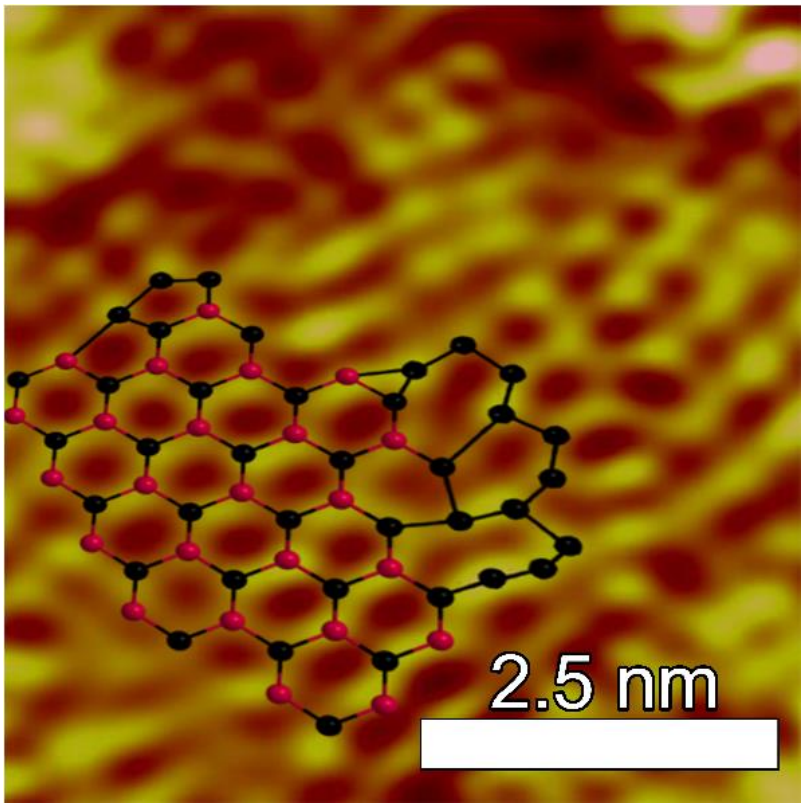

Figure 2.14. This figure was adopted from a previously published report by Bui *et al.*[27] A STM image of Au(111) in a pH 9 Ge solution. -1 V was applied to deposit Ge and probed to obtain the image, the image was then FFT filtered. Superimposed drawing of germanene, including 3, 5, 7, and 8 membered ring structures are surrounding a germanene domain, was added to illustrate the germanene domains.

Despite the EC-STM evidence of germanene formation seen in Figure 2.12, 2.13, and 2.14, spectroscopic evidence of germanene formation could not have been reproduced when using micro-Raman spectrometer on a flat sample surface. All Raman

spectra of electrochemically deposited Ge films on polycrystalline Cu and Au substrates, formed either by applying a negative potential or using the B&S method, only exhibited amorphous Ge signals as shown in blue spectrum in Figure 2.15. Even in conditions used in Figured 2.14 where germanene structures were visible. This may have been due to the aforementioned limited sensitivity of the Raman spectrometer. Also, it was impossible to guarantee that the germanene deposit remained pristine when exposed to air.

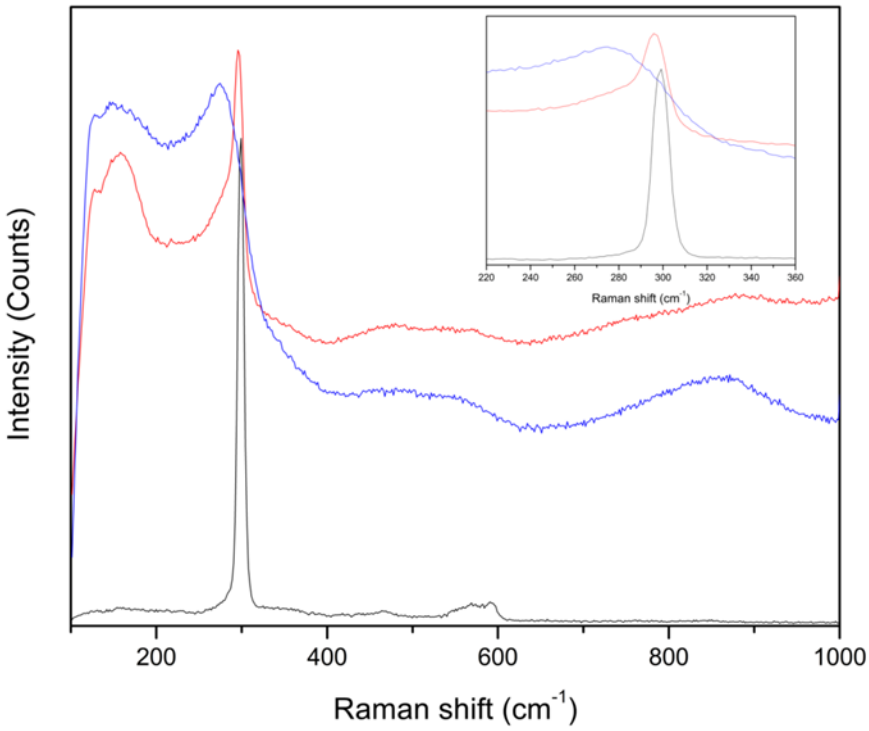

Figure 2.15. These three Raman spectra including crystalline Ge (black), amorphous Ge (blue), and germanene (red) have been adopted from a previously published report by Ledina *et al.*[20] The characteristic sharp symmetric peak centered at 300 cm^{-1} in the black spectrum is from sp^3 crystalline Ge. The broad peak centered around 270 cm^{-1} in the blue

spectrum is from amorphous Ge. The sharp symmetric peak centered at 296 cm^{-1} in the red spectrum is from germanene.

2.5 CONCLUSION

Close examination of electrochemical sub-ML Ge deposition on Au and Cu revealed a slow rate of deposition and surface limited amount of Ge on Au. The sub-ML deposition was further studied using EC-STM, revealing Ge-Au surface alloy formation and lines of germanene structure on the surface. B&S method program was modified by increasing volume of blank solution flown after Te strip and applying longer cathodic application time in Ge solution to deposit Ge. The newly formed Ge film showed a linear increase in Ge amount per cycle, and low Te content in the film, but Te content was never eliminated. Using Cu substrate for Ge deposition was investigated, Cu substrate in Ge acidic solution may have been not feasible, but the B&S method seemed more compatible with the Cu substrate. Micro-Raman spectroscopy on all samples did not have any evidence of germanene, despite evidence of germanene formation from EC-STM. Suggesting that either germanene on the surface is disrupted when exposed to air or the Raman spectroscopy has too poor sensitivity to measure a 3.5 ML thick material.

2.6 ACKNOWLEDGEMENT

Support from the National Science Foundation, DMR #1410109, is gratefully acknowledged.

REFERENCES

1. Bardeen, J.; Brattain, W. H., The Transistor, A Semi-Conductor Triode. *Physical Review* **1948,** *74* (2), 230-231.

2. Kamata, Y., High-k/Ge MOSFETs for future nanoelectronics. *Materials Today* **2008,** *11* (1), 30-38.

3. Nalwa, H. S., Handbook of thin film materials. In *Handbook of Thin Films*, Academic Press: Burlington, 2002; pp xxiii-xxvi.

4. Wilk, G. D.; Wallace, R. M.; Anthony, J. M., High-κ gate dielectrics: Current status and materials properties considerations. *Journal of Applied Physics* **2001,** *89* (10), 5243-5275.

5. Houssa, M., *High k Gate Dielectrics*. CRC Press: Boca Raton, 2003.

6. Szekely, G., Electrodeposition of Germanium. *Journal of The Electrochemical Society* **1951,** *98* (8), 318-324.

7. Endres, F., Electrodeposition of a thin germanium film on gold from a room temperature ionic liquid. *Physical Chemistry Chemical Physics* **2001,** *3* (15), 3165-3174.

8. Liang, X.; Kim, Y.-G.; Gebergziabiher, D. K.; Stickney, J. L., Aqueous Electrodeposition of Ge Monolayers. *Langmuir* **2010,** *26* (4), 2877-2884.

9. Endres, F.; Zein El Abedin, S., Nanoscale electrodeposition of germanium on Au(111) from an ionic liquid: an in situ STM study of phase formation Part I. Ge from GeBr4. *Physical Chemistry Chemical Physics* **2002,** *4* (9), 1640-1648.

10. Fahrenkrug, E.; Gu, J.; Jeon, S.; Veneman, P. A.; Goldman, R. S.; Maldonado, S., Room-Temperature Epitaxial Electrodeposition of Single-Crystalline Germanium

Nanowires at the Wafer Scale from an Aqueous Solution. *Nano Letters* **2014,** *14* (2), 847-852.

11. Martineau, F.; Namur, K.; Mallet, J.; Delavoie, F.; Endres, F.; Troyon, M.; Molinari, M., Electrodeposition at room temperature of amorphous silicon and germanium nanowires in ionic liquid. *IOP Conference Series: Materials Science and Engineering* **2009,** *6* (1), 012012.

12. Endres, F.; El Abedin, S. Z., Electrodeposition of stable and narrowly dispersed germanium nanoclusters from an ionic liquid. *Chemical Communications* **2002,** (8), 892-893.

13. Liang, X.; Zhang, Q.; Lay, M. D.; Stickney, J. L., Growth of Ge Nanofilms Using Electrochemical Atomic Layer Deposition, with a "Bait and Switch" Surface-Limited Reaction. *Journal of the American Chemical Society* **2011,** *133* (21), 8199-8204.

14. Liang, X.; Jayaraju, N.; Thambidurai, C.; Zhang, Q.; Stickney, J. L., Controlled Electrochemical Formation of GexSbyTez using Atomic Layer Deposition (ALD). *Chemistry of Materials* **2011,** *23* (7), 1742-1752.

15. Al-Salman, R.; Mallet, J.; Molinari, M.; Fricoteaux, P.; Martineau, F.; Troyon, M.; El Abedin, S. Z.; Endres, F., Template assisted electrodeposition of germanium and silicon nanowires in an ionic liquid. *Physical Chemistry Chemical Physics* **2008,** *10* (41), 6233-6237.

16. Electrochemical lithiation of thin silicon based layers potentiostatically deposited from ionic liquid. *Electrochimica Acta* **2015,** *168*, 403.

17. Carim, A. I.; Collins, S. M.; Foley, J. M.; Maldonado, S., Benchtop Electrochemical Liquid–Liquid–Solid Growth of Nanostructured Crystalline Germanium. *Journal of the American Chemical Society* **2011,** *133* (34), 13292-13295.

18. Mahenderkar, N. K.; Liu, Y.-C.; Koza, J. A.; Switzer, J. A., Electrodeposited Germanium Nanowires. *ACS Nano* **2014,** *8* (9), 9524-9530.

19. Ledina, M.; Liang, X.; Kim, Y.-G.; Jung, J.; Perdue, B.; Tsang, C.; Soriaga, M.; Stickney, J. L., (Invited) Investigations into the Formation of Germanene Using Electrochemical Atomic Layer Deposition (E-ALD). *ECS Transactions* **2015,** *66* (6), 129-140.

20. Ledina, M. A.; Bui, N.; Liang, X.; Kim, Y.-G.; Jung, J.; Perdue, B.; Tsang, C.; Drnec, J.; Carlà, F.; Soriaga, M. P.; Reber, T. J.; Stickney, J. L., Electrochemical Formation of Germanene: pH 4.5. *Journal of The Electrochemical Society* **2017,** *164* (7), D469-D477.

21. Schlecht, S.; Yosef, M.; Fröba, M., Synthesis and Raman Spectroscopy of Nanoparticles of Crystalline and X-ray Amorphous Germanium within Mesoporous SiO2. *Zeitschrift für anorganische und allgemeine Chemie* **2004,** *630* (6), 864-868.

22. Tsai, H.-S.; Chen, Y.-Z.; Medina, H.; Su, T.-Y.; Chou, T.-S.; Chen, Y.-H.; Chueh, Y.-L.; Liang, J.-H., Direct formation of large-scale multi-layered germanene on Si substrate. *Physical Chemistry Chemical Physics* **2015,** *17* (33), 21389-21393.

23. Zhuang, J.; Gao, N.; Li, Z.; Xu, X.; Wang, J.; Zhao, J.; Dou, S. X.; Du, Y., Cooperative Electron–Phonon Coupling and Buckled Structure in Germanene on Au(111). *ACS Nano* **2017**.

24. Flowers Jr, B. H.; Wade, T. L.; Garvey, J. W.; Lay, M.; Happek, U.; Stickney, J. L., Atomic layer epitaxy of CdTe using an automated electrochemical thin-layer flow deposition reactor. *Journal of Electroanalytical Chemistry* **2002,** *524–525*, 273-285.

25. Christensen, A.; Ruban, A.; Stoltze, P.; Jacobsen, K. W.; Skriver, H. L.; Nørskov, J. K.; Besenbacher, F., Phase diagrams for surface alloys. *Physical Review B (Condensed Matter and Materials Physics)* **1997,** *56* (10), 5822-5834.

26. Wang, Y.; Li, J.; Xiong, J.; Pan, Y.; Ye, M.; Guo, Y.; Zhang, H.; Quhe, R.; Lu, J., Does the Dirac cone of germanene exist on metal substrates? *Physical Chemistry Chemical Physics* **2016,** *18* (28), 19451-19456.

27. Bui, N. N.; Ledina, M.; Reber, T. J.; Jung, J.; Stickney, J. L., An Electrochemical Scanning Tunneling Microscopic Study of the Potential Dependence of Germanene Growth on Au(111) at pH 9.0. *ACS Nano* **2017**.

28. Venables, J. A.; Spiller, G. D. T., Nucleation and Growth of Thin Films. In *Surface Mobilities on Solid Materials: Fundamental Concepts and Applications*, Binh, V. T., Ed. Springer US: Boston, MA, 1983; pp 341-404.

CHAPTER 3

IN SITU SURFACE ENHANCED RAMAN SPECTROSCOPIC STUDIES OF ELECTROCHEMICALLY FORMED GERMANENE[1]

[1]Jung, J.; Bui, N. N.; Shen, S.; Reber, T. J.; Brezner, J. M.; Mubeen, S.; Stickney, J. L., In Situ Surface-Enhanced Raman Spectroscopic Studies of Electrochemically Formed Germanene. *The Journal of Physical Chemistry C* **2018,** *122* (27), 15696-15705.3.1. Reprinted here with permission of publisher.

3.1 ABSTRACT

Germanene is a 2D allotrope of germanium atoms arranged in a honeycomb structure with Dirac fermion characteristics analogous to graphene and silicene. Formation of germanene is a recent advance, based on evaporation of Ge in a UHV environment. An alternative method, developed by the authors, is its electrochemical growth from aqueous solutions. Initial studies were performed on Au(111) substrates in aqueous solutions of H_2GeO_3 using *in situ* STM, voltammetry, SXRD, and coulometry. Those results indicated that electrochemically formed germanene domains were formed and covered the surface, though the coherence lengths were short due to the presence of domain walls composed of five and seven membered defect rings. The present study has made use of an *operando* spectroelectrochemical flow cell with a Raman microscope to follow the growth of germanene. Deposits were formed on a SERS active Au substrate. Initial spectra did not indicate the presences of germanene. However, repeated exposure to the 780 nm laser resulted in development of a sharp 296 cm^{-1} peak from a couple layers of germanene. Laser exposure appeared to improve the crystallinity of the electrodeposited germanene, enabling reproducible spectroscopic characterization. It is proposed that the laser resulted in localized annealing and self-healing of defects in the germanene layers, due to interaction with SP of the Au nano-morphology and germanene creating larger coherent Raman active germanene domains.

3.2 INTRODUCTION

Interest in graphene has stimulated studies of other two-dimensional (2D) group 14 allotropes, such as silicene,[1,2] stanene,[3,4] germanane (hydrogenated germanene),[5] and

germanene.[6,7,8] Germanene, as shown in Figure 3.1, has a near-planar Ge honeycomb (HC) structure with low-buckling, 0.07 nm, and a Ge-Ge distance near 0.24 nm, resulting in a ring to ring distance of 0.41 nm.[6,9] Germanene does not appear to be naturally occurring, though is stable under reducing conditions.[10,11] Theoretical calculations have proposed that germanene should exhibit similar electronic and optical characteristics to graphene, including quantum spin Hall effects,[12] massless Dirac fermions,[13,14,15] and tunable bandgap,[16,17,18,19] making it an attractive material for future device applications and material science research.

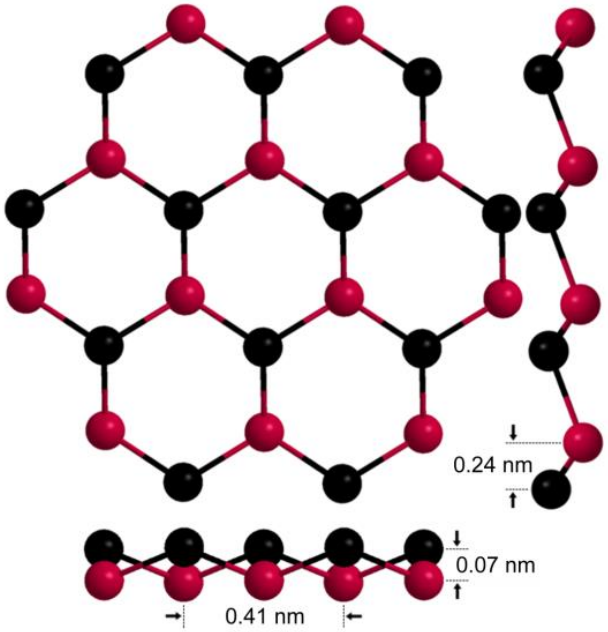

Figure 3.1. A top and side view of a sheet of germanene, the buckling distance is 0.07 nm, the bond length between Ge atoms is 0.24 nm, and the resulting ring to ring distance is 0.41 nm.

Recent experimental evidences for germanene formation have been reported. Those reports generally describe its formation in ultra-high vacuum (UHV) using techniques such

as chemical vapor deposition, and molecular beam epitaxy, together with high temperature annealing. Germanene formation in UHV has been reported on a variety of substrates including Au,[20] Pt,[21] Ag,[22] Al,[9] Si,[23] Graphite,[24] and MoS_2.[25] One paper suggest that high temperature annealing of the substrate may not be necessary for the formation of germanene in vacuum.[26]

However, germanene formation is not limited to UHV or gas phase growth, as the authors have described germanene formation electrochemically from aqueous solutions.[27,28,29] Ge electrodeposition has been previously studied, mostly in nonaqueous media to avoid hydrogen evolution.[30,31,32,33,34] One reported mechanism suggested that electrochemical deposition of Ge occurred by sequential reduction of Ge^{+4} to Ge^{+2} and then Ge^{+2} to Ge^{0}.[35] A previous report of direct Ge electrochemical deposition on Au in pH 9.0 by the authors indicated that Ge deposition was self-limited to approximately 3.5 monolayers (ML), assuming a four electron process and one ML being one deposited Ge atom for every surface Au atom.[32] The authors previously reported a method to electrochemically deposit thicker Ge film using a form of electrochemical atomic layer deposition,[36,37] where micro-Raman studies showed a broad Ge peak around 270 cm^{-1}, attributed to amorphous Ge.[38] However, a few spots on one sample displayed a distinct peak around 296 cm^{-1}, [27,28] a peak shift similar to germanene's theoretical in-plane vibration.[39] The same peak was also observed in UHV deposits of germanene on Au and Si. [23,40] In recent *in situ* scanning tunneling microscope (STM) studies by the authors, images of Ge electrodeposits exhibited arrays of six membered rings in a HC structure (Figure 3.1).[27,28,29] Reproducibility of the in-plane vibration peak from electrochemically formed germanene has been somewhat elusive. When the in-plane bonding of germanene

was first investigated using Raman spectroscopy, no fingerprint Raman peak was reproducibly observed. Raman spectroscopy is routinely used as a tool for rapid structural characterization of 2D materials.[41] Failure to capture Raman spectra from electrodeposited germanene may be a result of any of a number of issues.

To start with, the deposits were very limited in thickness and the spectrometer lacked high sensitivity. Another problem was the small coherent domains of the HC structure, observed with STM.[27,28,29] Coherent regions were broken up by the presences of five and seven membered defect rings, which created domain walls and result in small rotations of the lattice, with loss of structure coherence. Early Raman studies by the authors of Ge deposits were post deposition, where the samples were transferred through air to the spectrometer. The transfer from solution resulted in loss of potential control and exposure to oxygen. Problems with oxygen were not unexpected; silicene, an analogous Si based 2D Dirac material, was found to be chemically active and underwent rapid oxidation when exposed to O_2.[42,43,44] However, trends in standard redox potentials for Ge vs. Si suggest germanene should be more stable.

To address the above challenges, an *in situ operando* Raman spectroelectrochemical flow cell was used with a surface enhanced Raman spectroscopy (SERS) active substrate. The combination enabled real-time Raman analysis during the electrochemical deposition of single and multilayer Ge films by maintaining potential control during both formation and while acquiring spectra. In addition to the enhanced sensitivity, provided by the SERS active surface, surface plasmons (SPs) on the substrate may also have been critical to the appearance of the observed Raman features. SPs are collective conduction electron excitations that can be photo-induced in nanostructured

metals and other organic and inorganic conductors. SPs decay initially in tens to hundreds of femtoseconds, creating very energetic (hot) electrons and ultimately heat, over a time scales of a few picoseconds through various electron-electron and electron-phonon interaction pathways.[45] Such SP decay can result in large local temperature increases (>500 °C) in sub-micron sized hotspots. For example, plasmon-to-heat processes have been exploited for photothermal therapy,[46] to drive energetic chemical reactions,[47] and for the growth and patterning of nanostructures.[48] In this work, upon excitation with 780 nm excitation (resonant excitation, i.e., localized SP resonance of the underlying SERS substrate being matched with the laser excitation wavelength) a distinctive 296 cm^{-1} G-like Raman peak for germanene was observed. No Raman peaks were observed for as-synthesized germanene films with 532nm excitation (off-resonance condition). Remarkably, Raman peaks for germanene were observed from 532 nm excitation on samples previously illuminated with the 780 nm laser. A simple model suggested that the high electromagnetic field enhancement at the nanostructured Au surface during resonant excitation gives rise to strong photothermal effects, which may play a crucial role in the crystallization and structural transformation process of the 2D germanene films.

3.3 EXPERIMENTAL

Electrochemical experiments were performed using an automated electrochemical flow cell system (Electrochemical ALD L.C., Athens, GA).[49] The working electrode (substrate) was a 100 nm thick polycrystalline Au films vapor deposited on a 5 nm thick Ti film on glass. The reference electrode was Ag/AgCl (3 M NaCl, BASI, West Lafayette,

IN), and all potentials were reported with respect to it. The substrate was cycled in 0.1 M H_2SO_4 from -0.2 V to 1.45 V before each experiment.

Spectroelectrochemical experiments were performed using a Raman spectroelectrochemical flow cell (Electrochemical ALD L.C., Athens, GA).[49] Design of the new flow cell was similar to that described previously, but fitted with a quartz front window, and designed to fit in place of a microscope slide within the spectrometer (Figure 3.2).[36,49] The Ag/AgCl (3 M NaCl, BASI, West Lafayette, IN) reference electrode was placed up stream in a separate compartment. The Au SERS active working electrode was constructed on a polycrystalline Au film closely following the Bartlett et al. methodology, vapor deposited on a Ti adhesion layer, on glass. A layer of 600 nm diameter polystyrene spheres was then adsorbed on the surface, and Au was electrodeposited to partially cover the beads. Finally, the spheres were dissolved away using tetrahydrofuran, leaving a hexagonal array of 600 nm diameter hemispherical Au pits, which served as the SERS active substrate (Figure 3.3).[50,51] The thickness of the structured Au surface was approximately 360 nm.[52] Extinction spectra obtained on equivalent shallow Au pits in previous studies showed a strong plasmon resonance peak at 660 nm in solution and would be expected to red shift upon germanene deposition,[52] due to an increase in the dielectric constant.[53,54] Raman spectra were obtained using a DXR Raman microscope, controlled by OMNIC software (Thermo Scientific, Waltham, MA), and continuous wave 780 nm and 532 nm laser sources in a backscatter geometry mode. A 10x objective lens with a numerical aperture (NA) of 0.25 was used to focus the laser. The illuminated laser beam for the above NA had a focal diameter of 3.1 μm and power density of 1.06 $\frac{\mathrm{mW}}{\mu\mathrm{m}^2}$ (Table 3.1). The Raman spectrometer was calibrated daily using the calibration program in the

OMNIC software. Multiple neon emission lines were used to correct dispersion, into the grating, and correct laser wavelength. A pink light source was used to correct the relative band intensities, and a polystyrene sample was used to correct the Raman shift, in wavenumber. All Raman measurements were carried out under degassed aqueous environment.

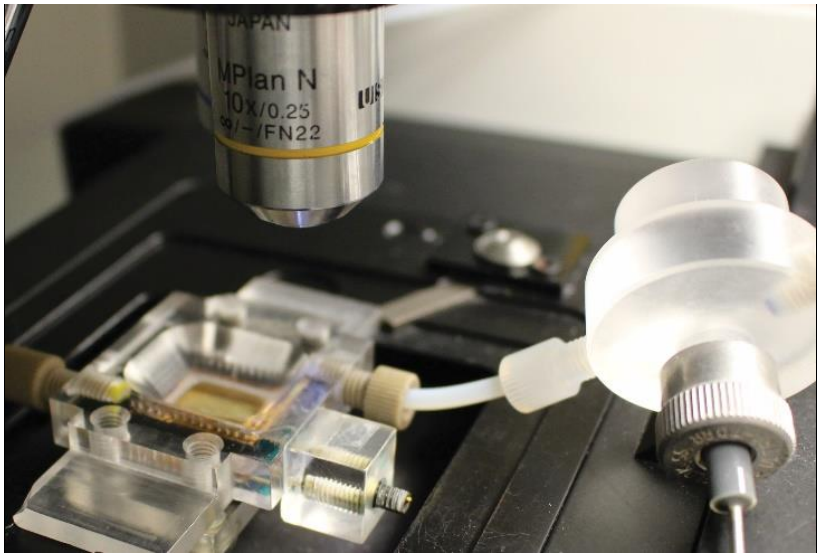

Figure 3.2. The spectroelctrochemical flow cell paced in a mirco-Raman spectrometer, the reference electrode compartment is placed on the inlet of the solution. The Au auxiliary electrode surrounds the quartz window, and gasket seals the solution from the environment. Reference electrode compartment is place at inlet of the solution.

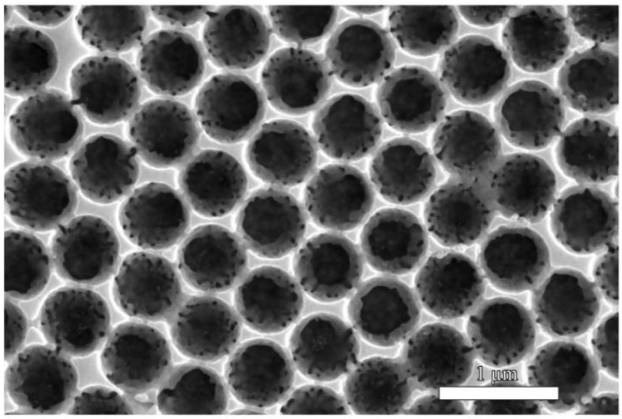

Figure 3.3. Secondary electron image of the SERS active Au surface obtained using SEM. Hemispherical structures with diameter of around 600 nm formed close packed structure. Brightness indicates height.

Table 3.1. Parameters involved in the two Raman excitation lasers and the corresponding Au reflectance and germanene absorption. The presented numbers are approximation assuming a monolayer of germanene and flat Au surface.

Maximum photon power output	532 nm laser 10 mW	780 nm laser 8 mW
Focal waist (µm)	2.1	3.1
Laser power density ($\frac{W}{cm^2}$)	2.89 x 10^5	1.06 x 10^5
Germanene absorbance[55]	0.052	0.062
Au reflectance[56]	0.70	0.97
Resulting total germanene absorbance	0.086	0.11
Resulting power absorption ($\frac{W}{cm^2}$)	2.48 x 10^4	1.17 x 10^4

All solutions were prepared using 18 MΩ ultrapure water from a Millipore-Q system (Barnstead, Dubuque, IA). GeO_2 and blank solutions were buffered to pH 9.0 using 50 mM $Na_2B_2O_4$ (Baker analyzed, 99.5%) and contained 0.1M perchlorate as a supporting electrolyte. The solutions were degassed for at least 2 hours with N_2 before experiments.SEM image was obtained using FEI Teneo (FEI Co., Hillsboro, OR) using Everhart-Thornley detector and secondary electron mode. The SEM was operated under high vacuum, 20 kV primary beam energy, working distance of 11 mm, and dwell time of 10 µm. The sample was rinsed with water prior to the measurement.

Simulation of temperature increase at the Au surface based on laser power was performed using SolidWorks (Dassault Systèmes, Waltham, MA). Parameters from the 780 nm laser in Table 3.1 were used. The thickness of Au was approximated to 200 nm and known thermal properties of Au were used.[57] The Au surface was submerged in water, 0.8 µl, flowing at of 1.7 $\frac{\text{ml}}{\text{min}}$.

3.4 RESULTS AND DISCUSSION

The cyclic voltammograms in Figure 3.4 were measured in a modified window opening experiment, with a polycrystalline Au substrate in pH 9.0 germanium oxide (GeO_2) solution. Each cycle was started at 0.5 V, and scanned to increasingly negative potential limits each time. The modification consisted of holding the potential constant for 5 minutes at the negative potential limit, to ensure complete deposition, as previous studies by this group have shown very slow kinetics for germanene deposition.[27,28,29] Significant Ge deposition began negative of -0.8 V, with reduction peaks at -0.9 V, -1.0 V and -1.1 V. Potentials negative of -1.4 V resulted in extensive current due to the

hydrogen evolution reaction (HER). In the subsequent positive (anodic) scans, oxidation began near -0.9 V, with peaks near -0.8 V, -0.3 V and -0.1 V. Previous *in situ* STM studies, in pH 9.0 solution, suggested the first layer of germanene could be completed by holding at -0.9 V, while reduction at more negative potentials resulted in formation of multilayer germanene deposits.[29] The total charge for oxidation, obtained by integration of the current time transient during the positive scan, after Ge deposition at -1.4 V, suggest a coverage of 3.5 MLs of Ge, based on four electrons per Ge atom, in agreement with previous reports.[32]

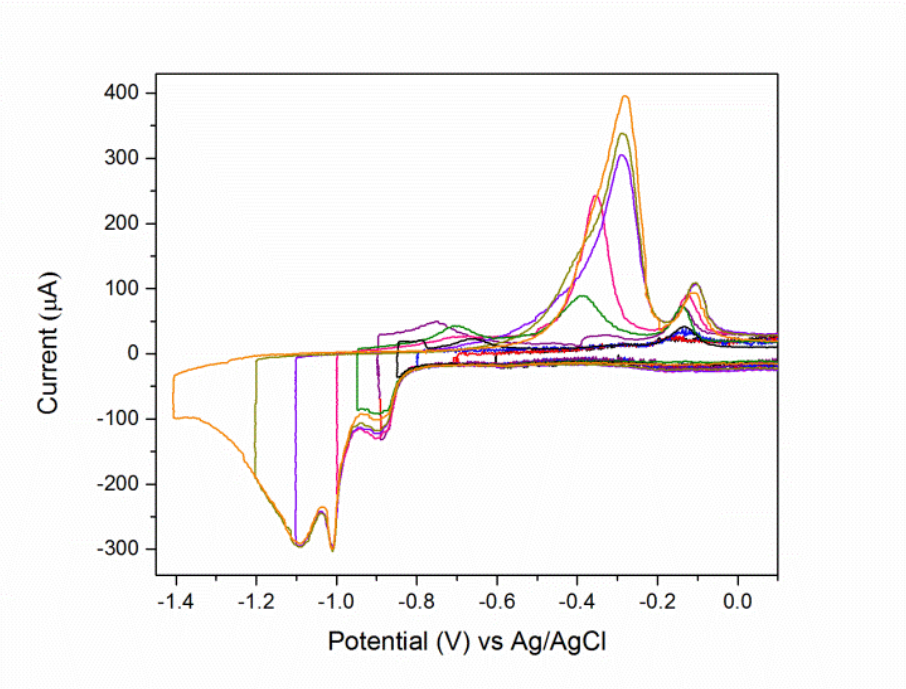

Figure 3.4. Window opening cyclic voltammograms of GeO_2 (0.1 mM GeO_2, 50 mM $Na_2B_2O_4$, pH 9.0) solution on a polycrystalline Au substrate from anodic limit at 0.5 V and various cathodic potential limit from -0.8 V to -1.4 V, cathodic potential was held constant

for 300 s at the cathodic potential limit before anodic scan. The scan rate was 10 mV/s and the area of the working electrode was 2 cm^2.

The electrochemically formed germanene deposits appeared susceptible to degradation under open circuit (OC) conditions (without potential control), which was monitored by measuring OC potential as a function of time Figure 3.5 displays the OC potential shift of germanene layers formed by first scanning to -1.35 V and holding for 5 minutes in the pH 9.0 GeO_2 solution. The solution was then exchanged for nitrogen degassed blank solution and left at OC. The OC potential shifted quickly from -1.35 V to -0.6 V within 10 minutes, plateauing at -0.55 V until the 105 minute mark, a potential consistent with the beginning of the large Ge oxidation peak in Figure 3.4. For the next 50 minutes, the OC potential slowly increased to -0.2 V, a potential equivalent to the start of the right most anodic peak, oxidation of the last germanene layer, in contact with the Au surface (Figure 3.4). The OC potential eventually reached around 0.1 V when left exposed to air for 12 hours. The positive drift in the OC potential indicates oxidation or loss of the germanene. A similar experiment using a blank solution which was equilibrated with air, produced a similar result. However the transition took about a tenth of the time, suggesting oxygen in the solution was at least partially responsible for the germanene deposit loss.

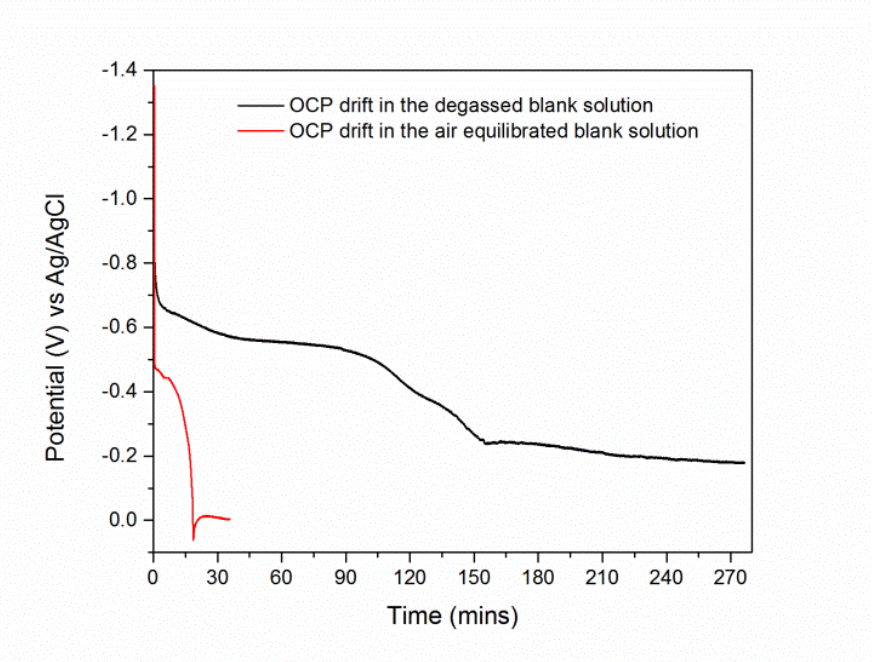

Figure 3.5. Ge was deposited on polycrystalline Au at -1.35 V in Ge solution for 300 s and the deposit was exposed to OC. Change in OC potential of the Ge in degassed blank solution (black) and in air equilibrated blank solution (red) with respect to the time toward oxidative potential was observed.

Above voltammetry and OC potential data suggested that by applying a potential between -1 V and -0.9 V, immediately after electrodeposition, loss of germanene was avoided and the HER was minimized. In a previous *in situ* STM study it appeared that hydrogen evolution could disrupt the germanene layers.[29] Overall, maintaining electrochemical control of the potential proved to be an inexpensive and scalable alternative to UHV for protecting germanene from oxidation. Figure 3.6a displays four

sequential spectra recorded of a germanene deposit formed by maintained the potential at -1.3 V in the pH 9.0 GeO_2 solution. The resulting deposit should consist of about 3 layers of germanene. The four spectra were recorded using a 780 nm laser focused on a 3.1 μm spot on a SERS active Au substrate. The orange spectra in Figure 3.6a was taken of a vapor deposited Au film under equivalent germanene deposition conditions. The first and second sequential spectra (black and red) in Figure 3.6a exhibited broad peaks centered around 270 cm^{-1}, which corresponds to amorphous Ge.[58] The sharp peak at 933 cm^{-1} is associated with perchlorate ions.[36,59] However, the third spectrum (green) displayed a broad peak around 290 cm^{-1}, as well as increased intensity between 150 and 200 cm^{-1} (165 cm^{-1}). The fourth spectrum (blue) displayed the same low intensity broad peak and a sharp peak at 296 cm^{-1}. Those two peaks are more clearly distinguishable in Figure 3.6b, where the second measurement (red) was subtracted as a background from the fourth measurement (blue). It appears that the 296 cm^{-1} peak corresponds to the germanene in-plane vibration, analogous to the G mode in graphene, while the low broad peak around 165 cm^{-1} corresponds to the out-of-plane vibration, analogous to the graphene D mode.[39] In the present report, the 296 cm^{-1} peak will be referred to as the G-like peak and the 165 cm^{-1} peak as the D-like peak. The new peaks in the purple spectrum (Figure 3.6b) are distinguishable from the amorphous Ge peak, centered around 270 cm^{-1}, and from the 300 cm^{-1} peak, observed for diamond structured Ge. The D-like peak was reproducible, but due to its low intensity and Raleigh scattering at low wavenumber, was distinguishable only after a background subtraction. The G and D like peaks were not present under equivalent conditions in the control experiments on plain Au substrate (Figure 3.6a, orange).

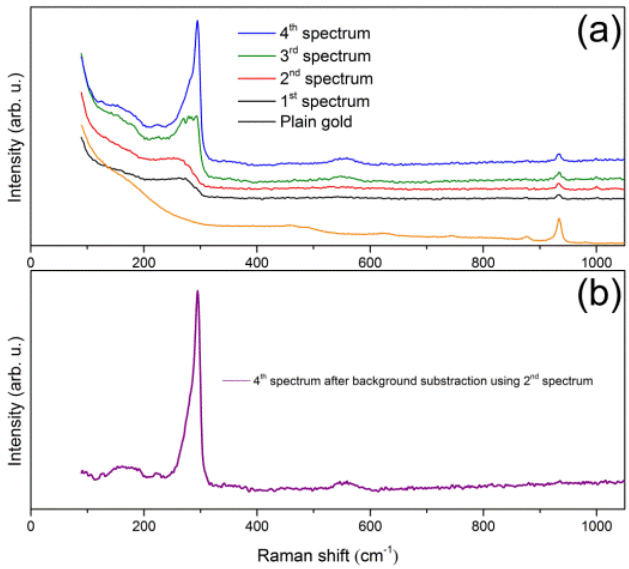

Figure 3.6. A series of sequential *in situ* Raman spectra from one spot on a Ge deposit formed on a SERS active Au substrate, and one *in situ* Raman spectra was from a plain Au substrate. In SERS substrate, the 296 cm^{-1} peak was developed in the 4th spectrum and the 165 cm^{-1} peak became apparent once 2nd spectrum was used as the reference in background subtraction in Figure 3.6b. Similar experiment using a plain polycrystalline Au substrate resulted in no discernable Ge peaks, change in measurement conditions did not change the result. Intensity in this figure has been offset for clarity. The maximum intensity of the 296 cm^{-1} peak in 4th spectrum (blue) was 324 counts per second per milliwatt (cps mW^{-1}). The measurement conditions for a spectrum were: 5 seconds laser irradiation, 3 measurements, and 6 mW 780 nm laser. Approximately 2 seconds were spent idle between each spectrum. Formation of the 296 cm^{-1} peak was reproducible when the listed conditions when SERS substrate was used, but was not exclusive to the listed conditions.

The peaks in Figure 3.6b are consistent with previously reported experimental and theoretical Raman spectra for germanene.[23,27,39,40] The G-like peak tails toward lower Raman shifts, as shown in the blue, green, and purple spectra in Figure 3.6, suggesting the presence of disordered and/or amorphous Ge, analogous to those observed in silicene formation.[60,61] The G-like peak formation was irreversible, being stable for at least 8 hours, under potential control at potentials negative of -0.5 V, with no further laser exposure. The D-like peak was stable as well, though was it was only discernable in spectra with high signal to noise.

As noted above, the G-like peak was not initially present in the Raman spectra (Figure 3.6). Previous in-situ STM studies have shown that the germanene HC structure is formed electrochemically on Au under equivalent deposition conditions (Figure 3.7).[29] However, the 6 membered ring domains were disrupted by five and seven membered rings domain walls, so that coherent HC domains were mostly a few nm in size. The five and seven membered rings result in rotations between coherent HC domains. Previous *in situ* STM studies suggest that the HC germanene is electrochemically grown by a by nucleation and 2D growth.[29] The resulting 2D HC islands grew from their edges until they meet, only forming larger coherent HC domains if their edges formed oriented six-membered rings. When they were not correctly oriented or spaced, five, seven, or eight membered rings could form, breaking the symmetry and limiting direct characterization by Raman spectroscopy and surface X-ray diffraction.[28] The presences of small coherent domains due to the defect rings and rotations should disrupt symmetry and alter the Raman signals.[62,63,64]

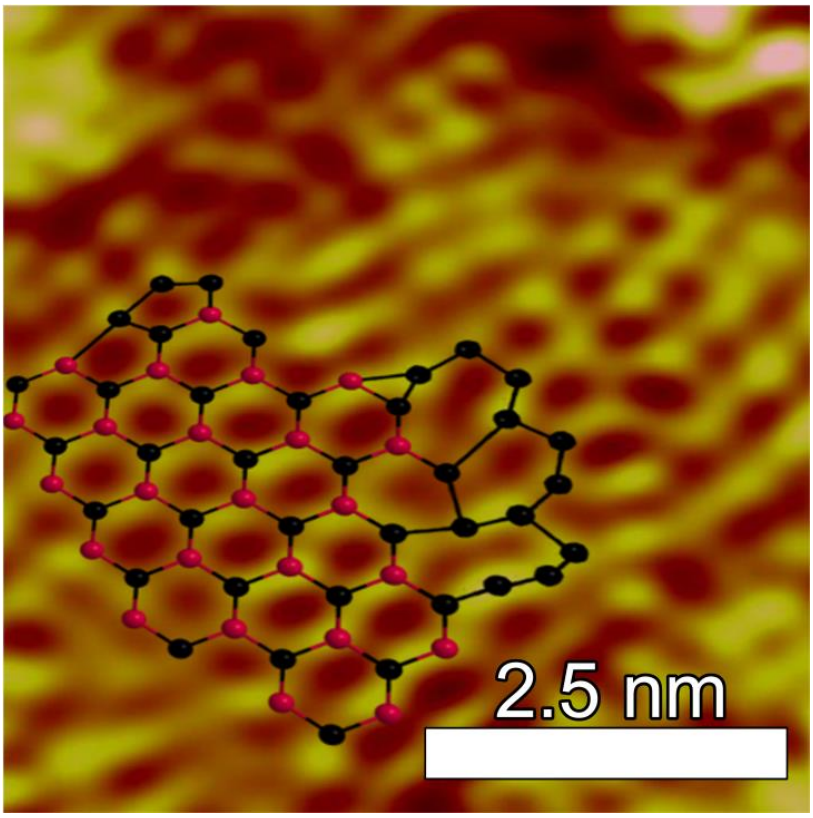

Figure 3.7. STM image of the first layer of germanene on Au (111), edited from a previously reported work.[29] Black and red hexagonal ring indicate complete germanene structure, and the black three, five, seven, eight-membered structures are examples of defective germanene structures surrounding a germanene domain. The image has been flattened and filtered via fast Fourier transform.

The laser exposure dependence (Figure 3.6) suggests that exposure to the micro-Raman spectrometer's 780 nm laser during measurements may be removing germanene defects and creating larger coherent domains of the germanene, thus allowing direct Raman

spectroscopic measurements of germanene in a process akin to the self-healing seen for graphene and silicene defects.[65,66]

Figure 3.8 illustrates changes is the G-like peak as a function of peak intensity (Figure 8a), FWHM (Figure 3.8b) and peak position (Figure 3.8c), as a function of the number of 1 second exposures to the 780 nm laser. The deposit was formed at -1.05 V, which corresponds to two layers of germanene. The spectra were measured on a single 3.1 μm diameter spot, using the 780 nm, 8 mW, laser, with 2 s off time between spectra. The GeO_2 solution was flowed continuously through the cell. Initially (Figure 3.8a, red arrow) the G-like peak was not evident. Around the 25th spectrum (green arrow) a broad peak, low intensity peak emerged, similar to the green spectrum in Figure 3.6a. By the 45th spectrum (blue arrow), a clearly defined G-like peak, similar to the blue spectrum in Figure 3.6a, was evident and its intensity continued to increase until about the 80th spectrum (purple arrow). By the 80th spectrum, the peak's intensity, peak position, and FWHM all plateaued, indicating maximum improvement in the quality of the germanene layer had been achieved under the applied conditions. The G-like peak's center plateaued around 296 cm^{-1}, while the FWHM had dropped to 10 cm^{-1}.

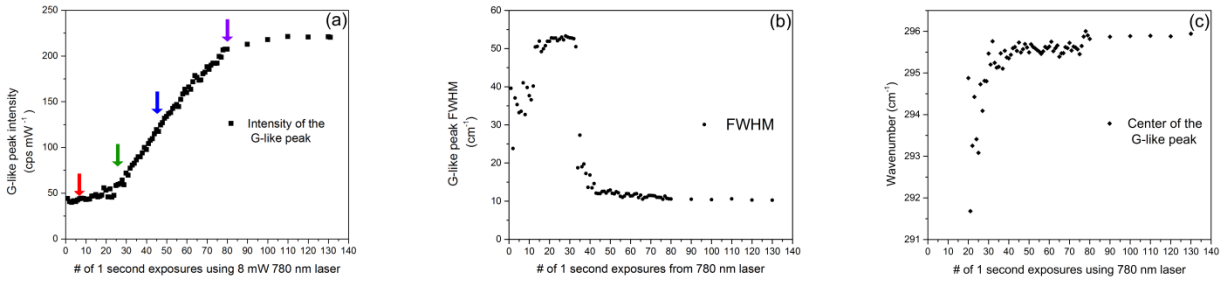

Figure 3.8. The progress of the G-like peak development from a sequential series of *in situ* Raman measurements on one spot using 780 nm wavelength laser on Ge deposited on Au by applying -1.05 V in the GeO_2 solution. The G-like peak's intensity in cps mW^{-1} is shown in (a), its FWHM in (b), and center of the peak in (c). Four distinctive phases in the development were presented around the 6^{th} (red), 25^{th} (green), 45^{th} (blue), and 80^{th} (purple) measurements. The initial broad peak starts to form near 291 cm^{-1} around the 5^{th} measurement and as the broad peak sharpens around the 34^{th} measurement the center of the peak shifts to near 295 cm^{-1}. The G-like peak does not develop further starting around the 80^{th} measurement when the center of the peak is close to 296 cm^{-1}. The measurement conditions for a spectrum were: sequential 1 second laser irradiation using the 8 mW 780 nm laser, approximately 2 seconds were spent idle between each spectrum.

The G-like peak was only observed when the deposit was formed at -1 V or lower, which corresponded to the formation of two or more layers of germanene. The absence of the G-like peak before deposition of the second layer may be the result of the first layer's interaction with the Au substrate.[10,20,67] Similar behavior has been reported for silicene and germanene, where the deposits were under significant strain at the substrate deposit interface.[40,44,60,68]

Formation of the G-like peak did not require the presences of H_2GeO_3 species in solution during exposure to the 780 nm laser, as long as germanene was first deposited at -1 V or below. That is, after electrodeposition of the germanene layer, the solution could be replaced with a blank, and exposed to the 780 nm laser would still produce the G-like

peak. Those results indicate that the appearance of the G-like peak was not a photoelectrochemical reaction with Ge precursor ions in solution during 780 nm exposure, but rather change in the nature of previously electrodeposited germanene upon exposure. In addition, the Raman measurements were not strongly dependent on the potential during 780 nm exposure, as long as more than one layer of germanene was present. For example, the full G-like peak was formed upon 780 nm exposure at -0.9 V, as long as the germanene was first deposited at -1.3 V.

Formation of the G-like peak using the micro-Raman spectrometer created a couple of artifacts on the surface, depending on the conditions used. Figure 3.9a is a visible light micrograph of the Au SERS active substrate in solution. The red circle surrounds a bright spot left after forming the G-like peak at -1.1 V with the 780 nm laser. The series of Raman spectra on the left of Figure 3.9a show that the bright spot is an area where the G-like peak is present. It should be noted that the bright area is broader then the predicted focus of the 780 nm laser, about 30 μm in diameter, or 10 times that quoted by the manufacturer (Table 3.1). SEM images of a bright spot (Figure 3.9b and 3.9c) showed that the substrate's surface was reconstructed into an array of 50-100 nm diameter nanorods, probably the result of localized annealing of the SERS active surface exposed to the 780 nm laser. The G-like peak was not immediately observed in Raman spectra, using the 780 nm laser on a newly formed germanene deposit, on a previously reconstructed Au spot. This suggests that changes in the SP at the reconstructed Au spot was not responsible for the observation of the G-like peak.

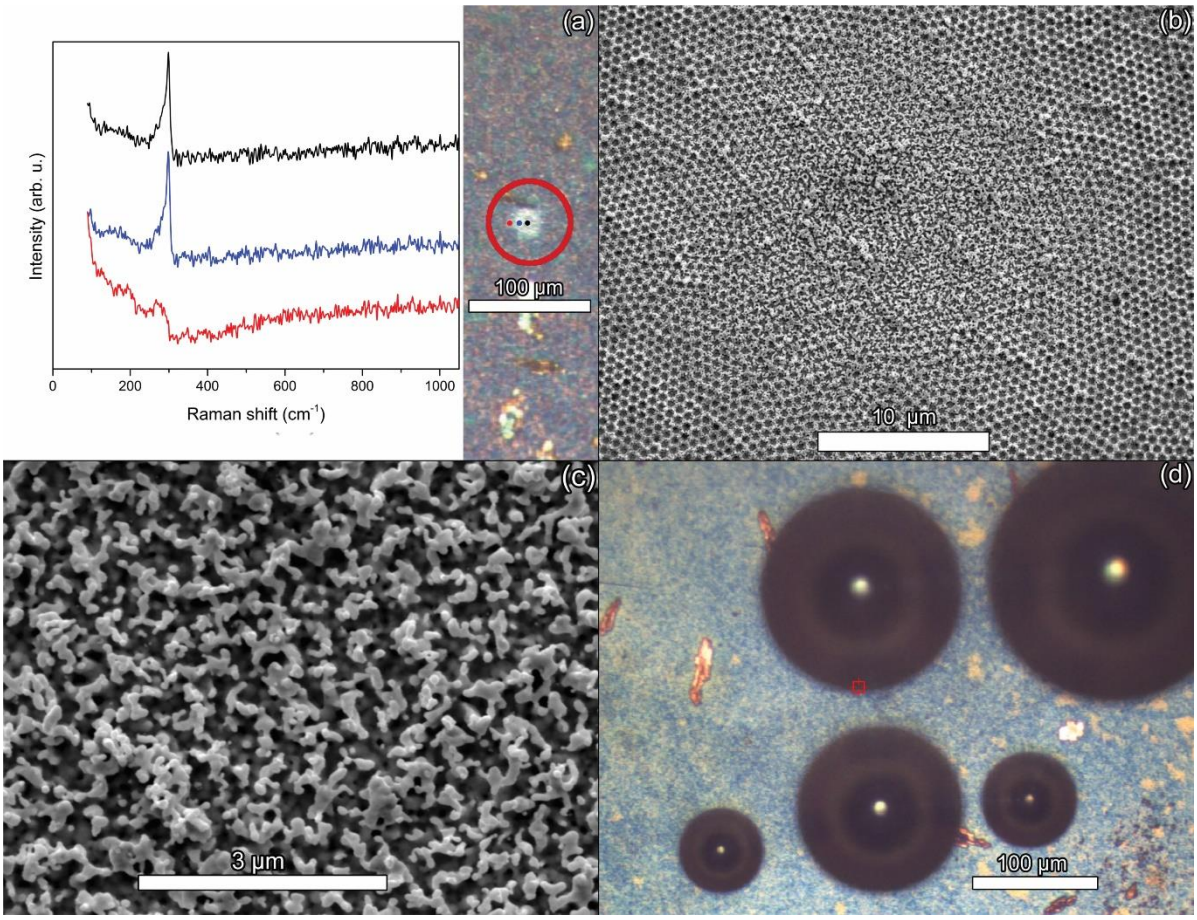

Figure 3.9. Ge was deposited by applying -1.1 V in (a), and bright spot highlighted by a red circle was formed after being irradiated by 8 mW 780 nm laser to form the G-like peak. The Raman spectra in (a) was obtained using 10 seconds long exposures of 1 mW of 780 nm laser to avoid further sample changes and intensity was offset for visibility. The maximum intensities of the G-like peak were 15 cps mW^{-1} (black), 15 cps mW^{-1} (blue), and 2 cps mW^{-1} (red). Each spectrum was measured on a spot focused on the corresponding color of the dot on the picture. The G-like peak was apparent throughout the bright spot, but not outside of it. No visible bubble formed after 5 minutes of continuous irradiation when using the 1 mW laser power. Surface electron microscope (SEM) images of a bright spot formed using the 780 nm laser indicated changes in the Au surface morphology (b). A close-up of the spot shows a new reconstructed array of nanostructures 50-100 nm in

size (c). Ge was deposited by applying -1.2 V in (d), and bubble formation on the surface was observed from irradiation by 8 mW 780 nm laser. The bubbles were stable for at least 8 hours.

Another artifact were bubbles formed on spots where the G-like peaks were produced by 780 nm exposure, when germanene was deposited at -1.2 V or lower (Figure 3.9d). Similar experiments using the 532 nm laser on germanene electrodeposited at -1.2 V resulted in neither bright spots nor bubbles, even with longer exposures with higher wattage (8 mW for the 780 nm and 10 mW for the 532 nm). In addition, no bubbles were produced using the 780 nm laser on the clean SERS active Au surface without germanene's presence, unless a potential negative of -1.4 V was used. The bubbles remained stable for at least 8 hours without further exposure. Possible bubble sources include water vapor from heating and hydrogen from the HER, which may occur simultaneously. Increased temperatures from laser absorption might result in water vapor bubbles on the surface. However, their dependence on applied potential, the surface composition, and stability are consistent with photocatalysis of the HER.

Raman studies were also performed using the 532 nm laser. The green spectrum (Figure 3.10) was recorded using the 532 laser on the Au surface at 0.5 V in the GeO_2 solution, a potential too positive for Ge deposition. The purple spectrum (Figure 3.10) was recorded at -1.35 V, where several layers of germanene were present. A broad peak centered at 270 cm^{-1} was present, characteristic of amorphous Ge. However, no G-like peak developed when the 532 nm laser was used. A range of laser powers, exposure times and

Ge deposition potentials were tried, with no significant change in the spectrum. However, if an equivalent deposit was first exposed to the 780 nm laser, producing the G-like peak, the G-like peak was then also observed using the 532 nm laser when focused on the same spot, as in the black spectrum (Figure 3.10). The G-like peak was not observed when the 532 nm laser was used on a newly formed germanene deposit, formed on a previously reconstructed Au spot. That suggests that changes in the SP at the reconstructed Au spot were not responsible for the observation of the G-like peak (Figure 3.10, black spectrum). Differences between the 780 nm and 532 nm lasers are noted in Table 3.1.

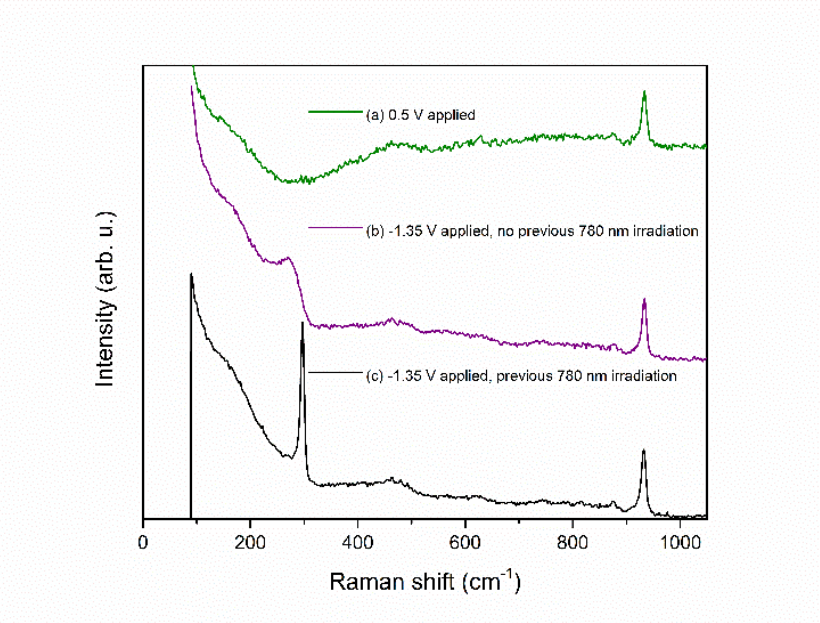

Figure 3.10. *In situ* Raman spectra of Ge deposit on SERS Au substrate using 532 nm laser. A broad peak around 266 cm^{-1}, belong to amorphous Ge, was visible when Ge was deposited on the surface at -1.35 V (purple). Clearly distinguishable from the clean Au surface when 0.5 V is applied (green). The measurement conditions for a spectrum were: 3 seconds laser irradiation, 10 measurements, and 10 mW 532 nm laser. Changing

measurement conditions or applied potential did not change the spectrum. After depositing Ge by applying -1.05 V, the G-like peak was first formed using 780 nm laser. Then, 532 nm laser was used to measure *in situ* Raman spectra of the same spot that was irradiated by 780 nm laser (black). The intensities at 296 cm^{-1} were 80 cps mW^{-1} (green), 52 cps mW^{-1} (purple), and 54 cps mW^{-1} (black). The measurement conditions for a spectrum were: 1 second laser irradiation, 10 measurements, and 10 mW 532 nm laser. Intensity of the spectra was offset for visibility.

The above results raise questions concerning how the 780 nm laser creates the G-like and D-like peaks. One possibility is that the micro-Raman spectrometer's laser acts as a local heating source, annealing the germanene, creating a longer range crystalline order. A study of laser modification of a deposit of carbon nanotubes in a micro-Raman spectrometer resulted in a decrease in the D-peak intensity, which was attributed to high laser power density purifying the carbon nanotube sample.[69] A study of a self-healing process for graphene, upon exposure to the electron beam of a tunneling electron microscope, was reported as due to localized heating.[65,70]

In the present study, Table 3.1 does not support simple power dependency to account for the absence of the G-like peak development with the 532 nm laser. From Table 3.1 the power density for the 532 nm laser should be about three times that for the 780 nm laser, and the power needed to initiate development of the G-like peak with the 780 nm laser is only a third of that available. Thus full power from the 532 nm should be about 3

times more than sufficient if it simply depends on power delivered. Those observations suggest strong wavelength dependence.

Figure 3.11 is a study of the temperature dependence for G-like peak development, where germanene was deposited at -1.05 V. Raman experiments were performed in-situ on two spots using the 780 nm laser at 2.5 mW. On the first spot, three sequential measurements were made, each consisting of 50 s of continuous exposure, separated by 3 s idle time between measurements. Those spectra are displayed in Figure 3.11: first (green), second (red), and third (blue). The G-like peak emerges in the second and third spectra. On a second spot, 45 measurements were performed, each was 3 s of exposure, with 120 s idle between measurements. The last 15 exposures were combined, producing the black spectrum in Figure 3.11, which did not displayed G-like peak. Those results indicate that the formation of the G-like peak was facilitated by long continuous exposure time, suggesting that higher temperatures were advantageous.

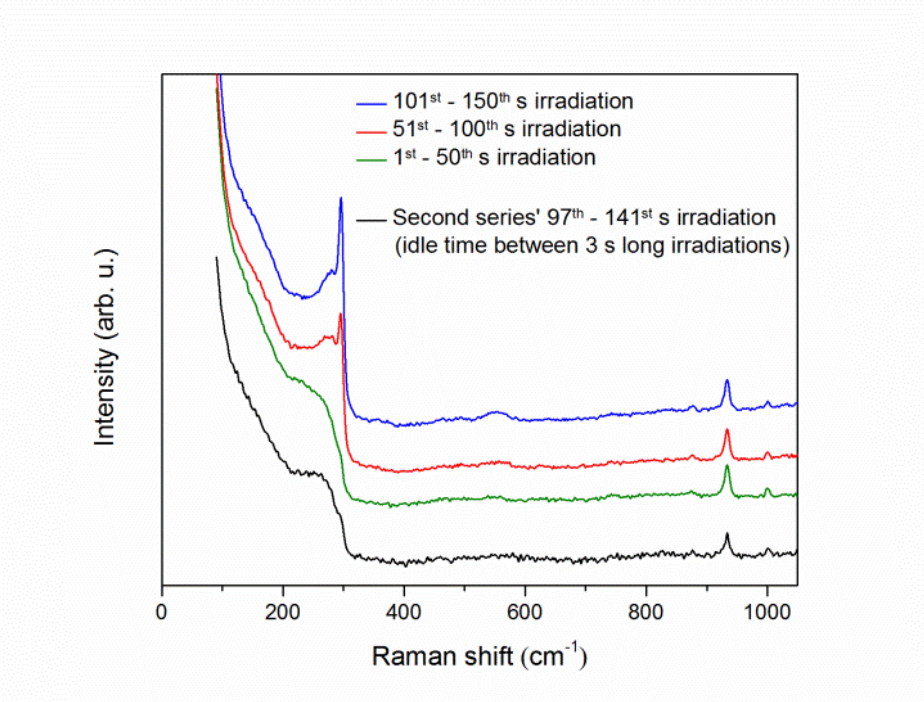

Figure 3.11. After depositing Ge at -1.05 V, two series of *in situ* Raman spectra were measured. First series of sequential measurements on one spot used prolonged continuous irradiation per spectrum (green, red, blue). Only amorphous Ge peak was evident in the first spectrum from the prolonged continuous irradiation (green). G-like peak is evident starting second spectrum (red). The G-like peak further developed in the third spectrum (blue). Second series of sequential measurements on a new spot used shorter irradiation of 3 s per spectrum, and the laser irradiated spot was given 2 mins to dissipate heat between measurements (black). The G-like peak seems to develop at much slower rate in the second series (black), suggesting that increased temperature from continuous laser irradiation helped improving germanene. The intensities at 296 cm^{-1} were 138 cps mW^{-1} (green), 210 cps mW^{-1} (red), 265 cps mW^{-1} (blue), and 96 cps mW^{-1} (black). The measurement conditions for the first series were 50 seconds laser irradiation, 1 measurement per spectra,

and 2.5 mW 780 nm laser. The measurement conditions for the second series were 1 second laser irradiation, 3 measurements per spectra, and 2.5 mW 780 nm laser. Intensity of the spectra was offset for visibility.

Given the results presented above, the G-like peak's development appears to be due to local temperature changes resulting from SP excitation of Au nanostructures on the surface, allowing recrystallization of the electrodeposited germanene. To further investigate any plasmon-mediated photothermal effect, local temperatures at the surface of the SERS substrate were calculated following thermal transport model developed by Brongersma.[71] The model developed for high density Au nanoparticle arrays on fused silica glass substrates (similar to substrate used here) assumes conduction to be the major thermal transport mechanism. With thermal conductivity and diffusivity of the substrate assumed to be temperature independent, the model predicts the temperature at the center of the laser spot to be equal to equation (3.1).

$$T = 0.5\,\varphi P/\sqrt{\tfrac{2}{\pi}}KD \tag{3.1}$$

In the equation, φ is the fraction of laser power absorbed, P is the laser power density, K is the thermal conduction coefficient and D is the diameter of the Gaussian laser beam. Based on the above model and laser beam characteristics used in this study, temperatures near 450℃ at the center of the laser spot could easily be obtained, further corroborating the photothermal effects on Raman spectra of Germanene observed in this study (Figure 3.8). Such localized heating would also account for the reconstructed spots (Figure 3.9c) left on the surface after exposure to the 780 nm laser. Such a mechanism

can be contrasted with a simple photon absorption and heat transfer model, a SolidWorks simulation, based on complete absorption of the laser power on a 3 μm spot, which suggested a temperature at the center of the 780 nm laser spot of only about 185 °C, too low to facilitate Ge recrystallization.[72] As noted, the sizes of coherent domains, as determined using in-situ STM, were a couple of nm at best. Analysis of graphene Raman signals as a function of domain size, or defect density, suggest they would be drastically affected for domains less than a few nm.[63,64]

The proximity between the G-like peaks measured in the present study (296 cm^{-1}) and the diamond structured crystalline Ge Raman peak (300 cm^{-1}) suggest that the peak may correspond to crystalline Ge formation, reported previously by others.[73,74,75] However, recent studies of germanene formation assigned the 296 cm^{-1} peak as the germanene G-like peak, not diamond structured Ge.[23,40] The presence of the D-like peak also suggests germanene formation (Figure 3.6b). The temperature required to anneal amorphous Ge thin films into crystalline Ge has been reported to be 300 °C – 450 °C,[72] under UHV conditions, which may be obtainable on the SERS active substrate. In solution, however, according to the Pourbaix diagram, crystalline Ge may be stable below -1V, but oxidizes to either GeO or $HGeO_3^-$ above -1.0 V.[76] However, the G-like peak was stable up to -0.55 V, and only slowly degraded starting around -0.5 V.

3.5 CONCLUSION

Previous *in situ* STM studies, by this group, have shown that germanene can be formed electrochemically on Au, although with a high fraction of defect rings. The present report describes a Raman spectroelectrochemical study of electrodeposited germanene on

plasmonically active Au substrates. The first spectrum after Ge deposition displayed no clear evidence for the presence of well-ordered germanene, although a feature characteristic for amorphous Ge was visible. However, with repeated exposure to the 780 nm laser, a sharp 296 cm^{-1} peak (G-like) grew in. The extent of the peak was a function of laser power, exposure time, wavelength, and electrode potential. Raman spectra collected using an off-resonance 532 nm laser, with equivalent power density, showed no such structural transformations. The potential controlled the amount deposited and only deposits formed at -1 V or below, where second layer of germanene was present on the surface, resulted in the G-like peak. It was not observed for deposits consisting of only first layer germanene, most likely due to its interaction with the substrate. The fact that the G-like peak grew with increased exposure suggests annealing of the deposit. However, the strong wavelength dependence was inconsistent with a simple heat transfer model based on complete absorption of all laser power. On the other hand, the use of a nanostructured Au electrode to enhance spectroscopic sensitivity suggests the importance of plasmonics in producing localized heating and self-healing of the germanene structure. It appears that larger coherent domains of the germanene structure resulted, producing stronger Raman signals. The formation of the reflective spots on the surface during analysis suggests heating sufficient to locally reconstruct the Au SERS active substrate.

3.6 ACKNOWLEDGEMENT

Support from the National Science Foundation, DMR #1410109, is gratefully acknowledged.

REFERENCES

1. Grazianetti, C.; Cinquanta, E.; Molle, A., Two-dimensional silicon: the advent of silicene. *2d Materials* **2016,** *3* (1).

2. Houssa, M.; Dimoulas, A.; Molle, A., Silicene: a review of recent experimental and theoretical investigations. *Journal of Physics: Condensed Matter* **2015,** *27* (25), 253002.

3. Zhu, F.-f.; Chen, W.-j.; Xu, Y.; Gao, C.-l.; Guan, D.-d.; Liu, C.-h.; Qian, D.; Zhang, S.-C.; Jia, J.-f., Epitaxial growth of two-dimensional stanene. *Nat Mater* **2015,** *14* (10), 1020-1025.

4. van den Broek, B.; Houssa, M.; Iordanidou, K.; Pourtois, G.; Afanas'ev, V. V.; Stesmans, A., Functional silicene and stanene nanoribbons compared to graphene: electronic structure and transport. *2d Materials* **2016,** *3* (1).

5. Bianco, E.; Butler, S.; Jiang, S.; Restrepo, O. D.; Windl, W.; Goldberger, J. E., Stability and Exfoliation of Germanane: A Germanium Graphane Analogue. *ACS Nano* **2013,** *7* (5), 4414-4421.

6. Acun, A.; Zhang, L.; Bampoulis, P.; Farmanbar, M.; Houselt, A. v.; Rudenko, A. N.; Lingenfelder, M.; Brocks, G.; Poelsema, B.; Katsnelson, M. I.; Zandvliet, H. J. W., Germanene: the germanium analogue of graphene. *Journal of Physics: Condensed Matter* **2015,** *27* (44), 443002.

7. Kaloni, T. P.; Schreckenbach, G.; Freund, M. S.; Schwingenschlogl, U., Current developments in silicene and germanene. *Physica Status Solidi-Rapid Research Letters* **2016,** *10* (2), 133-142.

8. Roome, N. J.; Carey, J. D., Beyond Graphene: Stable Elemental Monolayers of Silicene and Germanene. *ACS Applied Materials & Interfaces* **2014,** *6* (10), 7743-7750.

9. Derivaz, M.; Dentel, D.; Stephan, R.; Hanf, M.-C.; Mehdaoui, A.; Sonnet, P.; Pirri, C., Continuous Germanene Layer on Al(111). *Nano Letters* **2015,** *15* (4), 2510-2516.

10. Davila, M. E.; Le Lay, G., Few layer epitaxial germanene: a novel two-dimensional Dirac material. *Scientific Reports* **2016,** *6*.

11. Cahangirov, S.; Topsakal, M.; Aktürk, E.; Şahin, H.; Ciraci, S., Two- and One-Dimensional Honeycomb Structures of Silicon and Germanium. *Physical Review Letters* **2009,** *102* (23), 236804.

12. Liu, C.-C.; Feng, W.; Yao, Y., Quantum Spin Hall Effect in Silicene and Two-Dimensional Germanium. *Physical Review Letters* **2011,** *107* (7), 076802.

13. Novoselov, K. S.; Geim, A. K.; Morozov, S. V.; Jiang, D.; Zhang, Y.; Dubonos, S. V.; Grigorieva, I. V.; Firsov, A. A., Electric Field Effect in Atomically Thin Carbon Films. *Science* **2004,** *306* (5696), 666.

14. Wang, J.; Deng, S.; Liu, Z.; Liu, Z., The rare two-dimensional materials with Dirac cones. *National Science Review* **2015,** *2* (1), 22-39.

15. Ye, X.-S.; Shao, Z.-G.; Zhao, H.; Yang, L.; Wang, C.-L., Intrinsic carrier mobility of germanene is larger than graphene's: first-principle calculations. *RSC Advances* **2014,** *4* (41), 21216-21220.

16. Houssa, M.; Pourtois, G.; Afanas'ev, V. V.; Stesmans, A., Electronic properties of two-dimensional hexagonal germanium. *Applied Physics Letters* **2010,** *96* (8), 082111.

17. Ni, Z.; Liu, Q.; Tang, K.; Zheng, J.; Zhou, J.; Qin, R.; Gao, Z.; Yu, D.; Lu, J., Tunable Bandgap in Silicene and Germanene. *Nano Letters* **2012,** *12* (1), 113-118.

18. Wang, Y. P.; Ji, W. X.; Zhang, C. W.; Li, S. S.; Li, F.; Li, P.; Ren, M. J.; Chen, X. L.; Yuan, M.; Wang, P. J., Enhanced band gap opening in germanene by organic molecule adsorption. *Materials Chemistry and Physics* **2016,** *173*, 379-384.

19. Nijamudheen, A.; Bhattacharjee, R.; Choudhury, S.; Datta, A., Electronic and Chemical Properties of Germanene: The Crucial Role of Buckling. *The Journal of Physical Chemistry C* **2015,** *119* (7), 3802-3809.

20. Dávila, M. E.; Xian, L.; Cahangirov, S.; Rubio, A.; Lay, G. L., Germanene: a novel two-dimensional germanium allotrope akin to graphene and silicene. *New Journal of Physics* **2014,** *16* (9), 095002.

21. Bampoulis, P.; Zhang, L.; Safaei, A.; Gastel, R. v.; Poelsema, B.; Zandvliet, H J W., Germanene termination of Ge 2 Pt crystals on Ge(110). *Journal of Physics: Condensed Matter* **2014,** *26* (44), 442001.

22. d'Acapito, F.; Torrengo, S.; Xenogiannopoulou, E.; Tsipas, P.; Velasco, J. M.; Tsoutsou, D.; Dimoulas, A., Evidence for Germanene growth on epitaxial hexagonal (h)-AlN on Ag(111). *Journal of Physics-Condensed Matter* **2016,** *28* (4).

23. Tsai, H.-S.; Chen, Y.-Z.; Medina, H.; Su, T.-Y.; Chou, T.-S.; Chen, Y.-H.; Chueh, Y.-L.; Liang, J.-H., Direct formation of large-scale multi-layered germanene on Si substrate. *Physical Chemistry Chemical Physics* **2015,** *17* (33), 21389-21393.

24. Persichetti, L.; Jardali, F.; Vach, H.; Sgarlata, A.; Berbezier, I.; Crescenzi, M. D.; Balzarotti, A., van der Waals Heteroepitaxy of Germanene Islands on Graphite. *The Journal of Physical Chemistry Letters* **2016**, 3246-3251.

25. Zhang, L.; Bampoulis, P.; Rudenko, A. N.; Yao, Q.; van Houselt, A.; Poelsema, B.; Katsnelson, M. I.; Zandvliet, H. J. W., Structural and Electronic Properties of Germanene on MoS2. *Physical Review Letters* **2016,** *116* (25).

26. Satoshi, E.; Osamu, K.; Noriharu, N.; Seiya, I.; Riku, Y.; Yoshinari, K.; Hiroshi, T.; Mitsuhiro, K., ##IMG## [http://ej.iop.org/images/1882-0786/11/1/015502/toc_AP170768if001.gif] {$\sqrt{3} {\times} \sqrt{3} $} germanene on Al(111) grown at nearly room temperature. *Applied Physics Express* **2018,** *11* (1), 015502.

27. Ledina, M.; Liang, X.; Kim, Y.-G.; Jung, J.; Perdue, B.; Tsang, C.; Soriaga, M.; Stickney, J. L., (Invited) Investigations into the Formation of Germanene Using Electrochemical Atomic Layer Deposition (E-ALD). *ECS Transactions* **2015,** *66* (6), 129-140.

28. Ledina, M. A.; Bui, N.; Liang, X.; Kim, Y.-G.; Jung, J.; Perdue, B.; Tsang, C.; Drnec, J.; Carlà, F.; Soriaga, M. P.; Reber, T. J.; Stickney, J. L., Electrochemical Formation of Germanene: pH 4.5. *Journal of The Electrochemical Society* **2017,** *164* (7), D469-D477.

29. Bui, N. N.; Ledina, M.; Reber, T. J.; Jung, J.; Stickney, J. L., An Electrochemical Scanning Tunneling Microscopic Study of the Potential Dependence of Germanene Growth on Au(111) at pH 9.0. *ACS Nano* **2017**.

30. Szekely, G., Electrodeposition of Germanium. *Journal of The Electrochemical Society* **1951,** *98* (8), 318-324.

31. Endres, F., Electrodeposition of a thin germanium film on gold from a room temperature ionic liquid. *Physical Chemistry Chemical Physics* **2001,** *3* (15), 3165-3174.

32. Liang, X.; Kim, Y.-G.; Gebergziabiher, D. K.; Stickney, J. L., Aqueous Electrodeposition of Ge Monolayers. *Langmuir* **2010,** *26* (4), 2877-2884.

33. Endres, F.; Zein El Abedin, S., Nanoscale electrodeposition of germanium on Au(111) from an ionic liquid: an in situ STM study of phase formation Part I. Ge from GeBr4. *Physical Chemistry Chemical Physics* **2002,** *4* (9), 1640-1648.

34. Fahrenkrug, E.; Gu, J.; Jeon, S.; Veneman, P. A.; Goldman, R. S.; Maldonado, S., Room-Temperature Epitaxial Electrodeposition of Single-Crystalline Germanium Nanowires at the Wafer Scale from an Aqueous Solution. *Nano Letters* **2014,** *14* (2), 847-852.

35. Endres, F.; Zein El Abedin, S., Nanoscale electrodeposition of germanium on Au(111) from an ionic liquid: an in situ STM study of phase formation Part II. Ge from GeCl4. *Physical Chemistry Chemical Physics* **2002,** *4* (9), 1649-1657.

36. Liang, X.; Zhang, Q.; Lay, M. D.; Stickney, J. L., Growth of Ge Nanofilms Using Electrochemical Atomic Layer Deposition, with a "Bait and Switch" Surface-Limited Reaction. *Journal of the American Chemical Society* **2011,** *133* (21), 8199-8204.

37. Liang, X.; Jayaraju, N.; Thambidurai, C.; Zhang, Q.; Stickney, J. L., Controlled Electrochemical Formation of GexSbyTez using Atomic Layer Deposition (ALD). *Chemistry of Materials* **2011,** *23* (7), 1742-1752.

38. Schlecht, S.; Yosef, M.; Fröba, M., Synthesis and Raman Spectroscopy of Nanoparticles of Crystalline and X-ray Amorphous Germanium within Mesoporous SiO2. *Zeitschrift für anorganische und allgemeine Chemie* **2004,** *630* (6), 864-868.

39. Scalise, E.; Houssa, M.; Pourtois, G.; van den Broek, B.; Afanas'ev, V.; Stesmans, A., Vibrational properties of silicene and germanene. *Nano Research* **2013,** *6* (1), 19-28.

40. Zhuang, J.; Gao, N.; Li, Z.; Xu, X.; Wang, J.; Zhao, J.; Dou, S. X.; Du, Y., Cooperative Electron–Phonon Coupling and Buckled Structure in Germanene on Au(111). *ACS Nano* **2017**.

41. Paillet, M.; Parret, R.; Sauvajol, J.-L.; Colomban, P., Graphene and related 2D materials: An overview of the Raman studies. *Journal of Raman Spectroscopy* **2018,** *49* (1), 8-12.

42. Zhao, J.; Liu, H.; Yu, Z.; Quhe, R.; Zhou, S.; Wang, Y.; Liu, C. C.; Zhong, H.; Han, N.; Lu, J.; Yao, Y.; Wu, K., Rise of silicene: A competitive 2D material. *Progress in Materials Science* **2016,** *83*, 24-151.

43. Morishita, T.; Spencer, M. J. S., How silicene on Ag(111) oxidizes: microscopic mechanism of the reaction of O2 with silicene. *Scientific Reports* **2015,** *5*, 17570.

44. Galashev, A. E.; Ivanichkina, K. A.; Vorob'ev, A. S.; Rakhmanova, O. R., Structure and stability of defective silicene on Ag(001) and Ag(111) substrates: A computer experiment. *Physics of the Solid State* **2017,** *59* (6), 1242-1252.

45. Allmen, M. v.; Blatter, A., *Laser-Beam Interactions with Materials: Physical Principles and Applications*. 2nd ed.; Springer: New York, 1987.

46. Huang, X.; Jain, P. K.; El-Sayed, I. H.; El-Sayed, M. A., Plasmonic photothermal therapy (PPTT) using gold nanoparticles. *Lasers in Medical Science* **2007,** *23* (3), 217.

47. Linic, S.; Christopher, P.; Ingram, D. B., Plasmonic-metal nanostructures for efficient conversion of solar to chemical energy. *Nature Materials* **2011,** *10*, 911.

48. Duan, H.; Hu, H.; Kumar, K.; Shen, Z.; Yang, J. K. W., Direct and Reliable Patterning of Plasmonic Nanostructures with Sub-10-nm Gaps. *ACS Nano* **2011,** *5* (9), 7593-7600.

49. Flowers Jr, B. H.; Wade, T. L.; Garvey, J. W.; Lay, M.; Happek, U.; Stickney, J. L., Atomic layer epitaxy of CdTe using an automated electrochemical thin-layer flow deposition reactor. *Journal of Electroanalytical Chemistry* **2002,** *524–525*, 273-285.

50. Abdelsalam, M. E.; Bartlett, P. N.; Baumberg, J. J.; Cintra, S.; Kelf, T. A.; Russell, A. E., Electrochemical SERS at a structured gold surface. *Electrochemistry Communications* **2005,** *7* (7), 740-744.

51. Mahajan, S.; Baumberg, J. J.; Russell, A. E.; Bartlett, P. N., Reproducible SERRS from structured gold surfaces. *Physical Chemistry Chemical Physics* **2007,** *9* (45), 6016-6020.

52. Bartlett, P. N.; Baumberg, J. J.; Coyle, S.; Abdelsalam, M. E., Optical properties of nanostructured metal films. *Faraday Discussions* **2004,** *125* (0), 117-132.

53. Matthes, L.; Pulci, O.; Bechstedt, F., Optical properties of two-dimensional honeycomb crystals graphene, silicene, germanene, and tinene from first principles. *New Journal of Physics* **2014,** *16* (10), 105007.

54. Mahmoud, M. A.; Chamanzar, M.; Adibi, A.; El-Sayed, M. A., Effect of the Dielectric Constant of the Surrounding Medium and the Substrate on the Surface Plasmon Resonance Spectrum and Sensitivity Factors of Highly Symmetric Systems: Silver Nanocubes. *Journal of the American Chemical Society* **2012,** *134* (14), 6434-6442.

55. Matthes, L.; Gori, P.; Pulci, O.; Bechstedt, F., Universal infrared absorbance of two-dimensional honeycomb group-IV crystals. *Physical Review B* **2013,** *87* (3), 035438.

56. Johnson, P. B.; Christy, R. W., Optical Constants of the Noble Metals. *Physical Review B* **1972,** *6* (12), 4370-4379.

57. Haynes, W. M., CRC handbook of chemistry and physics. **1977**.

58. Wihl, M.; Cardona, M.; Tauc, J., Raman scattering in amorphous Ge and III–V compounds. *Journal of Non-Crystalline Solids* **1972,** *8* (Supplement C), 172-178.

59. Ruan, C.; Wang, W.; Gu, B., Surface-enhanced Raman scattering for perchlorate detection using cystamine-modified gold nanoparticles. *Analytica Chimica Acta* **2006,** *567* (1), 114-120.

60. Díaz Álvarez, A.; Zhu, T.; Nys, J. P.; Berthe, M.; Empis, M.; Schreiber, J.; Grandidier, B.; Xu, T., Scanning tunnelling spectroscopy and Raman spectroscopy of monolayer silicene on Ag(111). *Surface Science* **2016,** *653*, 92-96.

61. Mannix, A. J.; Kiraly, B.; Fisher, B. L.; Hersam, M. C.; Guisinger, N. P., Silicon Growth at the Two-Dimensional Limit on Ag(111). *ACS Nano* **2014,** *8* (7), 7538-7547.

62. Padilha, J. E.; Pontes, R. B., Electronic and transport properties of structural defects in monolayer germanene: An ab initio investigation. *Solid State Communications* **2016,** *225*, 38-43.

63. Cançado, L. G.; Jorio, A.; Ferreira, E. H. M.; Stavale, F.; Achete, C. A.; Capaz, R. B.; Moutinho, M. V. O.; Lombardo, A.; Kulmala, T. S.; Ferrari, A. C., Quantifying Defects in Graphene via Raman Spectroscopy at Different Excitation Energies. *Nano Letters* **2011,** *11* (8), 3190-3196.

64. Eckmann, A.; Felten, A.; Mishchenko, A.; Britnell, L.; Krupke, R.; Novoselov, K. S.; Casiraghi, C., Probing the Nature of Defects in Graphene by Raman Spectroscopy. *Nano Letters* **2012,** *12* (8), 3925-3930.

65. Zan, R.; Ramasse, Q. M.; Bangert, U.; Novoselov, K. S., Graphene Reknits Its Holes. *Nano Letters* **2012,** *12* (8), 3936-3940.

66. Özçelik, V. O.; Gurel, H. H.; Ciraci, S., Self-healing of vacancy defects in single-layer graphene and silicene. *Physical Review B* **2013,** *88* (4), 045440.

67. Cantero, E. D.; Solis, L. M.; Tong, Y.; Fuhr, J. D.; Martiarena, M. L.; Grizzi, O.; Sanchez, E. A., Growth of germanium on Au(111): formation of germanene or intermixing of Au and Ge atoms? *Physical Chemistry Chemical Physics* **2017,** *19* (28), 18580-18586.

68. Lin, C.-L.; Arafune, R.; Kawahara, K.; Kanno, M.; Tsukahara, N.; Minamitani, E.; Kim, Y.; Kawai, M.; Takagi, N., Substrate-Induced Symmetry Breaking in Silicene. *Physical Review Letters* **2013,** *110* (7), 076801.

69. Zhang, L.; Li, H.; Yue, K.-T.; Zhang, S.-L.; Wu, X.; Zi, J.; Shi, Z.; Gu, Z., Effects of intense laser irradiation on Raman intensity features of carbon nanotubes. *Physical Review B* **2002,** *65* (7), 073401.

70. Vicarelli, L.; Heerema, S. J.; Dekker, C.; Zandbergen, H. W., Controlling Defects in Graphene for Optimizing the Electrical Properties of Graphene Nanodevices. *ACS Nano* **2015,** *9* (4), 3428-3435.

71. Cao, L.; Barsic, D. N.; Guichard, A. R.; Brongersma, M. L., Plasmon-Assisted Local Temperature Control to Pattern Individual Semiconductor Nanowires and Carbon Nanotubes. *Nano Letters* **2007,** *7* (11), 3523-3527.

72. Chik, K. P.; Lim, P.-K., Annealing and crystallization of amorphous germanium thin films. *Thin Solid Films* **1976,** *35* (1), 45-56.

73. Carim, A. I.; Gu, J.; Maldonado, S., Overlayer Surface-Enhanced Raman Spectroscopy for Studying the Electrodeposition and Interfacial Chemistry of Ultrathin Ge on a Nanostructured Support. *ACS Nano* **2011,** *5* (3), 1818-1830.

74. Andreev, B. A.; Gavrilenko, L. V.; Drozdov, Y. N.; Yunin, P. A.; Pryakhin, D. A.; Mochalov, L. A.; Sennikov, P. G.; Bulkin, P.; Roca i Cabarrocas, P., Raman spectra of amorphous isotope-enriched 74Ge with low-strained Ge nanocrystals. *Thin Solid Films* **2014,** *552*, 46-49.

75. Sun, W.; Zhong, G.; Kübel, C.; Jelle, A. A.; Qian, C.; Wang, L.; Ebrahimi, M.; Reyes, L. M.; Helmy, A. S.; Ozin, G. A., Size-Tunable Photothermal Germanium Nanocrystals. *Angewandte Chemie International Edition* **2017,** *56* (22), 6329-6334.

76. Pourbaix, M., *Atlas of electrochemical equilibria in aqueous solutions*. 2d English ed. ed.; National Association of Corrosion Engineers: Houston, Tex. :, 1974.

CHAPTER 4

PRELIMINARY STUDY OF GERMANENE OXIDATION[1]

[1]Jung, J.; Bui, N.; Stickney J.L. To be submitted to Journal of the Electrochemical Society

4.1 ABSTRACT

Germanene's most notable properties are its electronic properties such as zero bandgap, ballistic conduction, and topological insulation. However, the electronic properties can get modified or disappear when the Ge-Ge sp^2 orbitals are disrupted via substrate lattice mismatch, electric field, physical adsorption, or chemical bonding.[1,2,3,4] Thus, it was important to study potential methods to control germanene's structure to either keep it protected or modified for potential applications. Specifically, oxidation of germanene from exposure to oxygen was the most worrisome due to likelihood of exposure to ambient environment, oxidation of germanene was briefly discussed in previous chapters, and silicene's tendency to oxidize when exposed to air has been reported by other researchers.[5] *In situ* Raman spectroelectrochemistry was utilized to further study germanene exposed to open circuit and more oxidizing anodic potentials. Germanene Raman peak degradation was both time and potential dependent. In addition, micron-sized bubble formation and the possibility of stanene formation were investigated. Stanene formation was investigated by depositing Sn on Au, but the resulting *in situ* Raman spectra suggested Sn oxide and Au-Sn alloy formation.

4.2 INTRODUCTION

Integrating 2D material such as graphene into an existing electronics device and material has been studied by researchers. For example, the high carrier mobility of graphene sheets is anticipated to provide unique properties.[6,7] The electronic properties are especially appealing because a single layer of graphene could operate as a field-effect transistor (FET), and that is why most of the work on integrating graphene into a device

has been focused on improving metal-oxide-semiconductor field-effect transistor (MOSFET).[8,9] Gapless 2D materials are not expected to entirely replace silicon and metal oxide materials, because MOSFET determines the on or off state of the circuit by maintaining bandgap between source and drain, thus a logic circuit cannot be entirely made out of gapless materials.[8] Furthermore, gapless 2D materials could be utilized in devices that a typical Si MOSFET cannot be used, such as transparent, flexible, or printable electronics.[10,11,12] The trend to make devices smaller to fit more transistors per area made 2D materials' ballistic transport also attractive.[13] Not simply because of the structure's improved conductivity from ballistic transport material, but because of decreased backscattering from ballistic transport at shorter lengths.[13] As discussed in chapter 1, germanene's electronic band structure is adjustable via substrate lattice mismatch, external electric filed, functionalization, tensile strain, and low temperature.[1,2,3,4] However, the induced bandgap is too small to be used for logic circuits.[8]

Visible micron meter-sized bubbles briefly mentioned in chapter 3 were further investigated. Unexpected bubble formation was undesirable because gas replacing electrolytic solution breaks the electronic connection at the surface of the working electrode, resulting in a localized open circuit. When irradiating with laser is a necessary process in forming long-range domain germanene, unpredictable bubble formation would make mass production challenging to implement. The most significant difficulty with analyzing the source of micron meter-sized bubbles was the inability to analyze the bubble's elemental and chemical composition, and analysis had to rely on examining the conditions that lead to bubble formation.

As previously mentioned, there are different methods to induce bandgap on 2D materials such as germanene. Oxidation of a 2D material is not necessarily undesirable. For example, a 2D material could be used as a sacrificial layer to protect the material underneath.[14] Also, silicene oxidation could be controlled by different silicene structures and oxygen availability.[15,16] Furthermore, oxide-terminated germanene nanoribbon was energetically favorable and could be used as an interconnect material.[17] Nonetheless, unexpected change in a material's property is undesirable when a device is designed to rely on the material to perform with an expected property. Protecting an easily oxidizable 2D material is possible, for instance, silicene covered in Al_2O_3 was protected from oxidation.

The initial approach to study germanene oxidation was to examine a change in cyclic voltammetry (CV) of deposited Ge and germanene, inspired by methods used to study electrochemical metal oxidation.[18] However, CVs and other surface analytical methods such as atomic force microscopy were inapplicable due to the low quantity of Ge deposit on the surface and small germanene domain sizes previously mentioned. To circumvent the issue, *in situ* Raman spectroscopy was used to analyze germanene Raman peak intensity when exposed to oxidation. This method was inspired by reports of using *in situ* Raman spectroscopy to study the reduction of graphene oxide.[19,20] In addition to the 296 cm^{-1} Raman peak previously discussed in chapter 3, two peaks around 200 cm^{-1} and 630 cm^{-1} peaks were observed. The 296 cm^{-1} peak corresponds to in-plane breathing mode of Ge atoms in germanene, and 630 cm^{-1} peak corresponds to the two-phonon of in-plane breathing mode.[21,22] These two peaks may be enhanced by defects in germanene, but their presence further support germanene formation. Two-phonon Raman peak

appears around twice the Raman shift of the corresponding one-phonon Raman peak because the two-phonon Raman scattering occurs when two phonons are created to scatter photon at a higher energy band.

4.3 EXPERIMENTAL

Electrochemical experiments were performed using an automated electrochemical flow cell system (Electrochemical ALD L.C., Athens, GA).[23] The working electrode (substrate) was a 100 nm thick polycrystalline Au film vapor deposited on a 5 nm thick Ti film on glass. The reference electrode was Ag/AgCl (3 M NaCl, BASI, West Lafayette, IN), and all potentials were reported with respect to it. The substrate was cycled in 0.1 M H_2SO_4 from -0.2 V to 1.45 V before each experiment.

Spectroelectrochemical experiments were performed using a Raman spectroelectrochemical flow cell (Electrochemical ALD L.C., Athens, GA).[23] Design of the new flow cell was similar to that described previously, but fitted with a quartz front window, and designed to fit in place of a microscope slide within the spectrometer (Figure 3.2).[23,24] The Ag/AgCl (3 M NaCl, BASI, West Lafayette, IN) reference electrode was placed upstream in a separate compartment. The Au SERS active working electrode was constructed on a polycrystalline Au film closely following the Bartlett et al. methodology, vapor deposited on a Ti adhesion layer, on glass. A layer of 600 nm diameter polystyrene spheres was then adsorbed on the surface, and Au was electrodeposited to partially cover the beads. Finally, the spheres were dissolved away using tetrahydrofuran, leaving a hexagonal array of 600 nm diameter hemispherical Au pits, which served as the SERS active substrate (Figure 3.3).[25,26] The thickness of the structured Au surface was

approximately 360 nm.[27] Extinction spectra obtained on equivalent shallow Au pits in previous studies showed a strong plasmon resonance peak at 660 nm in solution and would be expected to red shift upon germanene deposition,[27] due to an increase in the dielectric constant.[28,29] Raman spectra were obtained using a DXR Raman microscope, controlled by OMNIC software (Thermo Scientific, Waltham, MA), and continuous wave 780 nm and 532 nm laser sources in a backscatter geometry mode. A 10x objective lens with a numerical aperture (NA) of 0.25 was used to focus the laser. The illuminated laser beam for the above NA had a focal diameter of 3.1 μm and power density of 1.06 $\frac{\mathrm{mW}}{\mu\mathrm{m}^2}$ (Table 3.1). The Raman spectrometer was calibrated daily using the calibration program in the OMNIC software. Multiple neon emission lines were used to correct dispersion, into the grating, and correct laser wavelength. A pink light source was used to correct the relative band intensities, and a polystyrene sample was used to correct the Raman shift, in wavenumber. All Raman measurements were carried out under degassed aqueous environment.

All solutions were prepared using 18 MΩ ultrapure water from a Millipore-Q system (Barnstead, Dubuque, IA). GeO_2 and blank solutions were either adjusted to around pH 4.7 using perchlorate or buffered to pH 9.0 using 50 mM $Na_2B_2O_4$ (Baker analyzed, 99.5%) and contained 0.1M perchlorate as a supporting electrolyte. The solutions were degassed for at least 2 hours with N_2before experiments.

4.4 RESULTS AND DISCUSSION

After Ge is reductively deposited on the surface, forming small germanane domains, it can be irreversibly stripped off by applying positive potential, as shown in

Figure 4.1. It is believed that the ions diffuse away from the surface once Ge atoms are oxidized. However, the potential required to oxidize Ge depends on the reductive potential used to deposit the Ge. As shown in a red CV in Figure 4.1, when Ge was deposited by applying -0.7 V, the oxidation peak occurs at -0.1 V. The oxidation peak at -0.1 V is believed to be the first Ge layer in contact with Au, potentially forming a surface alloy. The initial alloy formation from low overpotential is supported by previous STM studies previously discussed, the -0.1 V oxidation peak's charge never reaches near 1 ML, but the peak also requires the highest potential to oxidize amongst all Ge oxidation peaks suggesting a strong Au-Ge interaction. When the more negative potential was applied, up to around -0.9 V, a new oxidation peak centered around -0.75 V was newly formed. The peak centered around -0.75 V however disappeared when the Ge was deposited at -1 V or more negative potentials, and a new oxidation peak centered around -0.3 V formed. The oxidation peak centered around -0.3 V had the most oxidative charge, and the high potential required to start the oxidation compared to the peak around -0.75 indicated that it was more stable species. The charge of the oxidation peak centered around -0.75 V indicated that the quantity of the Ge deposit was never over one ML. In addition, the Ge deposit formed at -0.9 V never formed 296 cm^{-1} from 780 nm laser irradiation, suggesting that the first ML of Ge heavily interacting with Au is formed at -0.9 V in pH 9.[30,31] It is suggested that the species oxidized at -0.75 V was incomplete germanene structures that were easily oxidizable.

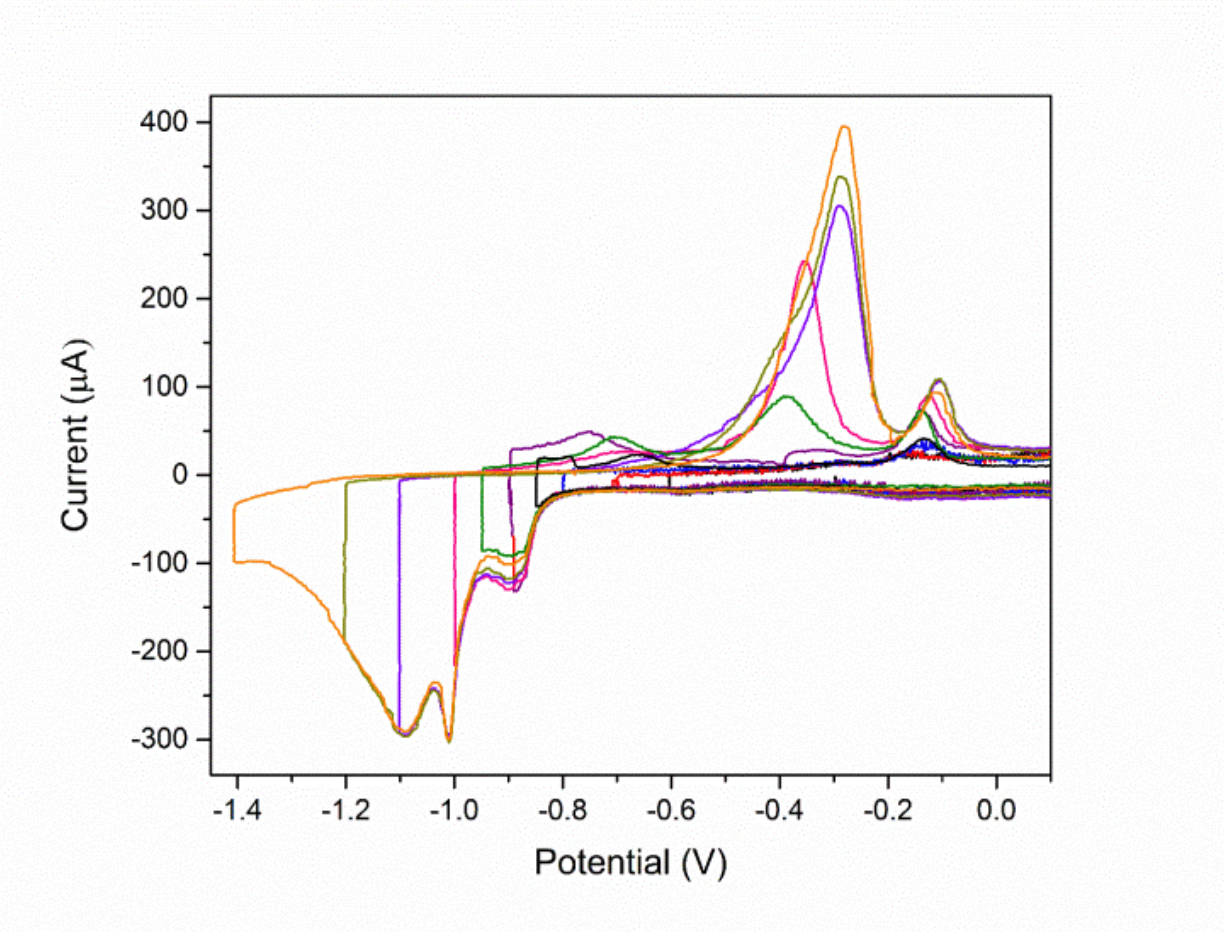

Figure 4.1. Adopted from chapter 3. Window opening cyclic voltammograms of GeO_2 (0.1 mM GeO_2, 50 mM $Na_2B_2O_4$, pH 9.0) solution on a polycrystalline Au substrate from anodic potential limit at 0.5 V and various cathodic potential limit from -0.8 V to -1.4 V, the cathodic potential was held constant for 300 s at the cathodic potential limit before the anodic scan. The scan rate was 10 mV/s, and the area of the working electrode was 2 cm^2.

The potential dependence of germanene oxidation was further studied using *in situ* Raman spectroscopy. In Figure 4.2, A series of *in situ* Raman spectra was measured at -0.7 V after forming the 296 cm^{-1} peak using 780 nm laser irradiation. As Raman

spectra were periodically measured, the 296 cm^{-1} peak remained consistent and did not disappear, indicating that germanene was present and stable at -0.7 V. This was expected, since no significant oxidation current is observed when -0.7 V was applied according to Figure 4.1. The 296 cm^{-1} peak seemed to remain stable until around -0.5 V was applied, an onset of Ge oxidation peak according to Figure 4.1. The 296 cm^{-1} peak started to broaden and turn into amorphous Ge peak 15 minutes after -0.5 V was applied, indicating that germanene structure potentially degraded. The eventual degradation from applying -0.5 V was expected, oxidation of thin films would induce significant structural changes. However, when either -0.7 V or -0. 5 V was applied, new unexpected peaks centered around 200 cm^{-1} and 625 cm^{-1} were observed and their intensity increased over time. The 200 cm^{-1} and 625 cm^{-1} peaks' intensities were proportional to each other and were always observed together in similar experiments, suggesting that those two are closely related. The 200 cm^{-1} and 625 cm^{-1} peaks were previously observed and reported in Bui's work but in a different conditions.[32] Nonetheless, according to a theoretical study, the peak around 200 cm^{-1} was identified as the out-of-plane breathing mode (ZO) and the peak around 265 cm^{-1} was identified as the two-phonon Raman peak of the 296 cm^{-1} (2TO).[21] The 296 cm^{-1} peak did not instantly change when the anodic potential was changed to -0.7 V or -0.55 V, but oxidative currents were observed at the potentials as shown in Figure 4.1 suggesting that some level of oxidation occurred and that the new 200 cm^{-1} and 625 cm^{-1} peaks may be due to the oxidation of germanene. The only differences between the spectra measured at 0^{th} minute and 30^{th} minute in Figure 4.2 were the amount of time spent in the potential and unknown amount of oxygen that may have leaked into the electrochemical cell, making oxidation more likely to occur.

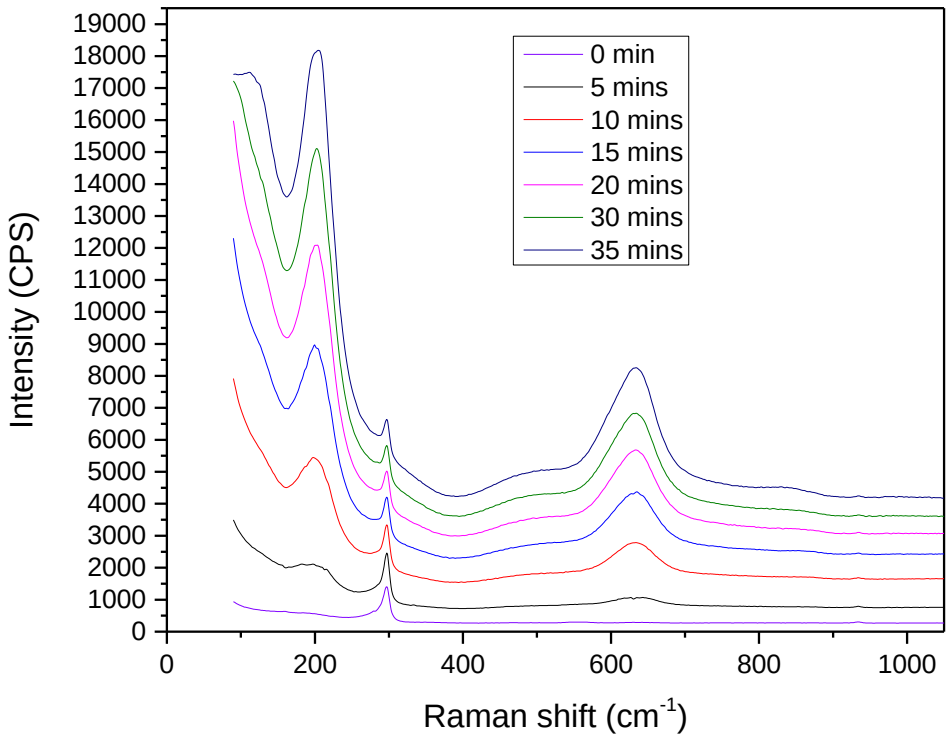

Figure 4.2. After depositing Ge at -1.3 V and forming the 296 cm^{-1} peak using 780 nm laser exposure, -0.7 V was applied, and a series of *in situ* Raman spectra was measured. After the first spectrum was measured at -0.7 V (purple), the Raman spectrum was measured every five minutes on the same spot. The 296 cm^{-1} peak's intensity relative to the baseline seemed to be unchanged despite anodic potential. ZO peak centered around 200 cm^{-1} and 2TO peak centered around 625 cm^{-1} started to develop and became the most prominent species. The measurement conditions for the series were 50 seconds laser irradiation, 5 measurements per spectrum, and 2 mW 780 nm laser.

The mechanism behind the 200 and 625 cm^{-1} peaks is not understood yet. As established in previous report by Bui, the two peaks seemed to be associated with the first germanene ML in contact with Au substrate. Bui's work demonstrated that ZO and 2TO peaks did not form when Ge was deposited on top of a Te ML that was in contact with Au.[32] Strong interaction between first ML Ge atoms and underlying Au atoms distorting germanene lattice could induce additional buckling, and the additional buckling could result in enhanced intensity of the ZO Raman peak.[21,30,31] As shown in Figure 4.2, ZO and 2TO peaks' intensities increased when germanene was exposed to an anodic potential. The two peaks' proportional intensities implied that there is one mechanism responsible for both peaks' increased intensities or multiple responsible mechanisms that are closely related. As previously discussed in chapter 3, EC-STM studies showed that the first germanene ML contained many defects. Therefore, it is proposed that the first ML germanene full of vacancy and Stone-Wales defects is stabilized by its heavy interaction with Au and applying more cathodic potential leads to increased hybridization and charge transfer between Ge and Au atoms.[31,33,34,35] Another possibility was that decreased hydrogen evolution may increase the interaction between Ge and Au, inducing structural stress on germanene.[36,37] Nonetheless, the ZO and 2TO peaks belonged to germanene and SERS Au surface enabled their measurements.

The ZO and 2TO peaks were not always present when germanene was oxidized away. In an experiment discussed in Figure 4.3, the 296 cm^{-1} peak was formed using 780 nm laser after Ge was deposited at -1.2 V and -0.15 V was applied to oxidize all deposited Ge. Afterward, the surface was studied using *in situ* Raman spectroscopy to

reveal that the 625 cm-1, 296 cm^{-1}, and 200 cm^{-1} peaks all disappeared, and only 270 cm^{-1} peak from amorphous Ge was present. The difference between the experiment in Figure 4.4 compared to experiments in Figures 4.2 and 4.3 was that more cathodic potential was applied, rapidly inducing oxidation when the potential was applied. The 270 cm^{-1} peak in in Figure 4.4 was attributed to amorphous Ge, caused by germanene after heavily disrupted to lose crystallinity obtained from 780 nm laser irradiation.

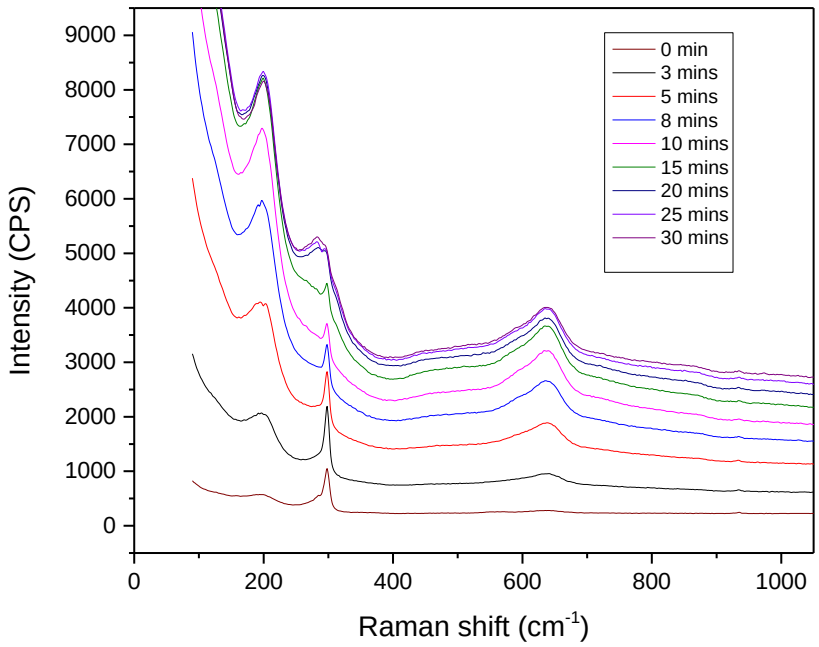

Figure 4.3. After depositing Ge at -1.3 V and forming the 296 cm^{-1} peak using 780 nm laser exposure, -0.5 V was applied, and a series of *in situ* Raman spectra was measured. After the first spectrum was measured at -0.5 V (purple), the Raman spectrum of the same spot was measured. The 296 cm^{-1} peak eventually broadened starting around 15^{th} minute after exposure to -0.5 V. ZO peak and 2TO peaks' intensity started to grow and

became the most prominent species just as in -0.7 V. The measurement conditions for the series were 20 seconds laser irradiation, 5 measurements per spectrum, and 2 mW 780 nm laser.

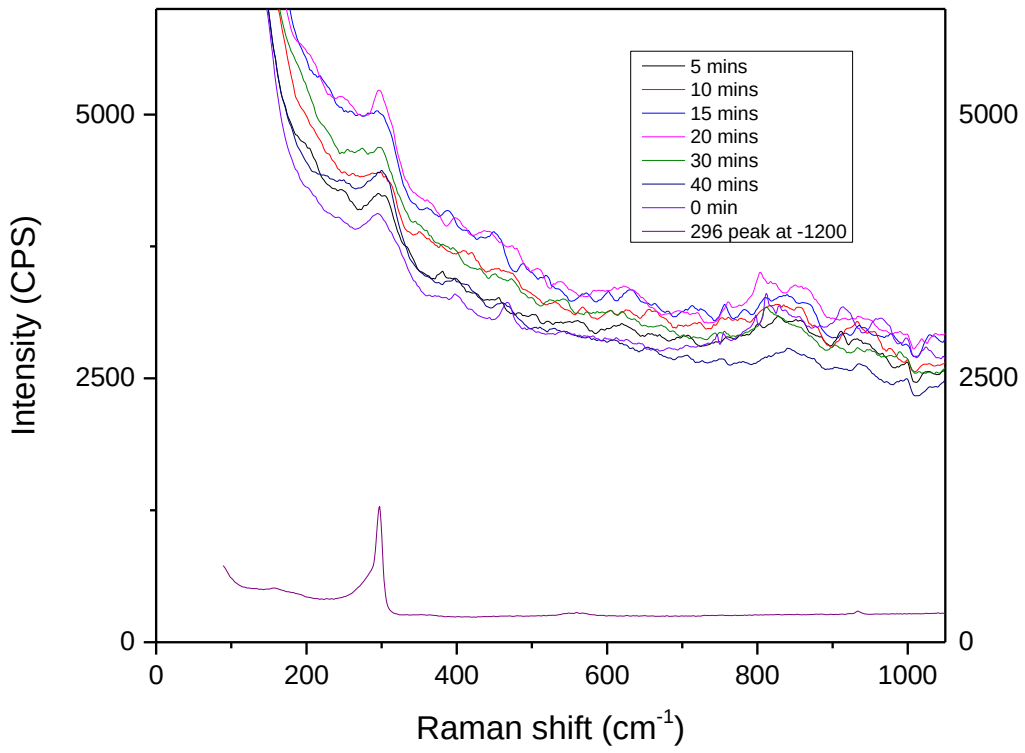

Figure 4.4. After depositing Ge at -1.3 V and forming the 296 cm^{-1} peak using 780 nm laser exposure, -0.15 V was applied, and a series of *in situ* Raman spectra was measured. After the first spectrum was measured at -0.5 V (purple), the Raman spectrum of the same spot was measured every five minutes. The 296 cm^{-1} peak disappeared and 270 cm-1 peak appeared after the first 5 minutes at -0.15 V. ZO peak and 2TO peaks did not grow. The measurement conditions for the this series were 20 seconds laser irradiation, 5 measurements per spectrum, and 2 mW 780 nm laser.

The partial oxidation of germanene described in Figure 4.4 behaved differently compared to the complete oxidation of deposited Ge. Total oxidation was illustrated in Figure 4.5, where OC was applied after forming the 296 cm^{-1} peak on Ge deposited at -1.35 V, the intensity of 296 cm^{-1} peak decreased over time and eventually disappeared without any sign of 170 cm^{-1}, 200 cm^{-1}, and 625 cm^{-1} peaks within 120 seconds. As discussed in chapter 3, OCP can quickly reach the potential for complete oxidation of Ge.

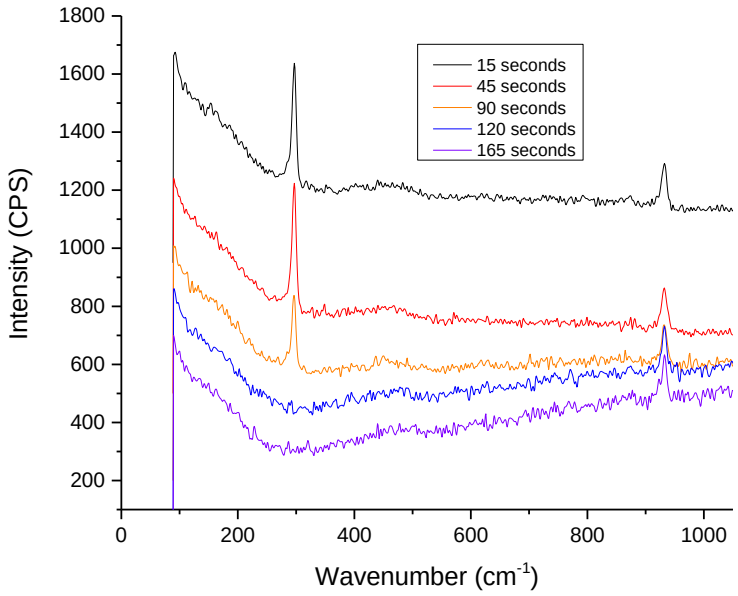

Figure 4.5. Ge was deposited on polycrystalline Au at -1.35 V in Ge solution for 300 s, and the deposit was exposed to OC in the Ge solution. After germanene was exposed to OC, the Raman spectrum was measured as frequently as the instrument allowed. The

measurement conditions were 5 seconds laser irradiation, 3 measurements per spectrum, and 2 mW 780 nm laser. ZO and 2TO peaks were not present, and their intensities did not seem to increase unlike in Figure 4.3 and 4.4.

Formation of micron-sized gas bubbles from the focus of Raman excitation laser was noticed early on during this project, but the experimental difficulty made it challenging to make a conclusion based on elemental analysis. Two possibilities have been considered: hydrogen gas evolution catalyzed by hot electrons and water boiling.[38] Water boiling has been considered due to increased temperature from Raman spectrometer's excitation laser heating the focused spot as previously discussed in chapter 3.[39] However, this was never experimentally proven and lacked any evidence. However, evidences of Raman excitation laser promoting hydrogen evolution were gathered, as shown in Figure 4.6. Formation micron-sized bubbles depended on multiple variables including Raman laser power, laser exposure length, Ge presence on the surface, and applied anodic potential. Higher Raman laser power tends to cause the bubble more reliably. In fact, low laser power below 2 mW in the Raman spectrometer never formed a visible bubble to the author's knowledge. Shorter laser radiation time also leads to less frequent bubble formation. However, a clear distinction between bubble forming laser power and irradiation time combinations and non-bubble forming combinations were not clearly defined. When moderate laser power and laser radiation time were used, the first Raman measurement may not have formed a bubble, but sequential measurements could have caused bubble formation, possibly due to residue

bubble-forming effects across multiple instances of Raman measurements collectively contributed to the bubble formation.

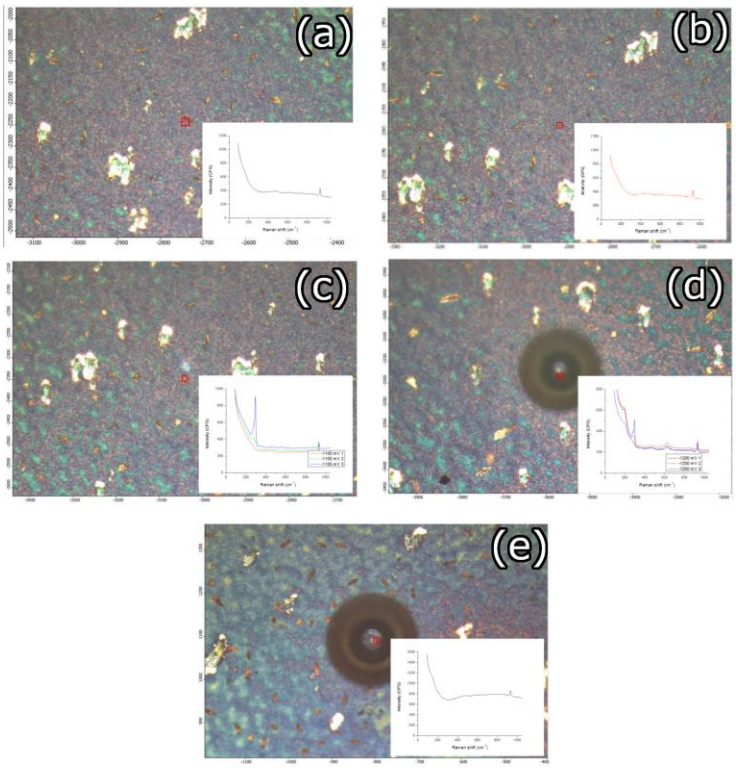

Figure 4.6. A series of *in situ* Raman spectroscopy was performed on an Au SERS surface. The picture was taken via 10x micro-Raman spectrometer objective after at least three 30 seconds long 5 mW measurements using 780 nm excitation laser, Raman spectra overlaid on right lower quarter were resulting Raman spectra from the image. Figure 4.6a was measured in pH 9.0 Ge solution at -1 V, neither germanene Raman peak nor bubble was present. Figure 4.6b was also measured in pH 9.0 Ge solution at -0.9 V, neither germanene Raman peak nor bubble was present. Figure 4.6c was measured in pH 9.0 Ge solution at -0.9 V, germanene Raman peak appeared but the bubble never appeared.

Figure 4.6d was measured in pH 9.0 Ge solution at -1.2 V, both germanene Raman peak ad bubble appeared. Figure 4.6e was measured in pH 8.9 blank at -1.4 V. This was the least anodic potential to form a bubble in a blank solution. It was demonstrated that bubble formation was correlated with anodic potential, and Ge presence on the surface decreases the necessary anodic potential to form the bubble.

As shown in Figure 4.6, there was a clear correlation between anodic potential and bubble formation. Applying more anodic potential made it more likely to form the bubble. Possibly due to hot electrons from laser irradiation promoting hydrogen evolution.[38] Ge presence was not required to form a bubble, but more cathodic potential had to be applied to form the bubble when Ge was not present on the surface. It should be noted that, without an excitation laser, the Ge-covered Au surface require more cathodic potential to start HER compared to a clean Au surface, meaning that Ge itself actually makes HER less energetically favorable. It has been hypothesized that germanene on the surface is increasing photon absorption to promote hydrogen evolution when Ge is present during Raman spectroscopy. This phenomenon has been also observed and reported by Bui.[32]

Inspired by the development of germanene Raman peaks from irradiating a laser at electrodeposited Ge on SERS surface, similar experiments were performed to form stanene. Stanene is a Sn elemental 2D material similar to germanene and graphene.[40] Sn was deposited on SERS active Au by applying -0.8 V for 30 seconds in an *in situ* spectroelectrochemical flow cell. Then, -0.25 V was applied to cease Sn reduction and

keep it stable under potential. Afterward, both 780 nm and 532 nm laser wavelengths were used to study the nature of Sn deposit and investigate if similar surface plasmon assisted annealing could be observed. However, resulting in spectra when the anodic potential was applied only exhibited a broad peak around 585 cm^{-1} as shown in Figure 4.7, indicating Sn^{+4} compound.[41,42] The 585 cm^{-1} peak disappeared when anodic potential around 0.5 V was applied, but the peak returned when cathodic potential around -0.25 V was applied again. It is believed that the Sn atoms alloyed with Au and were not easily oxidized away. When the anodic potential was applied, the Sn^{+4} compound may have been oxidized to a non-Raman active species but not dissolved into ions. Laser induced recrystallization did not seem to occur and stanene Raman peak was not found.

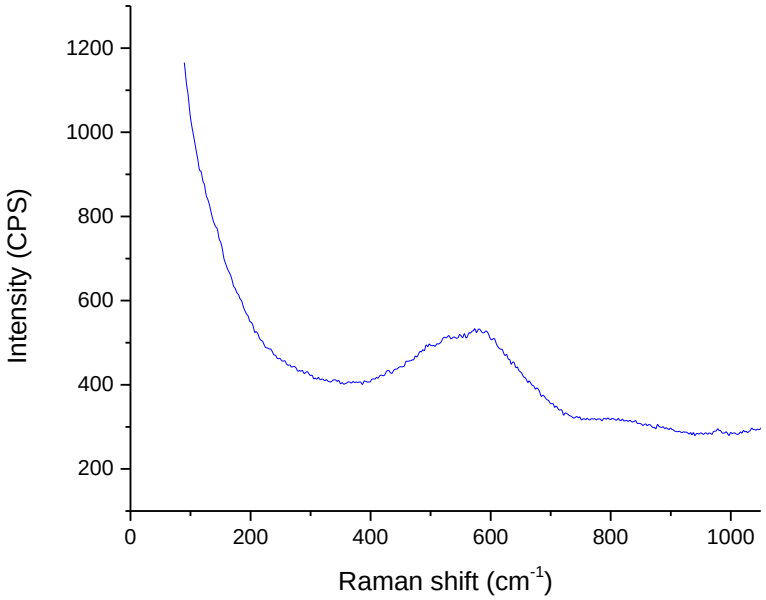

Figure 4.7. *In situ* Raman spectrum of Sn-Au alloy in -0.25 V in blank solution show a broad peak, with potentially two peaks centered around 495 cm^{-1} and 585 cm^{-1}. This Raman spectrum was measured after 10 cycles between -0.2 V and 1.45 V in 0.1 M sulfuric acid to clean the surface. This peak is believed to be from $Sn(OH)_4$.[42]

4.5 CONCLUSION

Previous chapters discussed electrochemical deposition of Ge and evidence of germanene formation, atomic resolution image of germanene and germanene's in-plane Raman peak around 296 cm^{-1} was reproducibly observed. In this chapter, a change in Raman spectra of the germanene deposit after exposure to anodic potential was reported. Two peaks, out-of-plane breathing mode scattering peak centered around 200 cm^{-1} and two phonon scattering of in-plane breathing mode scattering peak centered around 625 cm^{-1}, were enhanced when an anodic potential was applied. It is proposed that the interaction between first germanene ML and Au substrate strengthens via increased hybridization and charge transfer effects when the anodic potential is applied. Germanene seemed to be susceptible to oxidation when an anodic potential was applied, but the time required to entirely change deposited germanene depended on the applied potential. Nonetheless, additional Raman peaks originating from germanene were further evidence of the electrochemical formation of germanene. Ge assisted photon-driven hydrogen bubble formation was also observed when *in situ* spectroelectrochemical experiments were performed. The bubbles could have been avoided by adjusting Raman measurement conditions. Potential stanene formation was also investigated using *in situ* spectroelectrochemistry, but signs of stanene were not observed.

4.6 ACKNOWLEDGEMENT

Support from the National Science Foundation, DMR #1410109, is gratefully acknowledged.

REFERENCES

1. Wang, Y.; Li, J.; Xiong, J.; Pan, Y.; Ye, M.; Guo, Y.; Zhang, H.; Quhe, R.; Lu, J., Does the Dirac cone of germanene exist on metal substrates? *Physical Chemistry Chemical Physics* **2016,** *18* (28), 19451-19456.

2. Wang, Y. P.; Ji, W. X.; Zhang, C. W.; Li, S. S.; Li, F.; Li, P.; Ren, M. J.; Chen, X. L.; Yuan, M.; Wang, P. J., Enhanced band gap opening in germanene by organic molecule adsorption. *Materials Chemistry and Physics* **2016,** *173*, 379-384.

3. Liu, G.; Luo, W. W.; Wang, X.; Lei, X. L.; Xu, B.; Ouyang, C. Y.; Liu, S. B., Tuning the electronic properties of germanene by molecular adsorption and under an external electric field. *Journal of Materials Chemistry C* **2018,** *6* (22), 5937-5948.

4. Kaloni, T. P.; Schwingenschlögl, U., Stability of germanene under tensile strain. *Chemical Physics Letters* **2013,** *583*, 137-140.

5. Wang, R.; Pi, X.; Ni, Z.; Liu, Y.; Lin, S.; Xu, M.; Yang, D., Silicene oxides: formation, structures and electronic properties. *Scientific Reports* **2013,** *3*, 3507.

6. Saeed, M.; Hamed, A.; Wang, Z.; Shaygan, M.; Neumaier, D.; Negra, R., Graphene integrated circuits: new prospects towards receiver realisation. *Nanoscale* **2018,** *10* (1), 93-99.

7. Novoselov, K. S.; Geim, A. K.; Morozov, S. V.; Jiang, D.; Zhang, Y.; Dubonos, S. V.; Grigorieva, I. V.; Firsov, A. A., Electric Field Effect in Atomically Thin Carbon Films. *Science* **2004,** *306* (5696), 666-669.

8. Schwierz, F., Graphene Transistors: Status, Prospects, and Problems. 2013; Vol. 101, pp 1567-1584.

9. Wu, Y. Q.; Lin, Y.; Jenkins, K. A.; Ott, J. A.; Dimitrakopoulos, C.; Farmer, D. B.; Xia, F.; Grill, A.; Antoniadis, D. A.; Avouris, P. In *RF performance of short channel graphene field-effect transistor*, 2010 International Electron Devices Meeting, 6-8 Dec. 2010; 2010; pp 9.6.1-9.6.3.

10. Jo, G.; Choe, M.; Lee, S.; Park, W.; Kahng, Y. H.; Lee, T., The application of graphene as electrodes in electrical and optical devices. *Nanotechnology* **2012,** *23* (11), 112001.

11. Kim, B. J.; Jang, H.; Lee, S.-K.; Hong, B. H.; Ahn, J.-H.; Cho, J. H., High-Performance Flexible Graphene Field Effect Transistors with Ion Gel Gate Dielectrics. *Nano Letters* **2010,** *10* (9), 3464-3466.

12. Wang, S.; Ang, P. K.; Wang, Z.; Tang, A. L. L.; Thong, J. T. L.; Loh, K. P., High Mobility, Printable, and Solution-Processed Graphene Electronics. *Nano Letters* **2010,** *10* (1), 92-98.

13. Lundstrom, M. In *Device physics at the scaling limit: what matters? [MOSFETs]*, IEEE International Electron Devices Meeting 2003, 8-10 Dec. 2003; 2003; pp 33.1.1-33.1.4.

14. Kandemir, A.; Iyikanat, F.; Bacaksiz, C.; Sahin, H., α-Silicene as oxidation-resistant ultra-thin coating material. *Beilstein Journal of Nanotechnology* **2017,** *8*, 1808-1814.

15. Du, Y.; Zhuang, J.; Liu, H.; Xu, X.; Eilers, S.; Wu, K.; Cheng, P.; Zhao, J.; Pi, X.; See, K. W.; Peleckis, G.; Wang, X.; Dou, S. X., Tuning the Band Gap in Silicene by Oxidation. *ACS Nano* **2014,** *8* (10), 10019-10025.

16. De Padova, P.; Quaresima, C.; Olivieri, B.; Perfetti, P.; Le Lay, G., Strong resistance of silicene nanoribbons towards oxidation. *Journal of Physics D: Applied Physics* **2011,** *44* (31), 312001.

17. Sharma, V.; Srivastava, P.; Jaiswal, N. K., Edge-Oxidized Germanene Nanoribbons for Nanoscale Metal Interconnect Applications. *IEEE Transactions on Electron Devices* **2018,** *65* (9), 3893-3900.

18. Grishina, E. P.; Noskov, A. V., *Electrochemical Oxidation and Corrosion of Metals*. Nova Science Publishers, Inc: New York, 2010.

19. Ramesha, G. K.; Sampath, S., Electrochemical Reduction of Oriented Graphene Oxide Films: An in Situ Raman Spectroelectrochemical Study. *The Journal of Physical Chemistry C* **2009,** *113* (19), 7985-7989.

20. Berciaud, S.; Ryu, S.; Brus, L. E.; Heinz, T. F., Probing the Intrinsic Properties of Exfoliated Graphene: Raman Spectroscopy of Free-Standing Monolayers. *Nano Letters* **2009,** *9* (1), 346-352.

21. Kukucska, G.; Zólyomi, V.; Koltai, J., Resonance Raman Spectroscopy of Silicene and Germanene. *The Journal of Physical Chemistry C* **2019,** *123* (3), 1995-2008.

22. Scalise, E.; Houssa, M.; Pourtois, G.; van den Broek, B.; Afanas'ev, V.; Stesmans, A., Vibrational properties of silicene and germanene. *Nano Research* **2013,** *6* (1), 19-28.

23. Flowers Jr, B. H.; Wade, T. L.; Garvey, J. W.; Lay, M.; Happek, U.; Stickney, J. L., Atomic layer epitaxy of CdTe using an automated electrochemical thin-layer flow deposition reactor. *Journal of Electroanalytical Chemistry* **2002,** *524–525*, 273-285.

24. Liang, X.; Zhang, Q.; Lay, M. D.; Stickney, J. L., Growth of Ge Nanofilms Using Electrochemical Atomic Layer Deposition, with a "Bait and Switch" Surface-Limited Reaction. *Journal of the American Chemical Society* **2011,** *133* (21), 8199-8204.

25. Abdelsalam, M. E.; Bartlett, P. N.; Baumberg, J. J.; Cintra, S.; Kelf, T. A.; Russell, A. E., Electrochemical SERS at a structured gold surface. *Electrochemistry Communications* **2005,** *7* (7), 740-744.

26. Mahajan, S.; Baumberg, J. J.; Russell, A. E.; Bartlett, P. N., Reproducible SERRS from structured gold surfaces. *Physical Chemistry Chemical Physics* **2007,** *9* (45), 6016-6020.

27. Bartlett, P. N.; Baumberg, J. J.; Coyle, S.; Abdelsalam, M. E., Optical properties of nanostructured metal films. *Faraday Discussions* **2004,** *125* (0), 117-132.

28. Matthes, L.; Pulci, O.; Bechstedt, F., Optical properties of two-dimensional honeycomb crystals graphene, silicene, germanene, and tinene from first principles. *New Journal of Physics* **2014,** *16* (10), 105007.

29. Mahmoud, M. A.; Chamanzar, M.; Adibi, A.; El-Sayed, M. A., Effect of the Dielectric Constant of the Surrounding Medium and the Substrate on the Surface Plasmon Resonance Spectrum and Sensitivity Factors of Highly Symmetric Systems: Silver Nanocubes. *Journal of the American Chemical Society* **2012,** *134* (14), 6434-6442.

30. Dávila, M. E.; Xian, L.; Cahangirov, S.; Rubio, A.; Lay, G. L., Germanene: a novel two-dimensional germanium allotrope akin to graphene and silicene. *New Journal of Physics* **2014,** *16* (9), 095002.

31. Li, F.; Wei, W.; Yu, L.; Huang, B.; Dai, Y., Interface effects between germanene and Au(1 1 1) from first principles. *Journal of Physics D: Applied Physics* **2017,** *50* (11), 115301.

32. Bui, N. N. Electrodeposition of nanomaterials: examination of growth at the atomic interfaces. UGA, 2017.

33. Zhang, X.; Yu, Z.; Ji, W.; Sui, H.; Cong, Q.; Wang, X.; Zhao, B., Charge-Transfer Effect on Surface-Enhanced Raman Scattering (SERS) in an Ordered Ag NPs/4-Mercaptobenzoic Acid/TiO2 System. *The Journal of Physical Chemistry C* **2015,** *119* (39), 22439-22444.

34. Cao, C.; Tao, R.; Ford, D. C.; Klie, R. F.; Proslier, T.; Cooley, L. D.; Dzyuba, A.; Zapol, P.; Warren, M.; Lind, H.; Zasadzinski, J. F., Giant two-phonon Raman scattering from nanoscale NbC precipitates in Nb. *Physical Review B* **2015,** *91* (9), 094302.

35. Le Ru, E. C.; Blackie, E.; Meyer, M.; Etchegoin, P. G., Surface Enhanced Raman Scattering Enhancement Factors: A Comprehensive Study. *The Journal of Physical Chemistry C* **2007,** *111* (37), 13794-13803.

36. Zhuang, J.; Gao, N.; Li, Z.; Xu, X.; Wang, J.; Zhao, J.; Dou, S. X.; Du, Y., Cooperative Electron–Phonon Coupling and Buckled Structure in Germanene on Au(111). *ACS Nano* **2017**.

37. Galashev, A. E.; Ivanichkina, K. A.; Vorob'ev, A. S.; Rakhmanova, O. R., Structure and stability of defective silicene on Ag(001) and Ag(111) substrates: A computer experiment. *Physics of the Solid State* **2017,** *59* (6), 1242-1252.

38. Nedrygailov, I. I.; Moon, S. Y.; Park, J. Y., Hot electron-driven electrocatalytic hydrogen evolution reaction on metal–semiconductor nanodiode electrodes. *Scientific Reports* **2019,** *9* (1), 6208.

39. Lin, Y.; Yu, X.; Wang, Z.; Tu, S.-T.; Wang, Z., Effect of Laser-Induced Heating on Raman Measurement within a Silicon Microfluidic Channel. *Micromachines* **2015,** *6*, 813-830.

40. Deng, J.; Xia, B.; Ma, X.; Chen, H.; Shan, H.; Zhai, X.; Li, B.; Zhao, A.; Xu, Y.; Duan, W.; Zhang, S.-C.; Wang, B.; Hou, J. G., Epitaxial growth of ultraflat stanene with topological band inversion. *Nature Materials* **2018,** *17* (12), 1081-1086.

41. Akyil, C.; Akdas, G.; Afsin, P.; Ürgen, M., Freestanding SnO2 films produced with anodic polarization in acidic media containing colloidal tin hydroxides. *Materials Chemistry and Physics* **2019,** *221*, 263-271.

42. Huang, B. X.; Tornatore, P.; Li, Y.-S., IR and Raman spectroelectrochemical studies of corrosion films on tin. *Electrochimica Acta* **2001,** *46* (5), 671-679.

CHAPTER 5

CONCLUSION AND FUTURE STUDIES

Electrodeposited Ge has been studied using CV, EC-STM, and *in situ* Raman spectroscopy to investigate evidence of germanene. The CV of Au in pH 9 Ge solution suggested that multiple Ge species formed on the surface of Au, the slow rate of sub-ML Ge deposition, and the self-limiting amount is believed to be due to the lateral growth of germanene eventually covering the surface and eliminating further nucleation on the surface. EC-STM studies revealed Ge-Au surface alloy starting around -0.5 V vs. Ag/AgCl and germanene structures at anodic potentials starting around -0.9 V vs. Ag/AgCl. Approach to study germanene by forming a thick Ge deposit using the B&S method was futile. All Ge films deposited using the B&S formed exhibited amorphous Ge Raman peak only. The B&S method was further optimized to improve the homogeneity and look for the evidence of germanene formation. *In situ* Raman spectroelectrochemistry studies on electrodeposited Ge allowed observation of multiple germanene Raman scattering peaks when the deposit was irradiated with 780 nm excitation laser.

Using the B&S method on Cu and Au to form thick Ge films proved to be a reliable method, but the method required to exchange solutions between steps, making the overall process convoluted and slow for a practical application. One way to improve the B&S method would be eliminating solution exchange steps by depositing both Ge

and Te from one solution. Eliminating the solution exchange step would greatly decrease the amount of time it takes to deposit Ge and Te. Another possibility is to use pulse deposition similar to this group's previous work on CdTe deposition.[1]

One glaring limitation of electrochemically formed germane has been the small domain sizes without laser irradiation on SERS active substrate. It was speculated that the small domain sizes were due to simultaneous nucleation and growth at multiple nucleation sites. One possible way to increase germanene domain size could be using chemical additives to limit germanene nucleation sites and decreasing Ge ion concentration; they will effectively increase the distance between nucleation sites to promote larger germanene structures.[2,3] In addition, EC-STM could be used to identify germanene nucleation sites. Identifying favorable conditions for germanene nucleation could provide insight on how to control the electrochemical formation of germanene.[4,5]

The relationship between laser wavelengths and SERS active substrates used in the germanene recrystallization process was also not thoroughly studied. SERS enhancement factor is related to excitation laser wavelength and SERS surface morphology, but experiments reported in this dissertation were limited to two wavelengths of the laser and one SERS surface morphology. Experiments with a wide range of excitation laser wavelengths on different Ge deposited SERS substrates could discover conditions that do not disrupt the surface morphology or create hydrogen bubble during germanene recrystallization. Similarly, experiments on the electrochemical formation of stanene reported in this dissertation had a limited range of excitation laser wavelength and substrate. A notable difficulty with studying stanene reported in this dissertation was Sn forming an alloy with the metallic substrate. It may be challenging to

prohibit Sn-metal alloy formation, but non-metallic working electrode such as carbon electrode could be used to circumvent the problem.[6]

A method to keep germanene pristine in the ambient environment would be necessary to make it possible to integrate germanene into devices. One method to protect 2D materials from the environment is to encapsulate the 2D material in a protective layer. For example, multiple layers of germanene could be formed, utilizing some of the outer layers as the protective layer.[7] Also, germanene could be encapsulated in protective layers such as Au, transition-metal dichalcogenides, and aluminum nitride.[8,9]

It may be crucial to isolate free-standing germanene away from the substrate to utilize germanene, but 2D materials are too thin to be isolated using a mechanical tool. The most famous method to isolate a 2D material from a bulk material is using adhesive tape to isolate graphene from graphite or multilayered graphene.[10] However, the tape method may be incompatible with germanene because germanene is too fragile. Instead, intercalating gas molecules between the substrate and germanene could isolate the germanene layer.[11] Directly adopting other group's previous work may be difficult, but hydrogen gas evolution from laser irradiation may be utilized for this purpose.

REFERENCES

1. Zhang, X.; Shen, S.; Howell, P.; Cheng, W.; Mubeen, S.; Stickney, J., Potential Pulse ALD for Room Temperature Fabrication of Stoichiometric CdTe Nanofilms. *Journal of The Electrochemical Society* **2019,** *166* (5), H3249-H3256.

2. Radisic, A.; Vereecken, P. M.; Hannon, J. B.; Searson, P. C.; Ross, F. M., Quantifying Electrochemical Nucleation and Growth of Nanoscale Clusters Using Real-Time Kinetic Data. *Nano Letters* **2006,** *6* (2), 238-242.

3. Diao, Y.; Myerson, A. S.; Hatton, T. A.; Trout, B. L., Surface Design for Controlled Crystallization: The Role of Surface Chemistry and Nanoscale Pores in Heterogeneous Nucleation. *Langmuir* **2011,** *27* (9), 5324-5334.

4. Harniman, R. L.; Plana, D.; Carter, G. H.; Bradley, K. A.; Miles, M. J.; Fermín, D. J., Real-time tracking of metal nucleation via local perturbation of hydration layers. *Nature Communications* **2017,** *8* (1), 971.

5. Grujicic, D.; Pesic, B., Electrochemical and AFM study of nickel nucleation mechanisms on vitreous carbon from ammonium sulfate solutions. *Electrochimica Acta* **2006,** *51* (13), 2678-2690.

6. Kinoshita, K., *Carbon: Electrochemical and Physicochemical Properties*. Wiley: 1988.

7. De Padova, P.; Ottaviani, C.; Quaresima, C.; Generosi, A.; Paci, B.; Le Lay, G.; Olivieri, B.; Imperatori, P.; Salomon, E.; Angot, T.; Quagliano, L.; Romano, C.; Vona, A.; Muniz-Miranda, M., 24 h stability of thick multilayer silicene in air. *2D Materials* **2014,** *1* (2), 11.

8. Kou, L.; Ma, Y.; Yan, B.; Tan, X.; Chen, C.; Smith, S. C., Encapsulated Silicene: A Robust Large-Gap Topological Insulator. *ACS Applied Materials & Interfaces* **2015,** *7* (34), 19226-19233.

9. Van Bui, H.; Wiggers, F. B.; Friedlein, R.; Yamada-Takamura, Y.; Kovalgin, A. Y.; de Jong, M. P., On the feasibility of silicene encapsulation by AlN deposited using an atomic layer deposition process. *The Journal of Chemical Physics* **2015,** *142* (6), 064702.

10. Novoselov, K. S.; Geim, A. K.; Morozov, S. V.; Jiang, D.; Katsnelson, M. I.; Grigorieva, I. V.; Dubonos, S. V.; Firsov, A. A., Two-dimensional gas of massless Dirac fermions in graphene. *Nature* **2005,** *438* (7065), 197-200.

11. Du, Y.; Zhuang, J.; Wang, J.; Li, Z.; Liu, H.; Zhao, J.; Xu, X.; Feng, H.; Chen, L.; Wu, K.; Wang, X.; Dou, S. X., Quasi-freestanding epitaxial silicene on Ag(111) by oxygen intercalation. *Science Advances* **2016,** *2* (7), e1600067.